ADVANCED INTERMETALLICS/METALS AND COMPOSITES

Advanced Ordered Intermetallic Alloy Development

C. T. Liu and L. M. Pike
Metals and Ceramics Division
Oak Ridge National Laboratory
P.O. Box 2008, Oak Ridge, Tennessee 37831-6115

INTRODUCTION

The need for structural materials for use in corrosive environments has renewed interest in nickel silicide–based alloys. These alloys offer superior acid resistance and potentially could be used in a number of chemical industrial applications. Furthermore, nickel silicides offer many other attractive physical and mechanical properties that are common to intermetallic alloys. These include low density, high-temperature strength, oxidation resistance, and others. Previous investigations of nickel silicide alloys at ORNL were successful in developing alloys with good acid corrosion resistance. However, in alloys where corrosion resistance was optimized, a consequent loss in fabricability was observed. On the other hand, efforts to improve the fabricability resulted in reduced corrosion resistance. Another problem arose when considering high-temperature ductility vs low-temperature ductility. In general, it was found that while it was possible to achieve ductility in one temperature regime, it was considerably more difficult to have sufficient ductility in both regimes. It is apparent that although much knowledge has been obtained with regard to nickel silicide alloys, more work is needed to produce a single alloy with all of the desired properties present, that is, an alloy that exhibits excellent corrosion resistance, that is easy to fabricate, and that has sufficient low-temperature and high-temperature ductilities. The purpose of this project is to develop such an alloy based on the previous ORNL work as well as on recent studies reported in the scientific literature. This work is expected to lead to the development of a viable alloy with optimum properties for use as a structural material in a variety of chemical industrial applications.

TECHNICAL PROGRESS: FY 1998

Summary

A research project involving nickel silicide alloys was initiated during this year. The objective was to develop an alloy that exhibits good corrosion resistance, ease of fabricability, and good low- and high-temperature strength and ductility. A series of 8 alloys was produced with varying compositions. Alloying additions were chosen based on previous work performed at ORNL, as well as from information obtained from recent studies found in the literature. The compositions of these 8 alloys are listed in Table 1. The alloys were prepared from high-purity starting elements by arc melting in an inert argon atmosphere on a water-chilled copper hearth. The alloys then were drop cast into copper molds ($1/2 \times 1 \times 5$ in.). Sections of the ingots then were double clad in stainless steel and subjected to hot forging at 1050°C, followed by heat treatment for 3 d at 950°C.

Metallographic examination indicates that the alloys generally contain recrystallized two-phase microstructures.

With regard to fabricabilitity, it was found that all 8 alloys survived the first hot-forging step in excellent condition. However, after the second hot-forging step, a few of the alloys began to show signs of cracking. A list of the alloys that cracked is given in Table 2. Alloys that were easily fabricated (no cracking) included the base alloys (NSI-8 and NSI-1), as well as alloys doped with addition A. The alloy with 0.5% addition B also did not crack, but alloys with higher concentrations of addition B or with addition C were found to crack.

Table 1. Alloy Compositions (at. %)*

Alloy No.	Ni	Si	Cr	Mo	A	B	C	D
NSI-1	76.1	18.9	4.0	1.0	----	----	----	----
NSI-2	75.6	18.9	4.0	1.0	0.5	----	----	----
NSI-3	75.1	18.9	4.0	1.0	1.0	----	----	----
NSI-4	75.6	18.9	4.0	1.0	----	0.5	----	----
NSI-5	75.1	18.9	4.0	1.0	----	1.0	----	----
NSI-6	75.9	18.9	4.0	1.0	----	----	0.2	----
NSI-7	75.4	18.9	4.0	1.0	----	0.5	0.2	----
NSI-8	81.1	18.9	----	----	----	----	----	----

*Note: All alloys were doped with 50 wppm Boron.

Table 2. Fabricability and Oxidation Resistance of Alloys

Alloy No.	After 1st Forging	After 2nd Forging	Oxidation Resistance
NSI-1	Ok	Ok	Fair
NSI-2	Ok	Ok	Fair
NSI-3	Ok	Ok	Good
NSI-4	Ok	Ok	Fair
NSI-5	Ok	Cracked	Fair
NSI-6	Ok	Cracked	Fair
NSI-7	Ok	Cracked	Fair
NSI-8	Ok	Ok	Good

Tensile specimens were prepared from forged plate with an EDM and then hand-polished to eliminate surface imperfections. Tensile tests were performed in air with an Instron tensile testing machine at temperatures ranging from room temperature to 1000ºC. The yield strength of the alloys as a function of temperature is shown in Fig. 1. The yield strength of the base Ni-Si alloy (NSI-8) is seen to be the weakest. For this alloy, the yield strength is 95 ksi at room temperature, and it remains relatively constant up to 600ºC. At temperatures greater than 600ºC, the yield strength drops off sharply. Notably, by 1000ºC the strength has decreased to only 5 ksi. With the addition of Cr and Mo (alloy NSI-1),

the room-temperature yield strength has increased to 157 ksi. This high strength is maintained at elevated temperatures; in fact, a yield strength of 137 ksi is observed at temperatures as high as 600ºC. As with the base alloy, the yield strength of NSI-1 drops off sharply at temperatures greater than 600ºC. Also shown in Fig. 1 is the elevated temperature yield strength of alloys additionally alloyed with elements A and B (NSI-2, -3, -4, and -5). It can be seen that these yield strengths are quite similar to those of the NSI-1 alloy. However, it is observed that additions of element B (alloys NSI-4 and NSI-5) do increase the yield strength consistently over NSI-1 at all temperatures up to 600ºC. It is clear, however, that neither elements A nor B offer improvements at temperatures greater than 600ºC. It is important to point out that the yield strengths (~140 to 150 ksi) of these alloys at temperatures up to 600ºC are significantly high when compared with those of other corrosion-resistant alloys. For example, at 600ºC the yield strength of type 316 stainless steel and advanced Ni_3Al alloy is 62 and 100 ksi, respectively.

The ductility (elongation to fracture) of the alloys is shown in Fig. 2 as a function of temperature. The ductility of the base alloy (NSI-8) is seen to be around 18.9% at room temperature. However, this ductility drops off with increasing temperature, reaching a minimum of 1.6% at 600ºC. At greater temperatures the ductility is seen to increase, reaching 25.9% at 1000ºC. With the addition of Cr and Mo (NSI-1), the room-temperature ductility drops to 8.8%. A ductility minimum is still observed at 600ºC, but the minimum ductility of 3.0% is higher than that of the base alloy. At higher temperatures the ductility increases quickly, reaching an astonishing 193% at 1000ºC. The presence of the ductility minimum at 600ºC is a troublesome observation. If a useful Ni-Si alloy is developed, it will be necessary to eliminate this minimum as much as possible. It is noted in Fig. 2 that 0.5% additions of elements A and B increase the 600ºC ductility somewhat, but further increases (1%) show a negative effect.

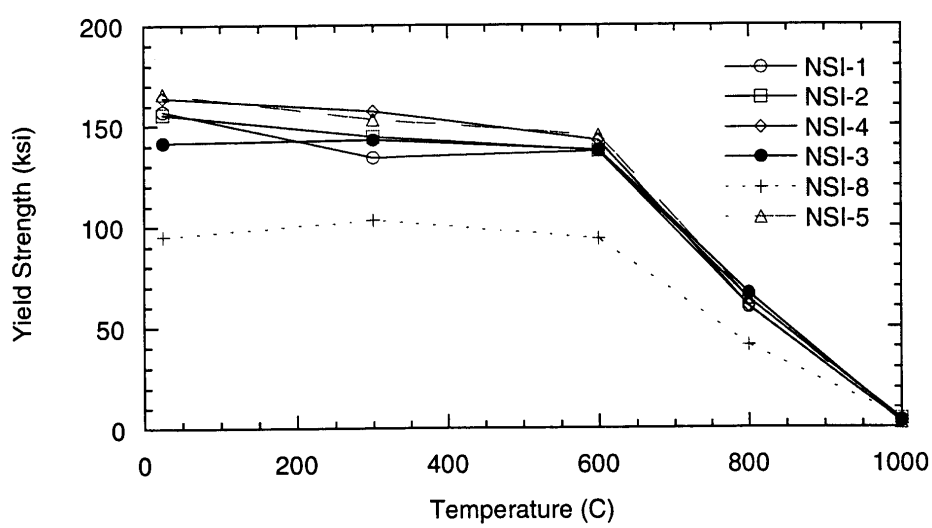

Fig. 1. The yield stress of Ni-Si alloys as a function of temperature.

Many intermetallic alloys show oxygen-induced environmental embrittlement at elevated temperatures. Recent studies indicate that in certain intermetallic alloys this kind of embrittlement can be alleviated by test in vacuum. To mechanistically understand the ductility minimum observed for NSI alloys at 600°C, the binary alloy NSI-8, the Cr+Mo modified alloy NSI-1, and the advanced alloy NSI-4 all were tensile tested in both air and vacuum. The test environment does not affect the yield strength but strongly influences the tensile ductility of these alloys at 600°C. Figure 3 compares the 600°C tensile ductility of the NSI alloys. The ductility of binary alloy NSI-8 is low and insensitive to test environment in air or vacuum. NSI-1 and -4 alloys exhibited a sharp increase in ductility as the test environment was changed from air to vacuum. This observation indicates that these alloys are proven to an oxygen-induced environmental embrittlement at 600°C. Since the ductility of NSI-1 and -4 in vacuum is distinctly higher than that of NSI-8, Mo and Cr additions seem to improve the intrinsic ductility at 600°C. The comparison of tensile ductilities in air and vacuum suggests that the alloying element B is very effective in improving the intrinsic ductility at 600°C but not effective in reducing the environmental embrittlement. In view of the fact that both alloys NSI-1 and NSI-4 showed a ductility of only 3% at 600°C, additional work certainly is required to improve the tensile ductility around this temperature in air.

Fig. 2. The ductility of Ni-Si alloys as a function of temperature.

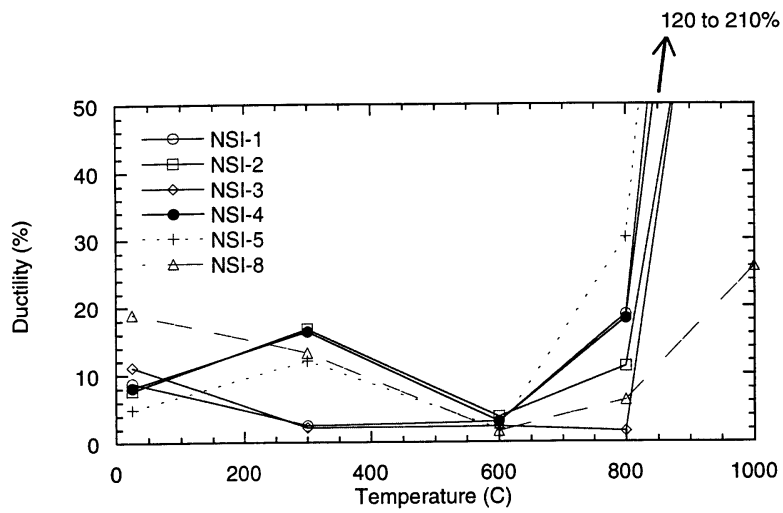

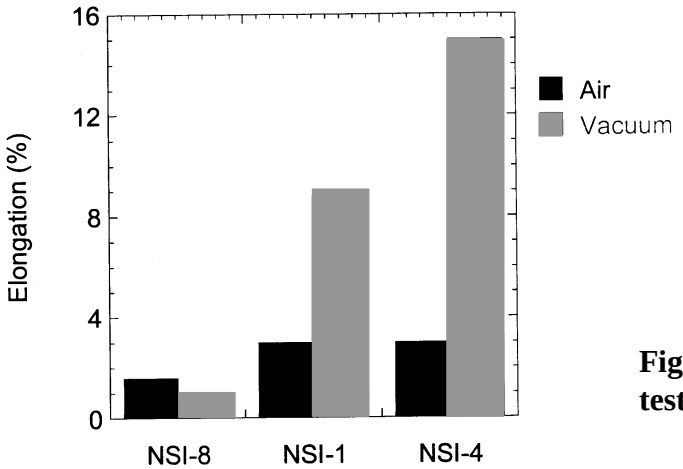

Fig. 3. Tensile ductility of NSI alloys tested at 600°C in air and vacuum.

A boiling-acid corrosion test was performed to characterize the corrosion behavior of the Ni-Si–based alloys. The tests were first performed in boiling sulfuric acid with a concentration of 60%. A reflux column was used to recapture acid vapors. The test was performed over a 96-h period with the solution being changed once every 24 h. The results are presented in Fig. 4, which plots the weight loss/unit area as a function of time. The graph shows that the alloys NSI-1 through NSI-5 offer substantial improvement over the binary Ni-Si alloy (NSI-8). The corrosion of these alloys at the end of the 96-h test is seen to be considerably less than half that of the binary alloy. Furthermore, the rate of corrosion is seen to be leveling off with time in these alloys (NSI-1 through NSI-5), while the corrosion rate of the binary NSI-8 alloy increases steadily with time. Trends among the well-performing alloys give further insight into the compositional dependence of the corrosion behavior. The alloy with only Cr and Mo additions had the highest corrosion rate in this set. Additions of element A improved corrosion resistance, and additions of B had an even greater beneficial effect.

The corrosion tests also were performed in 77% sulfuric acid solution. The results are shown in Fig. 5. The corrosion rates in this solution were found to be considerably less than in the 60% solution. In this case the corrosion rates of all of the alloys are fairly similar, with the worst performing alloy being NSI-1. As with the 60% solution data, the addition of 1% of element B (NSI-5) had the greatest beneficial effect. Additionally, corrosion tests will be performed at 99% sulfuric acid solutions. This concentration is similar to one commonly found in many industrial applications as reported recently at Haynes International.

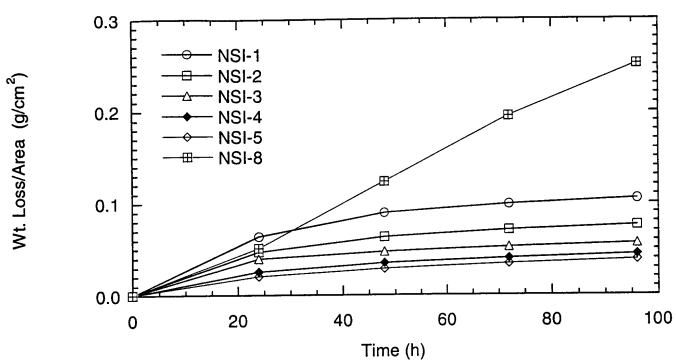

Fig. 4. The corrosion resistance of NSI alloys tested in boiling 60% sulfuric acid.

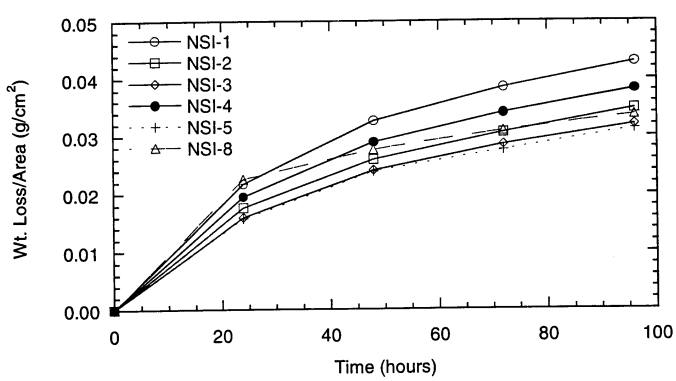

Fig. 5. The corrosion resistance of several NSI alloys tested in boiling 77% sulfuric acid.

PUBLICATIONS

A manuscript on the observed ductility minimum at 600ºC is in preparation and will be submitted in the following quarter.

PATENTS/DISCLOSURES

None. Project started October 1997.

LICENSES

None. Project started October 1997.

INDUSTRIAL INPUT AND TECHNOLOGY TRANSFER

At the DOE Workshop on Ordered Intermetallic Alloys held in Atlanta, Georgia, in June 1996, Cummins Engine Company and United Defense both expressed high interest in Ni_3Si-based alloys for petrochemical and chemical industries. We will contact these companies again when Ni_3Si alloys with improved corrosion resistance and cold and hot fabricability are developed through this project.

ESTIMATED ENERGY SAVINGS

The development of lightweight, high-strength, corrosion-resistant intermetallic alloys will lead to substantial improvement in performance (e.g., in terms of thermal efficiency and durability) of heat engines, energy-conversion devices, and industrial systems operated at elevated temperatures in hostile environments. This would result in substantial energy savings.

Development of Weldable, Corrosion-Resistant Iron-Aluminide (FeAl) Alloys

P. J. Maziasz, G. M. Goodwin, R. W. Swindeman, D. J. Alexander, and V. K. Sikka
Metals and Ceramics Division
Oak Ridge National Laboratory
P.O. Box 2008, Oak Ridge, Tennessee 37831

INTRODUCTION

A boron-microalloyed FeAl alloy [Fe-(36–38)Al-0.2Mo-0.05Zr-0.13C, at. %, with 100 to 400 appm B] with improved weldability and mechanical properties was developed in FY 1994. In FY 1995, a scaleup and industry technology-development phase was pursued along two parallel paths. One path was developing a monolithic FeAl component and application technology, while the other was developing coating/cladding technology for alloy steels, stainless steels, and other Fe-Cr-Ni alloys. During FY 1995–96, cast FeAl alloys were found to have good strength at 700 to 750°C, and some (2 to 5%) ductility in air at room temperature. A wide-ranging study of processing effects on properties showed that grain refinement, through hot extrusion of ingot or P/M FeAl alloys, significantly improved room-temperature tensile ductility and Charpy impact-toughness in air. However, the best high-temperature strength, creep resistance, and oxidation-corrosion resistance were found in cast FeAl alloys. In FY 1998, significant progress was made at developing an improved combination of mechanical properties, at developing methods for welding, and at extending studies of corrosion behavior of cast FeAl alloys. Potential applications in steel processing, chemical processing, and heat treating and furnace industries were pursued. This report concludes this project.

TECHNICAL PROGRESS: FY 1998

1. Industry Testing and Corrosion Resistance

In FY 1996, testing by INCO (G. Smith) showed that bare and preoxidized as-cast FeAl specimens were very resistant to carburization at 1000°C and 1100°C. The INCO carburizing gaseous environments simulated industrial steam/methane reformer and ethylene pyrolysis environments. In FY 1997, INCO (B. Baker and G. Smith) expanded testing and demonstrated outstanding oxidation resistance of FeAl in air + 5% water vapor at 1100°C up to 1000 h, carburization resistance at 1100°C in both oxidizing (H_2–5.5% CH_4–4.5% CO_2) and reducing (H_2–1% CH_4) atmospheres, and sulfidation resistance at 816°C. In FY 1998, INCO began testing on dusting resistance of FeAl alloys.

In FY 1997, large-scale castings of FeAl for skirt materials in aluminum refining applications were made and tested. A preliminary license was obtained for ORNL's FeAl

alloys for such applications by Anaconda Foundary and Fabrication Company (Anaconda, Montana), but this project ended in FY 1998.

During FY1997–98, cast FeAl grate bars and pallet tips for conveyors used in calcination of phosphate ores were produced and tested by FMC, Inc., in San Jose, California. This application involves both strength and oxidation/sulfidation resistance during cyclic exposures at 850 to 1000°C (1100 to 1200°C under extreme conditions). Cast FeAl components survived for over 6 months but then were removed due to sagging. There was no evidence of cracking, however, and they clearly showed good corrosion resistance, particularly compared with cast HH-35 or HH-40 cast austenitic alloys. Coupons of cast FeAl alloys were tested in FY 1998 at A. Finkl & Sons (C. Mante) for corrosion resistance relative to type 310 austenitic stainless steel in the molten neutral salt baths that are used for heat-treating steel die-blocks.

Cast FeAl coupons were tested for catalytic coking resistance at Dow Chemical Co. (C. Kneupper) in laboratory tests that simulate pyrolytic coking and de-coking treatments typical of ethylene cracking operations. The cast FeAl alloys typical of those being developed for commercial applications showed excellent resistance to pyrolytic coking compared with that of commercial cast austenitic stainless steels and alloys (HK-40, HP micro-alloyed alloys).

Discussions began in FY 1998 with Bethlehem Steel Corp. for use of FeAl alloys for steel rolls of the runout table in the hot-rolling mills, which currently are made of 400 series stainless steels. Discussions also were made with Weirton Steel Co. for FeAl alloys for use as rolls in molten zinc for producing galvanized sheet steel. In FY 1998, discussions continued with several different centrifugal casting companies (Duraloy, Inc., Alloy Engineering, and Shanango) for producing chemical and petrochemical tubing, radiant-heating tubes, or various steel processing rolls from cast FeAl alloys.

2. FeAl Fabrication Technology

Previous FeAl weld-overlay tests involved aspiration-cast wires for shielded-metal-arc (SMA) and gas-tungsten-arc (GTA) welding processes produced by Haynes International and others. Automated GTA and gas-metal-arc (GMA) commercial weld-overlay processing requires continuously coiled, small-diameter weld wire. Stoody Company was able to produce 1.6-mm–diam. solid- and powder-cored Fe-Al weld wire with compositions formulated to produce FeAl weld deposits with near-optimum Fe-36 to Fe-39 at. % Al compositions, with (Stoody I) and without (Stoody II) Cr. Crack-free FeAl weld-overlay test pads have been produced on 2¼Cr–1Mo and type 310 steels using the standard 350°C preheat and 750°C postweld heat treatment. Lower Al wires (Stoody III and IV) also were obtained.

Welding studies on monolithic FeAl components and thicker material began in FY 1996 and continued this year to solve the problem of cold cracking. Last year, initial efforts to weld FeAl centifugally cast (FA-385M2) tubes using filler wire were unsuccessful due to cold cracking without preheat and postweld heat treatment. Subsequent microstructural examination also revealed significant microcracks in the as-cast materials. To test the

hypothesis that cold-cracking and welding difficulties are related to the ductility in ambient air (an outcome that necessarily involves resistance to moisture-induced cracking), autogenuous automated GTA welds were made on hot-extruded P/M FeAl materials, with much higher ductility and significantly refined grain sizes. Good crack-free welds were made on the P/M FeAl material with no preheat or postweld heat treatment. This was a major breakthrough for welding/weldability of FeAl alloys. Previously, hot-extruded I/M FeAl alloys with 30- to 50-μm grain size and 8 to10% ductility in air at room temperature also were found to be weldable with no preheat or postweld heat treatment.

As-cast materials FeAl with only 3 to 4% ductility cold-cracked when welded without pre- and postweld heat treatment. However, there does appear to be a threshold ductility and strength level above which FeAl can be succesfully welded. In FY 1997, one of the heats (FA-386M2) was found not to cold-crack after a heat-treatment of 1 h at 1200°C. In FY 1998, a significant breakthrough in welding of cast FeAl alloys was achieved, because, with appropriate preheat and postweld heat treatment, ¼- and ½-in.–thick plates of several different FeAl alloys (and one Fe_3Al alloy) were welded successfully with no cold cracks.

3. Mechanical Properties of Cast FeAl

Mechanical properties of monolithic FeAl alloys have been examined previously as functions of alloy composition and processing-induced microstructures. Emphasis in FY 1998 was on as-cast FeAl alloys. Alloy compositional effects have focused mainly on minor variations and combinations of B, C, and Zr and other elements added to the FA-385/FA-385M2 base alloys, with Al contents ranging from 36 to 40 at. %. One goal microstructurally has been to enhance the formation and stability of MC carbides for improved high-temperature creep strength.

Previous work on the as-cast FeAl alloys with B microalloying additions showed that they had about 400 MPa yield strength (YS) up to about 700 to 750°C due to fine dispersions of ZrC precipitates. Heat-treatments of 1 h at 1200°C can increase room-temperature ductility in air to 3 to 4% and boost the YS to 500 to 550 MPa in new FeAl alloys with more added C and Zr, without sacrificing high-temperature strength and creep resistance at 700 to 800°C. Previously, such cast FeAl specimens heat-treated at 750°C or at 1200°C were found also to have Charpy impact energies of 11 to 14 J (Table 1). This is quite good, considering their coarse grain size (200 to 400 μm) and lower relative ductility. Previous Charpy impact testing of similar FA-350 alloys hot extruded to have more ductility and refined grain size (about 100 μm) showed only 3 to 5 J impact energy. The new FeAl alloys (FA-386 M3, M11, and M24) showed Charpy impact energies in the range of 8 to 10 J (full-sized specimens) regardless of heat treatment, and some alloys with tensile ductility above 5% also had impact energies close to 20 J (sub-sized specimens). TEM examination showed that the new FeAl heats also have more abundant dispersions of fine ZrC precipitates. High-temperature tensile testing also shows that these newer cast alloys have much better strength up to 800°C, and they have yield strength comparable to cast HU alloys at 900 and 1000°C.

Table 1. Charpy Impact Energy of Cast and Heat-Treated FeAl Alloys

Alloy	Heat Treatment	Temperature (°C)	Charpy Impact Energy (J)
FA386M1	1 h at 750°C	25	14.24
	1 h at 1200°C	25	13.56
FA386M2	1 h at 750°C	25	10.85
	1h at 1200°C	25	13.56
FA386M3	1 h at 750°C	25	8.14
	1 h at 1200°C	25	10.17
FA386M11	1 h at 750°C	25	8.81
	1 h at 1200°C	25	8.81
FA386M24	1 h at 750°C	25	8.81
	1 h at 1200°C	25	9.5

PUBLICATIONS

Journals

P. J. Maziasz, D. J. Alexander, and J. L. Wright, "High Strength, Ductility and Impact-Toughness at Room Temperature in Hot-Extruded FeAl Alloys," *Intermetallics* **5,** 547–62 (1997).

C. T. Liu, E. P. George, P. J. Maziasz, and J. H. Schneibel, "Recent Advances in B2 Iron Aluminide Alloys: Deformation, Fracture, and Alloy Design," to be published in *J. Materials Science and Engineering*, 1998/99 (invited Keynote paper).

D. J. Alexander, P. J. Maziasz, and J. L. Wright, "Processing and Alloying Effects on Tensile and Impact Properties of FeAl Alloys," to be published in *J. Materials Science and Engineering*, 1998–99.

Other Publications

P. J. Maziasz, G. M. Goodwin, D. J. Alexander, and S. Viswanathan, "Alloy Development and Processing of FeA: An Overview," in the *Conf. Proc. Nickel and Iron Aluminides: Processing, Properties and Applications*, eds. S. C. Deevi, P. J. Maziasz, V. K. Sikka, and R. W. Cahn, ASM-International, Materials Park, Ohio, pp. 157–76 (1997).

PRESENTATIONS

Oral Presentations

P. J. Maziasz, "Controlling Processing-Induced Microstructures to Dramatically Improve the Mechanical Properties of FeAl (B2) and γ-TiAl Alloys," Graduate Student Seminar presented at the Department of Materials Science and Engineering, University of Cincinnati, Cincinnati, Ohio, January 23, 1998.

P. J. Maziasz, R. W. Swindeman, and J. L. Wright, "Minor Alloying Additions for Improved High-Temperature Strength of FeAl Alloys," presented at Symposium on Strengthening in High-Temperature Intermetallics, 1998, TMS Annual Meeting, San Antonio, Texas, February 15–19, 1998.

D. J. Alexander, P. J. Maziasz, and J. L. Wright, "Processing and Alloying Effects on Tensile and Impact Properties of FeAl Alloys," presented at International Symposium on Iron Aluminides: Alloy Design, Processing, Properties and Applications, 1998, TMS Annual Meeting, San Antonio, Texas, February 15–19, 1998.

C. T. Liu, E. P. George, P. J. Maziasz and J. H. Schneibel, "Recent Advances in B2 Iron Aluminide Alloys: Deformation, Fracture and Alloy Design," presented at International Symposium on Iron Aluminides: Alloy Design, Processing, Properties and Applications, 1998, TMS Annual Meeting, San Antonio, Texas, February 15–19, 1998. [Invited Keynote Talk]

HONORS AND AWARDS

None.

PATENTS/DISCLOSURES

C. T. Liu, C. G. McKamey, P. F. Tortorelli, and S. A. David, "Corrosion Resistance Iron Aluminides Exhibiting Improved Mechanical Properties and Corrosion Resistance," U.S. Patent 5,320,802, granted June 14, 1994.

P. J. Maziasz, G. M. Goodwin, and C. T. Liu, "High-Temperature Corrosion-Resistant Iron-Aluminide (FeAl) Alloys Exhibition Improved Weldability," U.S. Patent 5,545,373, granted August 13, 1996.

P. J. Maziasz, A. M. Paris (Duraloy Technologies, Inc.), and J. D. Vought, "Mn Additions for Improved Fluidity of Cast B2-Phase FeAl Alloys," invention disclosure ERAD 0517, submitted June 2, 1998.

LICENSES

A preliminary license on FeAl was obtained by Anaconda Foundry and Fabrication Company (Anaconda, Montana) for use as a skirt material for an aluminum manufacturing process by Columbia Falls Aluminum Company. FeAl is currently in test for calcination of phosphate ores by FMC, Inc. (San Jose, California).

Duraloy continued discussions and has expressed written interested in licensing and/or a CRADA for FeAl. The benchmarks for comparison are the current heat-resistant cast austenitics like HK-40 or microalloyed HP alloys. Several other companies also have expressed interest in FeAl this quarter for a variety of applications.

INDUSTRIAL INPUT AND TECHNOLOGY TRANSFER

INCO has expressed interest in FeAl for weld-overlay technology. Finkl & Sons (C. Manthe) continues testing FeAl for resistance to corrosion in molten neutral-salts heat-treating baths and has inquired about FeAl for oxidation resistance and strength in a furnace-buck application.

FeAl has been tested as skirts around reduction cells that produce aluminum for Columbia Falls Aluminum Company, and significant erosion occurred. FeAl also has been cast as grid bars and pallet tips for application in calcination of phosphate ores by FMC, Inc., and has been in test for over 6 months at 850 to 1000°C in a highly oxidizing and sulfidizing environment.

Cast plates of FeAl have been sent to M-C Power Corporation for corrosion resistance in molten carbonate salts for a benign molten carbonate fuel cell (MCFC) application.

Cast FeAl specimens have been sent to Duraloy, Inc., for carburization and dusting-resistance testing relevant to chemical and petrochemical refinery applications. Continuous casting trials have been scheduled for early in FY 1999.

Cast FeAl specimens are being tested for resistance to coking by Dow Chemical Co. (Freeport, Texas). Resistance to dusting is being conducted by INCO, and dusting and carburization tests also are being conducted by the Swedish Institute for Metals.

ESTIMATED ENERGY SAVINGS

Very large energy savings accrue from using the Exo-Melt™ processing of FeAl compared with those of conventional metals melting processes (50%), and this use enables even larger savings in energy and in materials wastage when FeAl replaces steels, stainless steels, or Fe-Cr-Ni alloys as a longer-lasting “super” corrosion-resistant and heat-resistant alloy. Benefits for reduced metal loss or wear of FeAl also may be realized. FeAl also is a Cr- and Ni-free substitute for heat/corrosion-resistant steels and alloys for applications with such environmental and toxicity requirements. Coking resistance in ethylene-cracking applications would contribute to a very significant reduction in CO_2 emissions from the chemical industry.

High-Density Infrared Processing of Materials

C. A. Blue and V. K. Sikka
Metals and Ceramics Division
Oak Ridge National Laboratory
P.O. Box 2008, Oak Ridge, Tennessee 37831

INTRODUCTION

High-density infrared (HDI) heating has many advantages over commonly used heating techniques. This heating provides (1) an inherently clean noncontact heating method; (2) high heat fluxes resulting in heating rates up to 500°C/s, dependent on materials and mass because only the sample is heated to the desired temperature; (3) need for heating only the part (i.e., low thermal mass); (4) fast cooling rates due to the "cold-wall" nature of the process in which only the sample is heated; (5) high heat fluxes, which can be delivered unidirectionally over large areas; and (6) a precise process that essentially is shape independent, utilizing proper furnace designs (1).

High heat-flux heating is based on the transfer of thermal energy by electromagnetic radiation. There are three heat-transfer mechanisms: conduction, convection, and radiation. Conduction finds industrial application in the heating of liquids and solids. The heat system is based primarily on flame technology. Convection is used universally in drying applications where thermal energy needs to be transferred from a source to a workpiece without contact. Convection heating often can provide inefficiency, as the forced convection of heated air must be directed at the workpiece to break the boundary layer. In addition, forced convection requires enclosures and recirculating systems, and convection systems attract airborne dust and dirt. Radiation, particularly infrared radiation, suffers none of these disadvantages, and it is rapid. Thus, high heat-flux heating provides a versatile and flexible answer to heat-transfer problems throughout the industrial spectrum (2).

OAK RIDGE NATIONAL LABORATORY TECHNICAL PROGRESS: FY 1998

Summary

Infrared transient-liquid coating

Infrared transient-liquid coating (ITLC) gained a tremendous amount of interest this year. Application of tungsten carbide– and chromium carbide–reinforced nickel-based coatings to die inserts, wear parts, and corrosion-exposed parts was investigated with substantial success. The process involves a room-temperature spray process to coat a given specimen or part only where the coating is needed. After application of the coating material at room temperature, the specimen or part is fused rapidly in seconds to minutes in an infrared-type furnace. In the area of ITLC, two new funding sources were obtained. The first is a Cooperative Research and Development Agreement with the Y-12 Plant in the area of coating die inserts to resist thermal fatigue and aluminum attack. In this program, the

coating did not spall even under severe thermal fatigue, 200°C/s to 660°C followed by water quenching. This is due to the controlled dissolution of the base material during the infrared fusing. The system used in this work employs tungsten halogen lamps that are capable of delivering a maximum of 500 W/cm^2. In certain coating fusing applications, this is not high enough to fuse the coating without affecting the base material. Therefore, a new high-density transient-liquid coating system is being installed that is capable of delivering up to 3500 W/cm^2.

High-density infrared transient-liquid coating process

ORNL has developed an HDI transient-liquid coating (TLC) process to produce wear- and corrosion-resistant coatings on a multitude of surfaces. The HDI TLC process combines infrared with power densities up to 3.5 kW/cm^2 with a room-temperature spray process to form wear- and/or corrosion-resistant coatings in seconds to minutes. This process has been demonstrated with Cr_2C_3- and WC-reinforced coatings with nickel-based binders. Volume fractions as high as 70% have been accomplished with coating thicknesses of 10 μm to 2 mm. Examples of WC coatings of 10, 40, and 500 μm are shown in Figs. 1 and 2. These coatings have been tested under severe thermal cycling, 200°C/s to 650°C followed by water quenching and wear testing. Under no condition has coating delamination been observed.

The HDI TLC process allows for applying wear- and corrosion-resistant coatings where they are needed in seconds, with minimal effects on the base material to which it is being applied, and delamination is a nonissue.

Fig. 1. High-density infrared transient-liquid coating of steel parts.

(a)

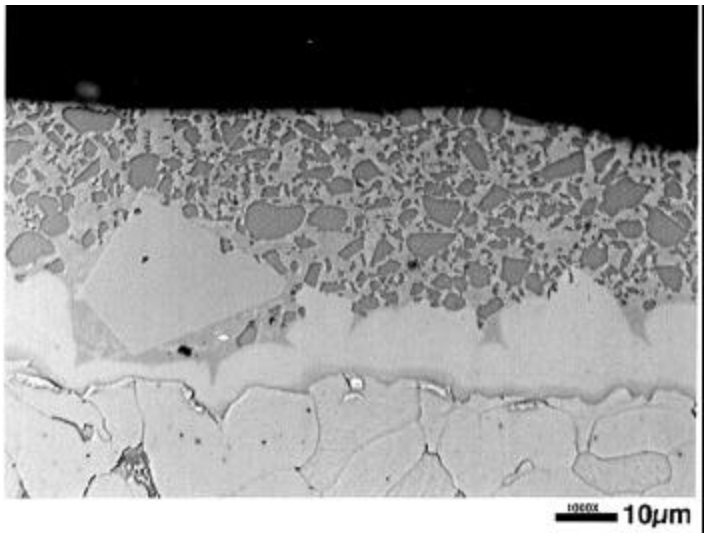

(b)

Fig. 2. High-density transient-liquid coating: (a) thick coating (60 to 70 mil) and (b) thin coating (1 to 2 mil).

References

1. N. C. Cox and D. E. McGee, "Use of High Density IR for the Rapid Heating of Metals," *Industrial Heating* **4,** 46–48 (1989).

2. H. Bischof, "The Answer is Electrical Infrared," *J. Microwave Power and Electron Energy* **25**(1), 47–52 (1990).

Presentations/Theses

C. A. Blue and V. K. Sikka, "Rapid and Highly Efficient Heating Source for the Die Casting Industry," Die Materials Committee Meeting, Sheraton Airport, Cleveland, Ohio, October 9, 1997, invited special technical presentation.

C. A. Blue, V. K. Sikka, and E. K. Ohriner, "Rapid Fusing of Coatings for the Automotive Industry," USCAR Meeting, Southfield, Michigan, May 21, 1998.

C. A. Blue, V. K. Sikka, and E. K. Ohriner, "Infrared Processing of Materials," AIM Meeting, Jackson Hole, Wyoming, June 23–25, 1998, invited special technical presentation.

C. A. Blue and V. K. Sikka, "Infrared Processing of Materials—Past, Present, and Future," 1998, Materials Solutions Conference, Rosemont Convention Center, Rosemont, Illinois, Life Cycle Issues and Technologies Session.

C. A. Blue and V. K. Sikka, "Infrared Processing of Materials," Cincinnati Milicron Consumable Products Division, October 22–23, 1998, Pebble Creek, Cincinnati, Ohio, 8th Annual Engineering Development Seminar, invited.

PUBLICATIONS

None.

PRESENTATIONS

None.

HONORS AND AWARDS

None.

PATENTS/DISCLOSURES

C. A. Blue, V. K. Sikka, and M. Patel, "Infrared Transient-Liquid-Phase Joining of TiAl to Steel," Lockheed Martin Energy Research Corporation, Invention Disclosure ERID No. 0344, S-88,687, submitted by Cummins Engine Company, 1998.

C. A. Blue, V. K. Sikka, and B. G. Whitson, "Infrared Heater for Boot Assembly," Lockheed Martin Energy Research Corporation, Invention Disclosure ERID No. 0306, S-87,645.

C. A. Blue, V. K. Sikka, E. C. Hatfield, and R. D. Seals, "Rapid Infrared Processing of Thermally Sprayed Materials," Lockheed Martin Energy Research Corporation, Invention Disclosure ERID Nos. 0438, S-90,007 and 1952-Y, S-90,007.

C. A. Blue, V. K. Sikka, and E. K. Ohriner, "Low Temperature Vacuum Heat Treating Utilizing Infrared," Lockheed Martin Energy Research Corporation, Invention Disclosure ERID No. 0317.

C. A. Blue, E. K. Ohriner, and V. K. Sikka, "Methods for Fabrication of Intermetallic Alloys," Lockheed Martin Energy Research Corporation, Invention Disclosure ERID No. 0509, S-90,099.

V. K. Sikka, C. A. Blue, and S. C. Deevi, "Flash Annealing of Iron Aluminide," filed by Philip Morris U.S.A., 1998.

Two additional patents filed by Smith & Nephew Richards.

The above nine patents have been forwarded to the U.S. Patent Office this year, and two are being licensed currently; approximately four additional patents have been filed.

LICENSES

"Infrared Heater for Boot Assembly," Invention Disclosure ERID No. 0306, S-87,645.

INDUSTRIAL JOINING AND TECHNOLOGY TRANSFER

Iron, Titanium, and Nickel Aluminide, Oak Ridge National Laboratory

Diamond Inserts to Steel Wheels, Blazer Diamond, and York Saw & Knife

TiAl Turbo-Chargers to Steel Shafts, Cummins Engine Company

Titanium to Steel Brazing and Heat Treating, Adaptive Coating Technologies

Titanium to Steel, TACOM, and General Dynamics

Zirconium to Copper, Montec

Titanium to Tungsten, Callaway Golf

Hafnium to Copper, EASB Welding & Cutting Products

Automotive Parts, General Motors

Titanium Honeycomb, Rohr

Inconel Honeycomb, Rohr

Intermetallic Alloy Development and Technology Transfer

V. K. Sikka, M. L. Santella,
R. W. Swindeman, and G. Aramayo
Metals and Ceramics Division
Oak Ridge National Laboratory
P.O. Box 2008, Oak Ridge, Tennessee 37831

Introduction

Ductile Ni_3Al and Ni_3Al-based alloys have been identified for a range of applications. These applications require the use of material in a variety of such product forms as sheet, plate, bar, wire, tubing, piping, and castings. Although significant progress has been made in the melting, casting, and near-net-shape forming of nickel aluminides, some issues still remain. These include the need for (1) high strength/high room-temperature hardness; (2) castability (e.g., mold type, fluidity, hot-shortness, and porosity); (3) welding and weld reparability of castings; (4) workability of cast or powder metallurgy product to sheet, bar, and wire; and (5) technology transfer.

All of the issues listed above can be "show stoppers" for the commercial applications of nickel aluminides.

In addition to Ni_3Al-based alloys, FeAl-based alloys have progressed to a stage for commercial applications. For successful applications of FeAl-based alloys, some issues still remain. These include the need for (1) identification of castable compositions, (2) development of melting practice to minimize/eliminate the furnace build-up issue, (3) properties of castings, and (4) technology transfer.

TECHNICAL PROGRESS: FY 1998

Summary

Major accomplishments have occurred during this year and are summarized briefly below.

1. Identified IC-438 as the Ni_3Al-based alloy for higher-temperature use than IC-221M. Thermal expansion, tensile, creep, and fatigue data of IC-438 are presented.
2. Heavy wall tubes of IC-221M were successfully cast by the centrifugal casting method.
3. Details of weld microstructure of IC-221LA in IC-221M are presented. Thermal-aging response of the welded IC-221M after 900°C for 5000 h was investigated.
4. Two radiant burner tube assemblies were welded at the Oak Ridge National Laboratory (ORNL) for Alloy Engineering & Casting (AEC) Company. These assemblies are going into operation at Ford and The Timken Company.

5. Initial welding trials of Ni_3Si-based alloys are presented. The results are very encouraging with the potential for their successful weldability.
6. Preliminary deformation maps for nickel-aluminide alloy.
7. Significant technology-transfer activities occurred with our licensees and potential new users.

Task 1. High-Strength Castable Ni_3Al Compositions (start 10/97, end 9/98)

The applications of the cast IC-221M alloy [8.0 Al-7.7 Cr-1.43 Mo-1.7 Zr-0.008 B-Balance Ni (wt %)] continued to expand. The new applications included radiant burner tubes, center posts for pit-carburizing furnaces, and guide rolls for continuous casters. However, a great demand has arisen from the potential users for extending the use temperature from the maximum allowed of 1100°C for IC-221M to 1250 to 1300°C. The IC-438 alloy, a eutectic-free modification of alloy IC-221M, has been identified for possible applications between 1150 and 1300°C. The IC-438 consists of 8.1 Al-5.23 Cr-7.02 Mo-0.13 Zr-0.005 B-Balance Ni (wt %). More than ten 15-lb heats of IC-438 alloy were air-induction melted using the Exo-Melt™ process and cast into $4 \times 6 \times 1$ in. thick plates and round, 2.85-in.–diam ingots. The cast ingots were used to measure thermal-expansion data, tensile properties, and selected creep properties.

The thermal-expansion data for IC-438 are plotted and also listed in Fig. 1. Its values are compared with those for IC-221M in Fig. 2. A set of tensile properties measured on cast IC-438 alloy are summarized in Table 1. The tensile properties of IC-438 are compared with those of IC-221M, HU, and SUPERTHERM™ in Figs. 3–5.

The creep rupture data on IC-438 are compared with those of IC-221M in Fig. 6. This plot shows that the rupture strength of IC-438 is equal to or even higher than IC-221M. The creep curves for the same test conditions for IC-438 and SUPERTHERM™ are compared in Fig. 7. This figure clearly demonstrates the superior creep resistance of IC-438 as opposed to SUPERTHERM™.

The fatigue data on several IC-438 samples are presented in Table 2. The fatigue data converted to equivalent creep life are presented as a Larson Miller plot in Fig. 8. This figure shows that IC-438 delivers significantly higher creep life under fatigue conditions as opposed to static loading. Figure 9, a plot similar to Fig. 8, shows IC-438 to have better fatigue life than SUPERTHERM™.

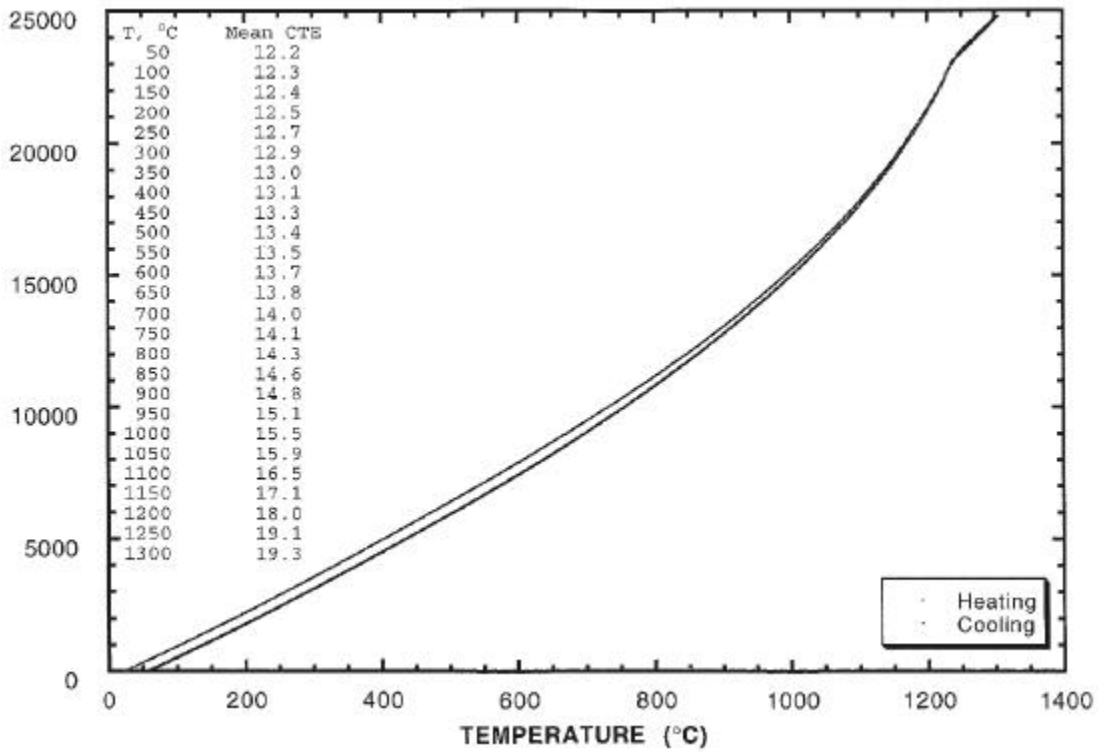

Fig. 1. Linear thermal expansion of IC-438 alloy in the as-cast condition.

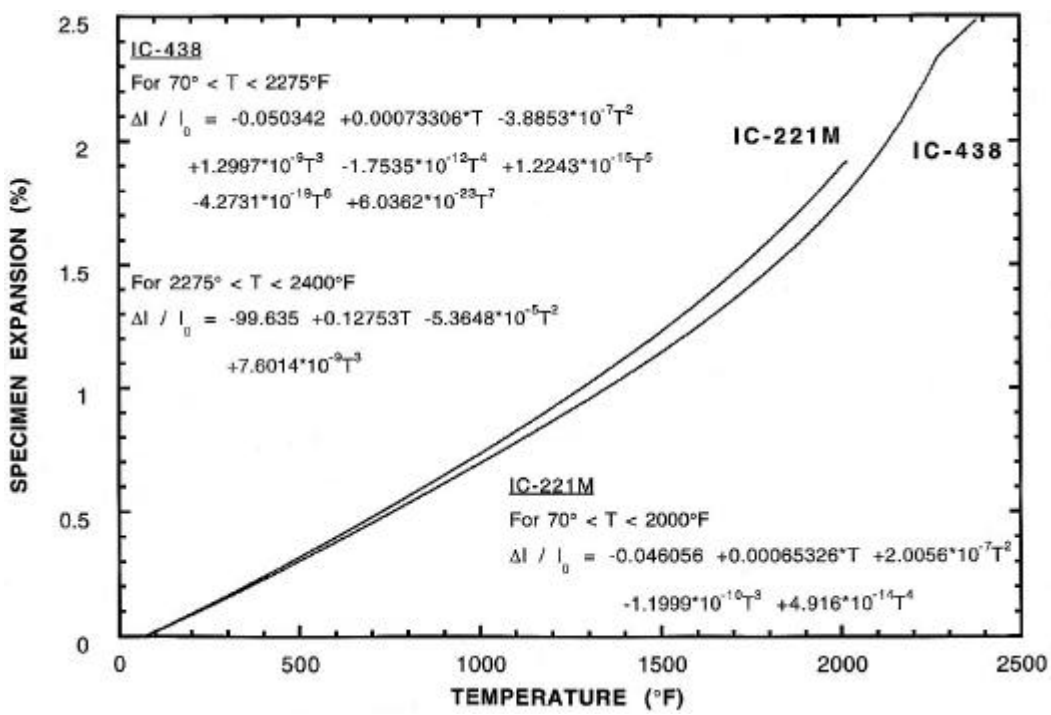

Fig. 2. Linear thermal expansion of IC-438 alloy compared with the data for IC-221M.

Table 1. Tensile Properties of IC-438 as a Function of Temperature

Temperature (°F)	Strength (ksi)		Elongation (%)
	Yield	Ultimate tensile	
	Small Heat Data		
RT[a]	82.9	135	20.8
572	83.4	133	24.6
1112	100.0	129	15.0
1472	108.0	122	4.8
1832	90.0	93.7	5.5
2012	53.7	55.3	2.2
2192	18.4	18.9	1.0
	Air-Melted Larger Heat Data		
2102	22.26	22.66	1.43
214	16.86	19.95	2.56
2192	13.04	15.40	4.97
2372	--	25.97	1.01
2372	--	14.26[b]	4.64
2462	--	4.88[b]	1.16

[a]RT = Room temperature.

[b]Tests run at a strain rate of 0.05/min. All other tests at 0.2/min.

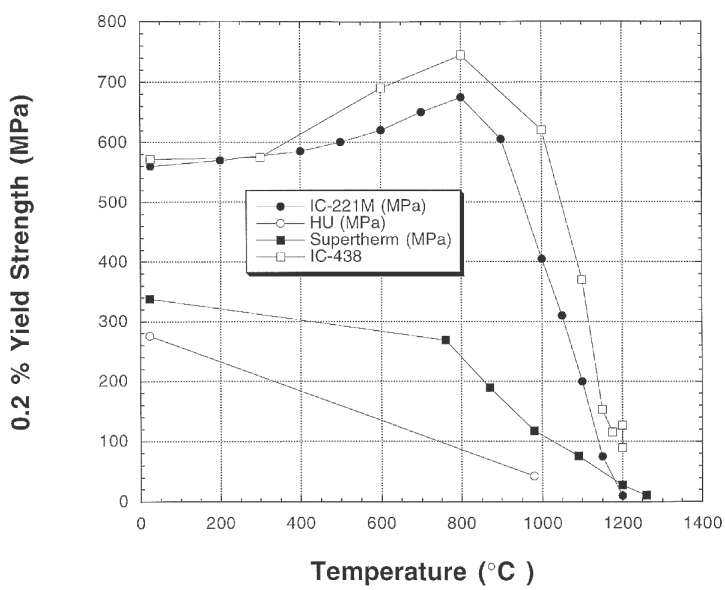

Fig. 3. Comparison of 0.2% yield strength of IC-438 with IC-221M, HU, and SUPERTHERM™.

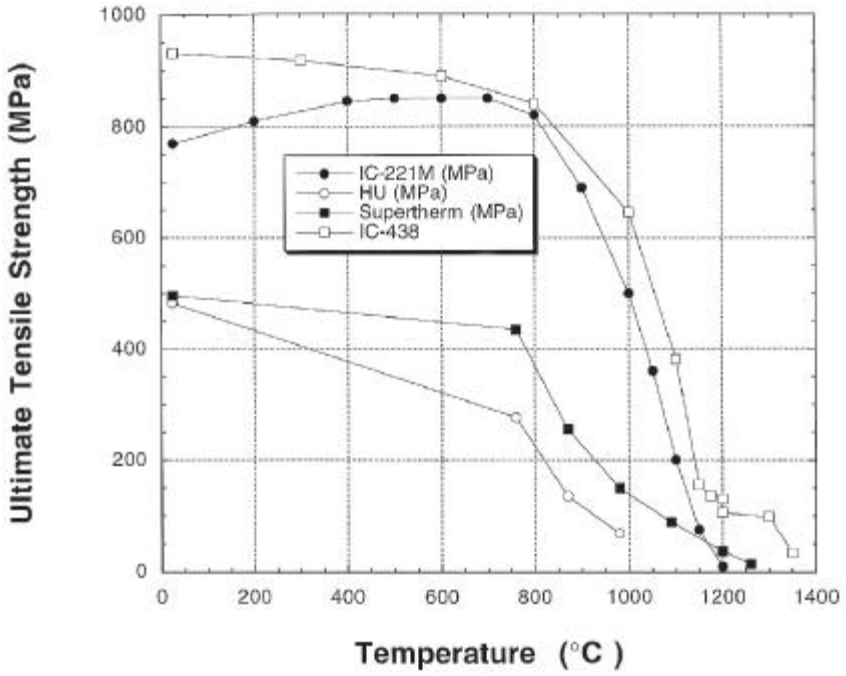

Fig. 4. Comparison of ultimate tensile strength of IC-438 with IC-221M, HU, and SUPERTHERM™.

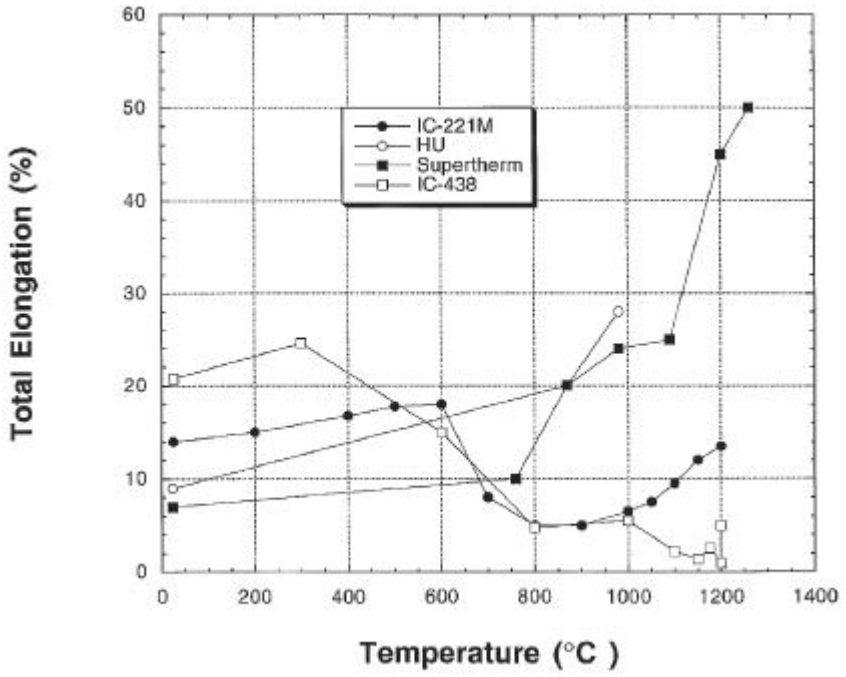

Fig. 5. Comparison of total elongation of IC-438 with IC-221M, HU, and SUPERTHERM™.

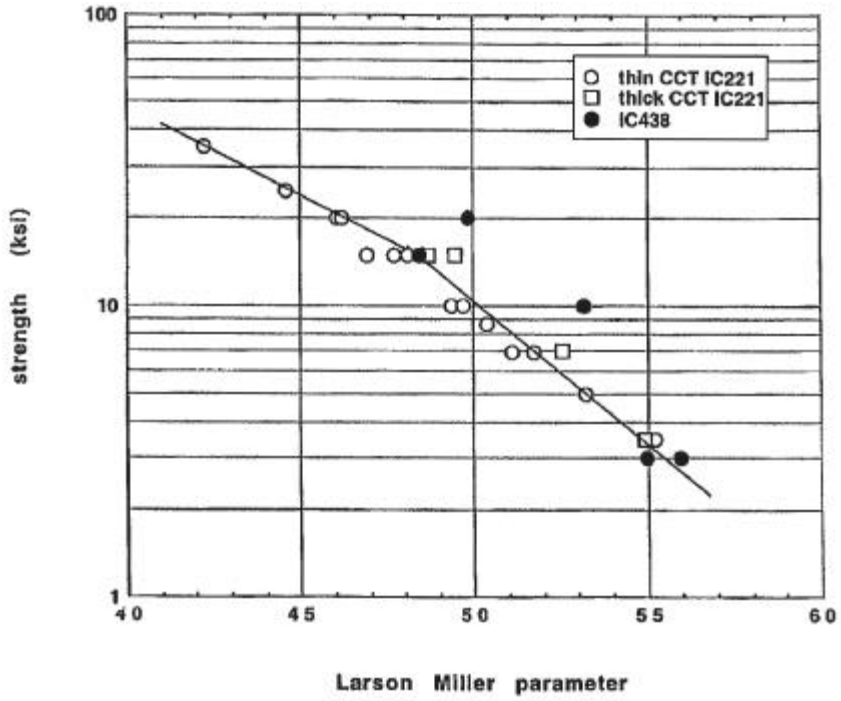

Fig. 6. Comparison of creep-rupture strength of IC-438 with the data for IC-221M.

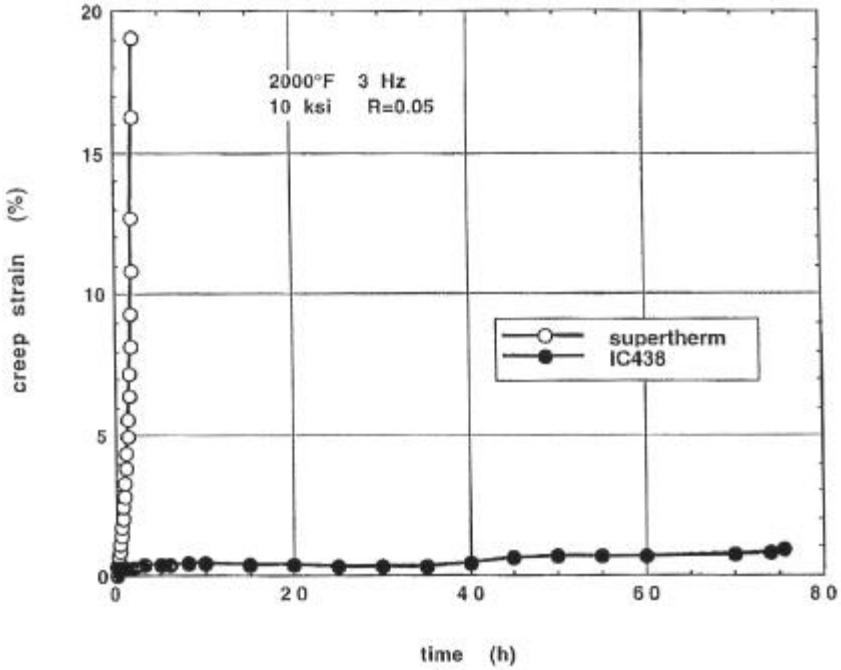

Fig. 7. Comparison of creep curves at 2000 °F and 10 ksi for IC-438 with SUPERTHERM™.

Table 2. Results of Cyclic Fatigue Tests on IC-438

Specimen No.	Temperature (°F)	Cyclic Amplitude (Ksi)	Number of Cycles	Notes
1	1600	+24.3/–28.8	22	Flawed specimen; fractured before cycled to the intended full load of ±50 ksi
2	1900	±10	>1,232,430	Increased the cyclic load to ±15 ksi
2	1900	±15	>265,300	Increased again to ±20 ksi
2	1900	±20	>256,200	Increased again to ±25 ksi
2	1900	±25	1,653	Fractured
			1,755,583	Total number of cycles to failure
3	200	±5	>759,100	Increased the cyclic load to ±7.5 ksi
3	2200	±7.5	>54,146	Fractured
			813,246	Total number of cycles to failure
4	1600	±40	71	Fractured at the transition radius; the specimen appeared to be defective.
5	1600	±40	>273,370	Increased the cyclic stress to ±45 ksi
5	1600	±45	>212,002	Increased the cyclic stress to ±50 ksi.
5	1600	±50	29,628	Fractured
			515,000	Total number of cycles to failure
6	Rt[a]	+39.2/–46	55	Flawed specimen; cycled to check out test system; fractured prematurely.

[a]RT = room temperature.

Physical and mechanical properties data presented in this report are the first set of data available on IC-438. Additional testing will continue on both laboratory and commercially melted heats of IC-438.

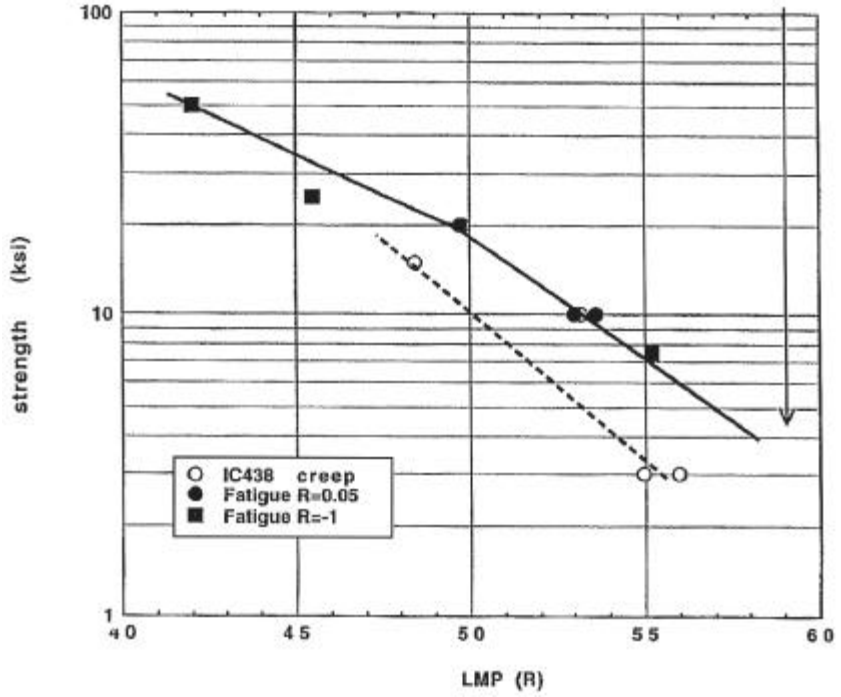

Fig. 8. Comparison of estimated creep life under fatigue vs static creep loading for IC-438.

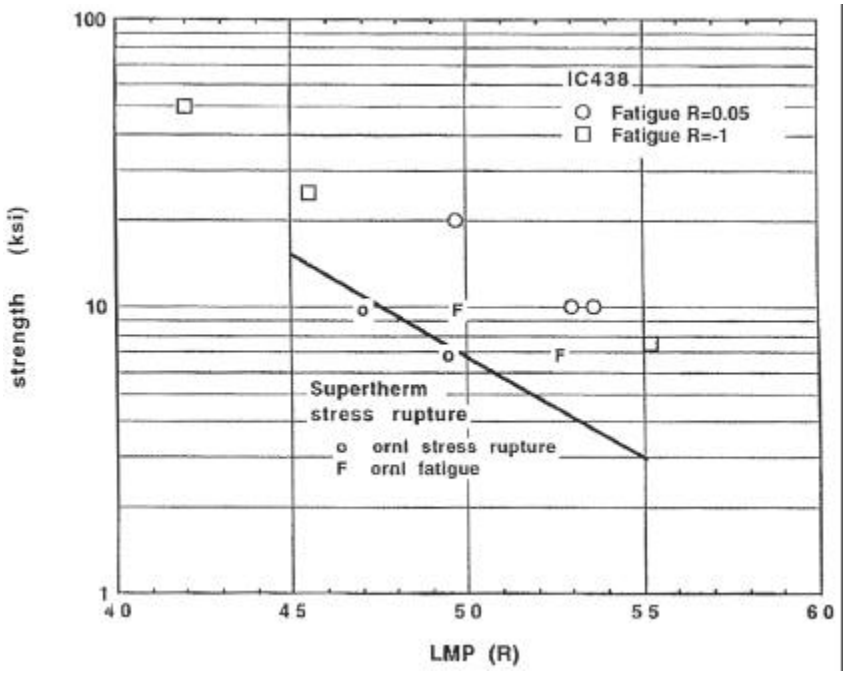

Fig. 9. Comparison of estimated creep life under fatigue conditions for IC-438 with similar data for SUPERTHERM™.

Task 2. Castability of Nickel Aluminides (start 10/97, end 9/98)

Casting trials of nickel aluminide by static and centrifugal methods continued. In one of the trials, the IC-221M was centrifugally cast into a variety of thick wall tubes at AEC. Photographs of various cast tubes are shown in Fig. 10. This trial demonstrated that the alloy can be cast into a 3-in.–OD tube with a 1-in. wall thickness, which is the smallest feed hole that has been tried for feeding the IC-221M into a centrifugal mold. The heavy wall tubes were cast for possible applications in the steel casters.

Static casting trials were carried out at our new licensee, Alcon Industries, Inc. These trials included heat-treating trays and other castings.

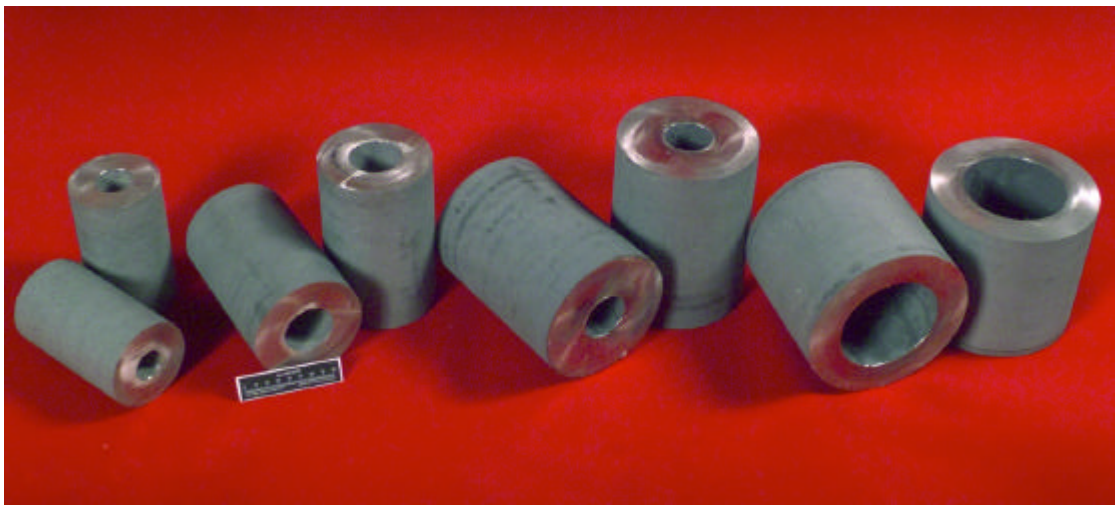

Fig. 10. Photograph of various sizes of heavy-wall centrifugally cast tubes of IC-221M.

Task 3. Welding and Weld Repairability of Ni_3Al Castings (start 10/97, end 9/98)

A. Annealing behavior of IC-221M weldments

One of the weldments (JDM1) made during the process of developing welding procedures for fabricating transfer roll assemblies is being used for testing purposes. Tensile and stress-rupture specimens were made from this weldment, and these results were contained in previous reports. Specimens also are being used for a study of the annealing behavior of the alloys. The annealing treatments were done in air at 900°C. The microstructures in the as-welded ring assembly are given in Fig. 11. The weld metal consists of a very fine dispersion of the γ'-ordered precipitates in a matrix of disordered γ phase. The γ' precipitates are barely visible at this magnification. The dendritic nature of the microstructure is apparent in the top left micrograph. The interdendritic regions contain the Ni-Ni_5Zr eutectic. The large blocky particle visible in the lower left micrograph is probably a ZrN particle, which is known to form in both the weld deposits

and castings of IC-221M. The centrifugally cast IC-221M contains the same basic microstructure, but the sizes and distributions of the various constituents are different. As in the weld deposit, the γ phase is continuous in the cast IC-221M. However, the casting contains relatively large γ′ particles, as shown in the lower right micrograph of Fig. 11. The casting also contains the Ni-Ni_5Zr eutectic, but these particles also are relatively large.

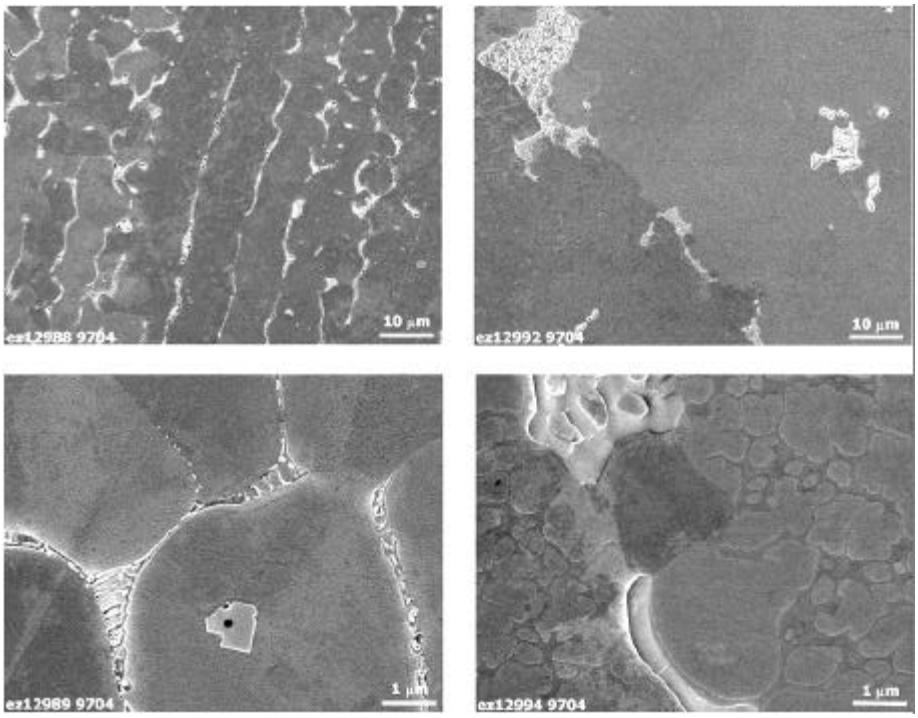

Fig. 11. As-welded microstructures of IC-221LA weld deposit (left top and bottom) and centrifugally cast IC-221M (right top and bottom).

The microstructures of the IC-221LA weld deposit and IC-221M casting after annealing for 2500 h are shown in Fig. 12. Coarsening of the Ni-Ni_5Zr eutectic is clearly evident, but the amount is relatively unchanged from the as-welded condition. After 2500 h, the γ′ precipitates also are coarsened, and they are clearly visible in the lower left micrograph. Changes in the cast microstructure are not as dramatic. Coarsening of the Ni-Ni_5Zr eutectic and the γ′ particles is only slightly evident. Comparison of the lower left micrographs in Figs. 11 and 12 suggests that the amount of γ′ in the casting increased slightly during annealing. The lower micrographs in Fig. 11 indicate the IC-221LA weld deposit contains a smaller amount of γ′ than the casting as would be expected because of its lower aluminum concentration (4.5 compared with 8 wt % for the IC-221M casting).

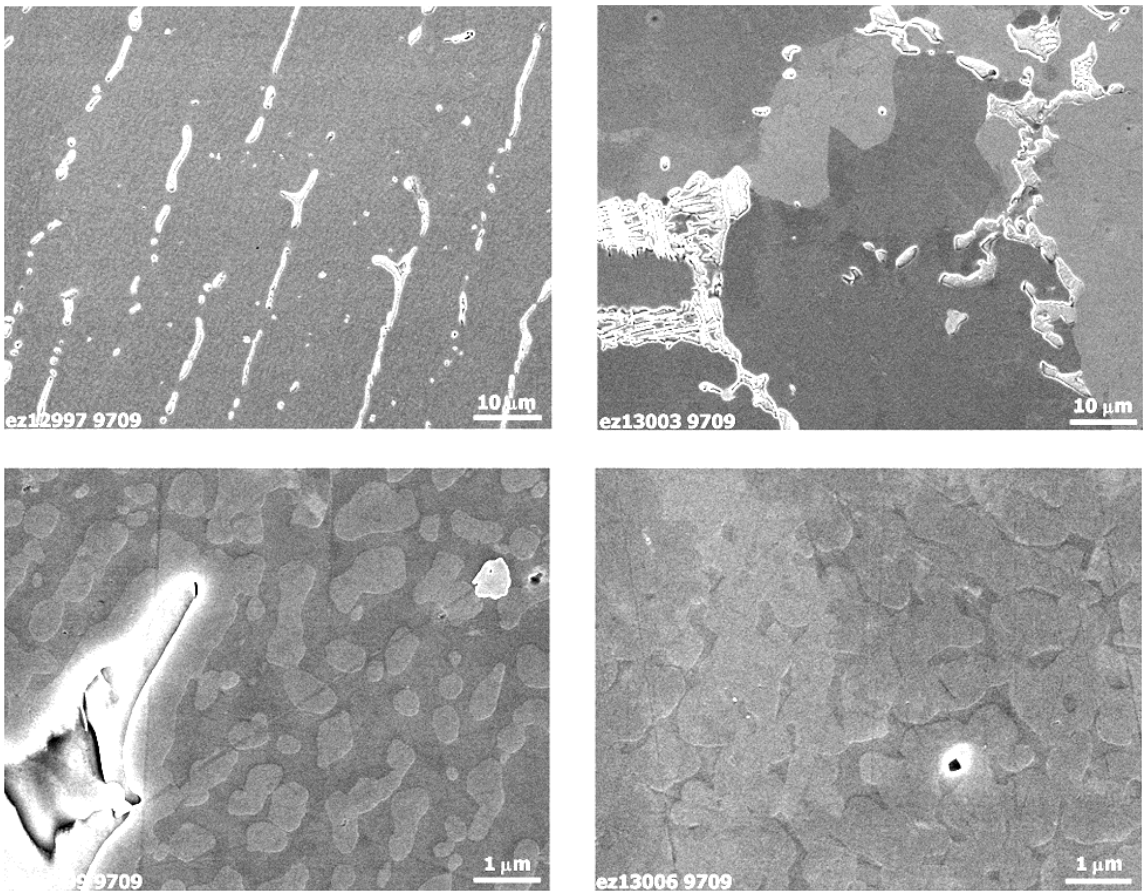

Fig. 12. Microstructures after annealing for 2500 h in air for IC-221LA weld deposit (left top and bottom) and centrifugally cast IC-221M (right top and bottom).

The variations of hardness for the weld deposit and the casting are shown in Fig. 13. The IC-221LA filler metal experienced a slight increase in hardness during annealing for 500 h. After that, its hardness returned to near its level in the as-welded condition and remained there for annealing up to 5000 h. The IC-221M cast base metal initially was much harder than the weld deposit. However, within 250 h, its hardness decreased from near 380 DPH to about 260 DPH, where it remained during further annealing up to 2500 h. This behavior could be the result of stress relieving in the casting. During the period from 2500 to 5000 h, the IC-221M hardness increased slightly. For these annealing conditions, the IC-221LA weld deposit maintained a higher hardness than the IC-221M casting.

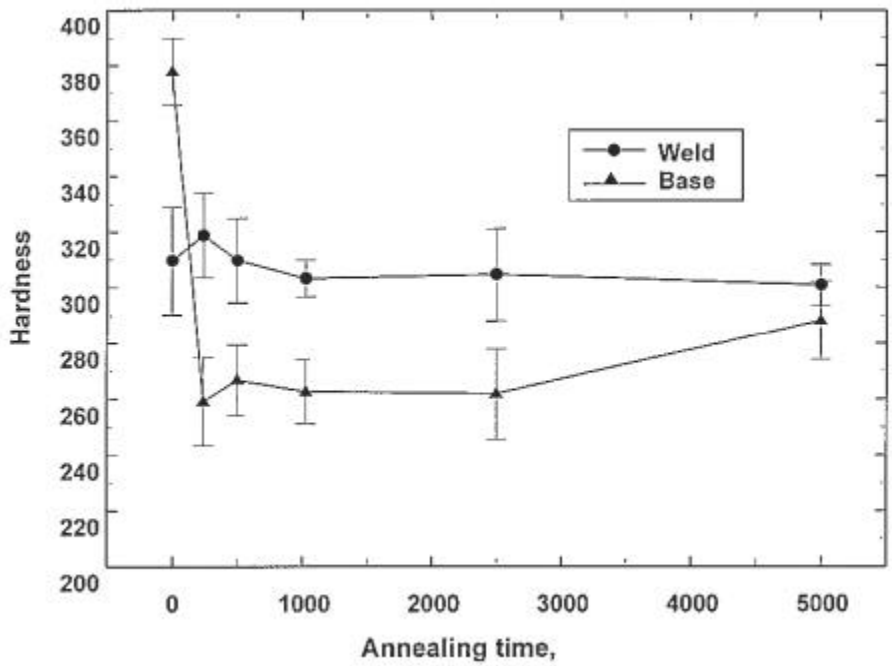

Fig. 13. Variation of hardness with annealing time at 900 ℃ for centrifugally cast IC-221M welded with IC-221LA filler metal.

B. Technical support for fabrication

On-site technical support was provided for licensees at AEC, Sandusky International, and United Defense LP.

Also, two radiant burner tube assemblies were fabricated at ORNL for AEC. Each assembly consisted of two centrifugally cast tubes that were welded to a U-shaped return bend. The tubes had dimensions of 54-11/16 in. long × 6-5/8 in. OD × 6-1/8 in. ID. Also, a tube support was welded to each return bend, and a reinforcing sleeve was welded to one tube of each assembly. Figure 14 shows an IC-221M reinforcing sleeve being welded to the outside diameter of an IC-221M tube. Welding was done by manual gas tungsten arc welding using previously established procedures. All welds were examined by dye-penetrant inspection upon completion. A completed radiant burner tube assembly is shown in Fig. 15. The tube assemblies were installed subsequently in the heat-treating facility of a customer of AEC.

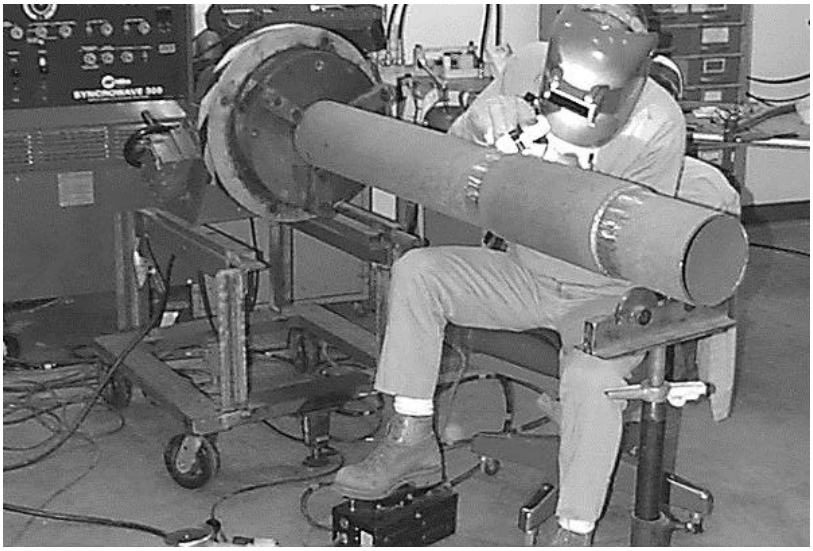

Fig. 14. ORNL technician welding reinforcing sleeve to centrifugally cast IC-221M radiant burner tube.

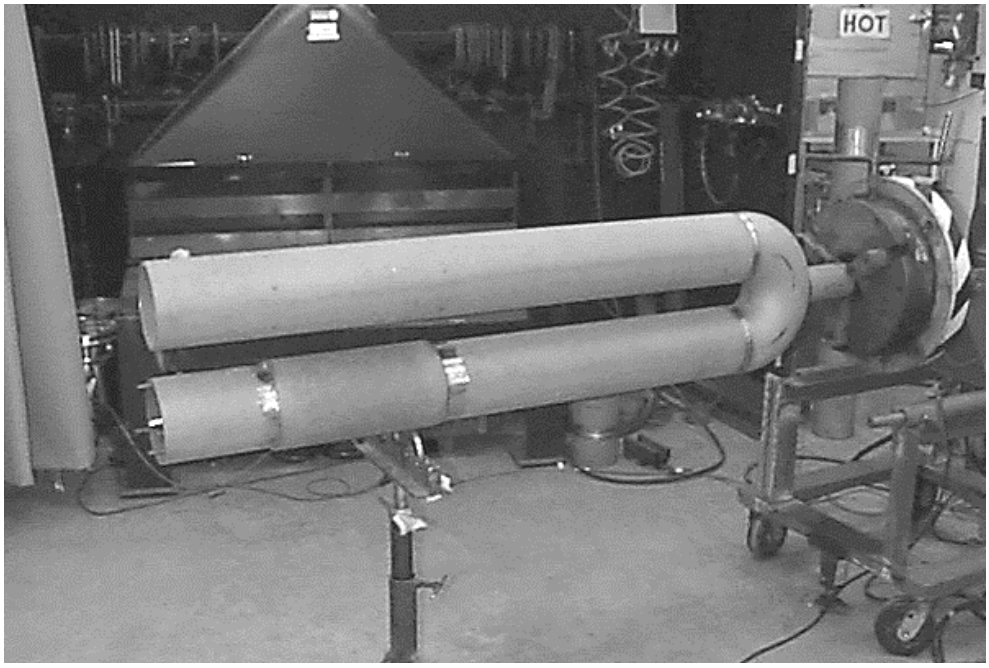

Fig. 15. Completed IC-221M radiant burner tube assembly.

C. Welding of nickel-silicide alloys

Several nickel-silicide alloys were melted and cast to begin evaluating the welding behavior of these alloys. The two alloys used for this initial evaluation were Ni–7.8 Si–0.01 B and Ni–10 Si–0.01 B (wt %). The composition of the Ni–7.8 Si alloy is near the silicon solid solubility limit in the binary system; the Ni–10 Si alloy composition is about midway between the solid solubility limit and the most nickel-rich nickel-silicon eutectic point. Castings of the alloys were made by induction melting under an argon cover and pouring into $6 \times 6 \times 1$ in. graphite permanent molds. Several $6 \times 1 \times 1/8$ in. slices were cut from the castings and further sliced into $6 \times 1/8 \times 1/8$ in. rods for use as welding filler metal. Bars with dimensions of $6 \times 1 \times 1$ in. also were cut from the cast plates for welding trials. Two 0.25-in.–deep slots were machined into opposing faces of these bars.

The welds were made by gas tungsten arc welding with argon shielding gas using the filler metal rods of identical chemical composition. No preheating or unusual cleaning or other preparations were made prior to welding. On both castings, a weld bead was deposited on a flat surface and in the 0.25-in.–deep slot. A cross-sectional view of the weld in the slot in the Ni–7.8 Si casting is shown in Fig. 16. The weld contained a small amount of porosity but otherwise appeared to be free of cracks and other significant defects. This result indicates that the Ni–7.8 Si composition has relatively good weldability. The welds of the Ni–10 Si casting are shown in Fig. 17. The weld on the flat surface was defect free, but the weld made in the machined slot contained a prominent weld bead centerline crack. The weld made in the slot would be subjected to conditions of higher mechanical restraint than the one made on the flat surface. These results indicate that increasing the silicon content from 7.8 to 10 wt % in nickel causes an increase in the susceptibility to weld-induced cracking. Comparison of the two weld beads in Fig. 17 also indicates that the cracking depends on mechanical restraint conditions.

Task 4. Workability of Cast or Powder Metallurgy Product to Sheet, Bar, and Wire (start 10/97, end 9/98)

Workability of nickel aluminides using conventional processing techniques such as forging, rolling, and extrusion are essential in developing a widespread use of these materials. In order to be successful in processing aluminides, we need a comprehensive knowledge of flow-stress data at a wide range of temperatures and strain rates approaching those used in commercial techniques. A test program to develop such data was set up with Prof. Y.V.R.K. Prasad at the Indian Institute of Science (IIS) (Bangalore, Karnataka State, India). The program is best on the unique capability of equipment and expertise of IIS in developing such data and its analysis into deformation maps. The test program exchanges no funds and is based on ORNL supplying the specimens and some metallurgical characterization of tested specimens and on IIS carrying out the data development. The program was put in place in September 1997.

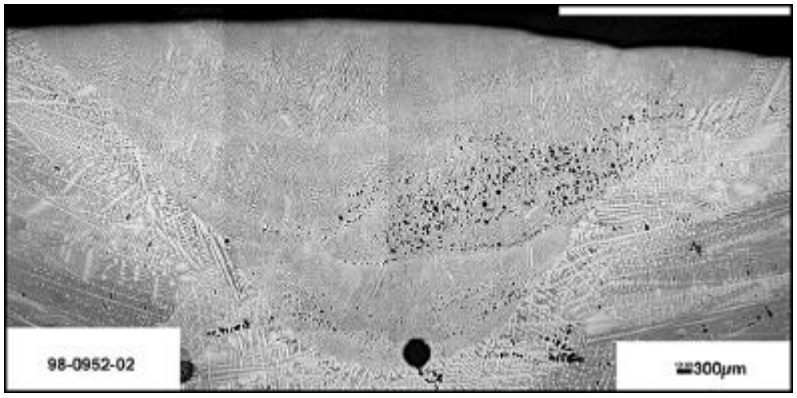

Fig. 16. Composite optical micrograph showing a cross-sectional view of a gas tungsten arc weld in a Ni–7.8 Si casting made with filler metal of the identical chemical composition.

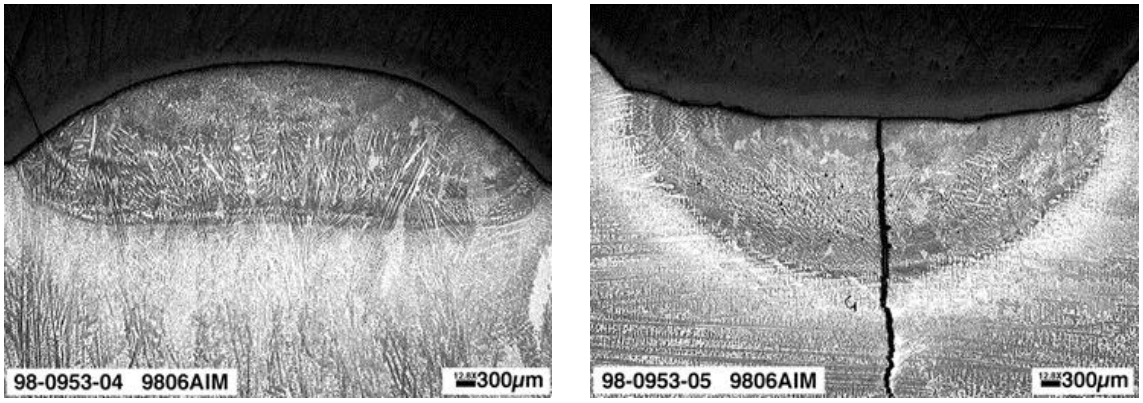

(a) **(b)**

Fig. 17. Optical micrographs showing cross-sectional views of gas tungsten arc welds in a Ni–10 Si casting: (a) weld bead deposited on flat surface, and (b) weld bead in slot.

Specimens for testing were supplied in November 1997. Testing of all the specimens has been completed at a broad range of combinations of test temperatures and strain rates. Preliminary deformation maps for nickel aluminide also have been plotted. Metallographic analysis of the data are needed now to characterize the regions of the deformation map. Such characterization will help to develop the predictable window for processing of nickel aluminides. If successful, it will open up the opportunity for developing the wrought nickel-aluminide product.

Task 5. Technology Transfer Activities (start 10/97, end 9/98)

Strong technology-transfer activities continued with the current and potential users and producers. Specific examples of interactions are listed below.

A. Bethlehem Steel/Sandusky interactions

ORNL continued to play a very active role in the successful manufacture and installation of rolls in the austenitizing furnace at Bethlehem Steel. Specific contributions included visits to (1) Bethlehem Steel Corporation-Burns Harbor Plant for examination of rolls in service and (2) Sandusky International to assist in welding issues and welder training, conducting stress analysis for various combinations of roll and trunnion combinations, and examining weld vs pinned-roll design. A lot of additional mechanical property data were developed. This has been the most demanding interaction with significant benefits to the steel industry, once the nickel aluminide technology is fully implemented. Our interaction has helped to extend the use of nickel-aluminide rolls from 2 to 20 at Bethlehem Steel Corporation.

B. United Defense LP

In this interaction, ORNL assisted with the computer modeling of the castings, weld repair of the castings, and training of the welders. A significant amount of Ni-Cr-Zr weld wire was supplied for repair of castings.

C. Alloy Engineering & Casting Company

We assisted AEC with (1) technical data, (2) welding process details, (3) welding training, (4) welding assemblies at ORNL, and (5) answering questions from AEC's customers.

D. Chemical Industry interactions

Interactions continued with E. I. DuPont and Dow. Many test coupons were supplied for testing at Dow.

E. Coronado Steel

Coronado Steel Company [(Coronado) Youngstown, Ohio] is a small foundry that can produce small production orders on a very rapid basis. ORNL personnel have trained several of Coronado's personnel on the Exo-Melt™ process and property data on nickel aluminides. They have demonstrated skills in the production of small pilot heats of specialty shapes and currently are looking at a potential license. They are developing applications in the area of cast heating elements, dies for intricate extrusion processed shapes, and permanent molds for copper alloy casting and burners for gas-fired furnaces. Coronado is a very progressive company, and a strong interaction with them has a strong potential for many new applications of nickel aluminides.

F. Alcon Industries, Inc.

Alcon Industries, Inc., is our newest licensee for casting nickel aluminides. We have provided them extensive help in the areas of (1) general training of employees on nickel aluminides and the Exo-Melt™ process, (2) standards for developing calibration curves for Alcon Industries' spectrometer, and (3) welding wire and welding procedure details.

G. Other interactions

Many other companies were sent the data packages and test coupons of nickel aluminide for potential new applications.

H. FeAl

Several activities were initiated in the transfer of FeAl technology to industry, including the following:

1. A visit to Bethlehem Steel-Homer Labs was made to discuss the possible use of FeAl alloy for the transfer of table rolls in the hot strip rolling line. A detailed written response to a long list of questions was prepared. The details of the actions needed for this application still are being finalized.
2. Melting of two 500-lb heats and their casting into heavy wall tubes was completed at AEC.
3. A visit was made by Duraloy Technologies, Inc., to ORNL for their involvement in casting of FeAl alloys.

PUBLICATIONS

P. J. Maziasz, G. M. Goodwin, X. L. Wang, R. W. Swindeman, D. J. Alexander, and V. K. Sikka, "Development of Weldable, Corrosion-Resistant Iron-Aluminide (FeAl) Alloys," pp. 97–106 in *Advanced Industrial Materials (AIM) Program Annual Progress Report FY 1997*, ORNL/TM-13494, Oak Ridge National Laboratory, Oak Ridge, Tennessee, May 1998.

S. C. Deevi, V. K. Sikka, B. J. Inkson, and R. W. Cahn, "Effect of Boron on the Vacancy Hardening of FeAl," *Scr. Mater.* **8,** 899–904 (1997).

V. K. Sikka, G. Aramayo, M. L. Santella, R. W. Swindeman, and S. Viswanathan, "Ni_3Al and FeAl Technology Transfer," pp. 143–69 in *Advanced Industrial Materials (AIM) Program Annual Program Report FY 1997*, ORNL/TM-13594, Oak Ridge National Laboratory, Oak Ridge, Tennessee, May 1998.

PRESENTATIONS

P. J. Maziasz, G. M. Goodwin, X. L. Wang, R. W. Swindeman, D. J. Alexander, and V. K. Sikka, "Development of Weldable, Corrosion-Resistant Iron-Aluminide (FeAl) Alloys," Advanced Industrial Materials (AIM) Program Annual Meeting, Oak Ridge, Tennessee, May 1998.

V. K. Sikka, J. Liebetrau, B. Mackey, and D. Wilkening, "Fabric Cutting Appliction of FeAl-Based Alloys," TMS Spring Meeting, International Symposium on Iron Aluminides Alloy Design, Processing, Properties, and Applications, San Antonio, Texas, February 15–19, 1998.

J. E. Orth and V. K. Sikka, "How to Double or Triple Your Alloy Life," Heat Treat Only FNA'98, Las Vegas, Nevada, March 27, 1998.

S. C. Deevi, M. R. Hajaligol, V. K. Sikka, and C. Scorey, "Manufacturing of Iron Aluminide Sheets by Thermomechanical Processing," 1998 TMS Fall Meeting on Processing of High Temperature Alloys, Rosemont, Illinois, November 1998.

V. K. Sikka and M. L. Santella, "Manufacturing Processes for Nickel Aluminides," International Symposium on Advanced Manufacturing Technologies, Rosemont, Illinois, October 12–15, 1998.

M. L. Santella, R. W. Swindeman, and R. J. Barkman, "Mechanical Properties of a Nickel Aluminide Weldment," 5th International Conference on Trends in Welding Research, Pine Mountain, Georgia, June 3, 1998.

V. K. Sikka, J. Liebetrau, B. Mackey, and D. Wilkening, "Melting and Casting of FeAl-Based Cast Alloys," TMS Spring Meeting, International Symposium on Iron Aluminides Alloy Design, Processing, Properties, and Applications, San Antonio, Texas, February 15–19, 1998.

V. K. Sikka, "Nickel Aluminide Rolls," Energy Technology Showcase, Bethelhem's Burns Harbor Plant, April 30, 1998.

V. K. Sikka, G. Aramayo, M. L. Santella, R. W. Swindeman, and S. Viswanathan, "Ni_3Al and FeAl Technology Transfer," Advanced Industrial Materials (AIM) Program Annual Meeting, Oak Ridge, Tennessee, May 1998.

10. V. K. Sikka and M. L. Santella, "Ni_3Al-Based Alloys in Steel and Heat Treating Industry," Materials Research Society 1998 Fall Meeting, Boston, Massachusetts, November 30–December 4, 1998.

S. C. Deevi, K. Sadananda, and V. K. Sikka, "Processing and Creep Behavior of Functionally Graded $MoSi_2Si_3N_4$ Composites," 1998 International Conference on Powder Metallurgy and Particulate Materials, Las Vegas, Nevada, May 31–June 4, 1998.

S C. Deevi, M. R. Hajaligol, V. K. Sikka, J. McKernan, and C. Scorey, "Processing and Properties of FeAl Sheets Obtained by Roll Compaction and Sintering of Water Atomized FeAl Powder," Materials Research Society 1998 Fall Meeting, Boston, Massachusetts, November 30–December 4, 1998.

V. K. Sikka, "Tape Casting Development—Thermomechanical Processing Review," Ametek Specialty Metal Products Division, Wallingford, Connecticut, November 6, 1997.

M. L. Santella and A. B. Patterson, "Wetting Behavior of Iron Aluminide," TMS Annual Meeting, San Antonio, Texas, February 18, 1998.

HONORS AND AWARDS

Ten research and support staff associated with nickel aluminide were awarded the International Hall of Fame Technology Transfer Support Award. This award consists of

sharing part of the royalty money with staff other than inventors who made significant contributions.

PATENTS/DISCLOSURES

M. L. Santella and V. K. Sikka, "Filler Metal Alloy for Welding Cast Nickel Aluminide Alloys," U.S. Patent 5,725,693, March 10, 1998.

LICENSES

The new licenses signed include:

Alcon Industries, Inc.—for sand castings.

Stoody Company—for welding wire.

Polymet Corporation—for welding wire.

Materials for the Pulp and Paper Industry

Section 1. Development of Materials for Black Liquor Recovery Boilers

J. R. Keiser, C. M. Hoffmann, C. R. Hubbard, P. J. Maziasz,
G. Sarma, R. W. Swindeman, and X. L. Wang
Metals and Ceramics Division
Oak Ridge National Laboratory
P.O. Box 2008, Oak Ridge, Tennessee 37831

D. L. Singbeil, P. Eng, L. Frederick, and R. Prescott
Pulp and Paper Research Institute of Canada
3800 Wesbrook Mall, Vancouver, BC, Canada V6S 2L9

P. M. Singh and J. Mahmood
Institute of Paper Science and Technology
500 10th St., NW, Atlanta, Georgia 30318

INTRODUCTION

Black liquor recovery boilers are critical components of kraft pulp and paper mills because they are an essential part of the system used to recover the pulping chemicals required in the kraft pulping process. In addition, the steam produced by these boilers generates a significant portion of the electrical power used in the mill. Recovery boilers require the largest capital investment of any individual component of a paper mill, and these boilers are a major source of material problems in a mill. The walls and floors of these boilers are constructed of tube panels that circulate high-pressure water. Molten salts (smelt) are present on the floor of recovery boilers, and leakage of water into the boiler can result in a violent explosion when the leaked water instantly vaporizes upon contacting the smelt. Tube leaks, sometimes leading to such explosions, have occurred with some regularity in the paper industry.

Because corrosion of the conventionally used carbon steel tubing was found to be excessive in the lower section of recovery boilers, use of stainless steel/carbon steel coextruded tubing was adopted for boiler walls to lessen corrosion and reduce the likelihood of smelt/water explosions. Eventually, this coextruded or composite (as it is known in the industry) tubing was selected for use as a portion or all of the floor of recovery boilers, particularly those operating at pressures greater than 6.2 MPa (900 psi), because of the corrosion problems encountered in carbon steel floor tubes.

However, cracking into, or through, the stainless steel outer layer of this composite tubing was subsequently encountered. Almost without exception in sloped-floor boilers, cracks have been seen first in the wall tubes that form the smelt spout openings through which molten salts are removed. Subsequently, cracks have been found in floor tube membranes and eventually in floor tubes themselves in both sloped-floor and flat-floor types of boilers.

Since neither the cause of the cracking nor an effective solution has been identified, this program was established to develop a thorough understanding of the degradation that occurs in the composite tubing used for walls and floors. This is being accomplished through a program that includes collection and review of technical reports; examination of unexposed and cracked tubes from boiler floors; collection and analysis of smelt samples; collection and tabulation of temperature data; measurement of residual stresses in as-produced, as-formed, and exposed composite tubing; computer modeling to predict residual stresses under operating conditions; and operation of laboratory tests to study corrosion, stress-corrosion cracking, and thermal fatigue. From this work it is anticipated that alternate materials or operating procedures will be identified, and these will be tested in recovery boilers. Significant progress has been made to determine the stresses that are present in composite floor tubes and to characterize the nature of cracking found in floor tubes. Recently, emphasis has been put on characterizing the tube environment and identifying stress-corrosion cracking mechanisms that could cause the type of cracking seen.

The staff members working on this project continue to produce reports that are being submitted to the open literature as well as for publication in conference proceedings. Of special note are four papers presented at the 9th International Symposium on Corrosion in the Pulp and Paper Industry and one paper presented at the International Chemical Recovery Conference. One of the papers presented at the 9th International Symposium received the best paper award for that meeting. Project results also are being reviewed at tri-annual review meetings as well as at meetings sponsored by AF&PA and BLRBAC.

TECHNICAL PROGRESS: FY 1998

1. Examination of Exposed Recovery Boiler Composite Tubes

During the last few years, a significant number of cracked composite tubes from boiler manufacturers, inspection companies, and paper mills have been carefully examined in order to define the characteristics of the cracking. In some cases, large panels have been provided when all or significant portions of a floor have been replaced, while others have come from floors in which single tubes, or no more than a pair of adjacent tubes, have been removed. A large number of these floor tubes have been examined and characterized. Also of interest are samples of cracked membranes and spout-opening tubes because these generally show cracking before the floor tubes.

Coextruded 304L/CS spout-opening tubes from a mill in the south central United States were examined. A dye-penetrant examination showed extensive cracking on the inner surface of the spout opening. Examination of samples taken from the cracked areas of the tubing shows that some of the cracking does not reach the SS/CS interface, while cracking in other areas appears to proceed a very short distance across the interface (see Fig. 1). No cracks were found that penetrate a significant distance into the carbon steel, but several areas were found in which penetration into the carbon steel had more the appearance of an advancing crack than a corrosion pit.

The other spout-opening tubes examined were from another boiler in the south central United States The spout openings had been replaced in June 1994, and four openings

constructed of coextruded modified Alloy 825/CS and one opening constructed of Alloy 625/CS were used as the replacements. It is reported that minor indications of surface cracking were removed by buffing the surface of the modified Alloy 825/CS tubes during the annual outages. In January 1998, cracking was found in the Alloy 625/CS spout opening, so the opening was removed and half was sent to ORNL for examination. The first tube forming the opening was, as noted, coextruded 625/CS. The second tube was coextruded 304L/CS, and the sample sent to ORNL included parts of this second tube.

The dye-penetrant examination of this spout opening showed "spider-web–type cracking in the 304L stainless, while circumferential cracking was seen on the 625/CS tube. Microscopic examination of a cross section of the cracking in the 304L stainless showed transgranular cracking that was typical of that seen in most other 304L/CS tubes. Microscopic examination of the circumferential cracks in the 625/CS section showed that cracking was intergranular, unlike that reported in the 304L stainless. An example of this cracking is shown in the low- and high-magnification micrographs in Fig. 2.

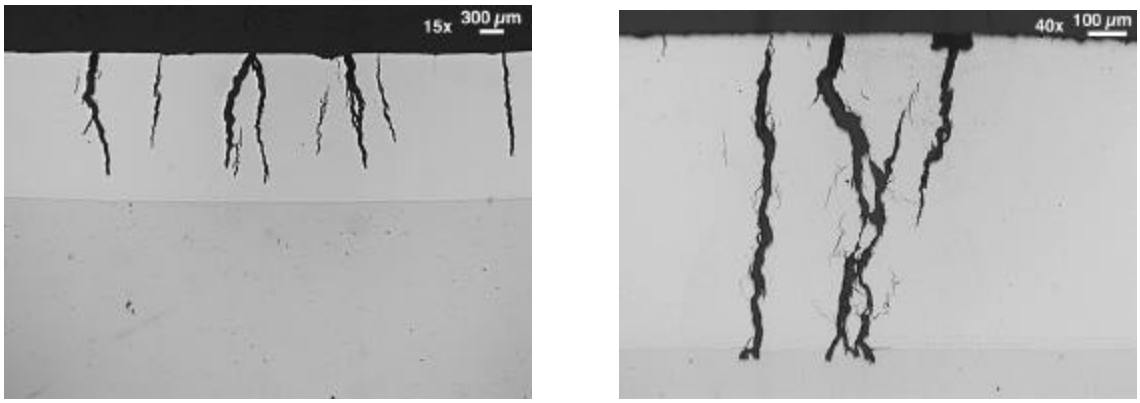

Fig. 1. Micrographs of samples taken from a 304L/CS smelt spout-opening tube showing (l) cracking that does not reach the SS/CS interface and (r) cracking that may be progressing into the carbon steel.

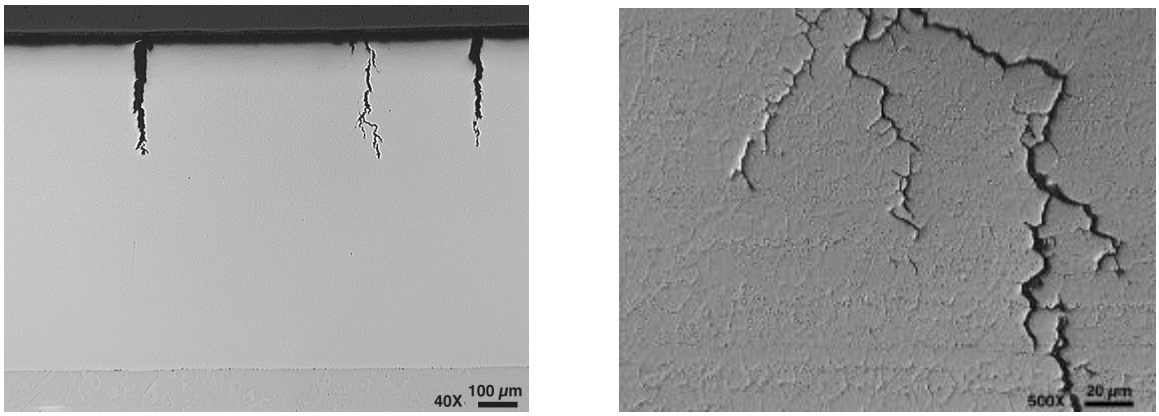

Fig. 2. (l) Low- and (r) high-magnification micrographs of intergranular cracks in the 625 layer of coextruded Alloy 625/CS that formed a smelt spout opening.

2. Characterization of Floor Tube Environment

It is becoming apparent that the thermal and chemical environments of recovery boiler floor tubes are not static. In order to determine the extent of the variations, an array of thermocouples has been installed in the floor of Weyerhaeuser's Prince Albert #1 recovery boiler. Figure 3 shows the shield on a floor tube that protects the thermocouple that is in contact with the crown of the tube. These thermocouples are providing information about the temperature variations that occur during operation as well as information about the cooling and heating rates during water washes and shutdowns. Wash-water samples have been collected to determine the compositional variations in the water that contacts the floor tubes during water washes.

Fig. 3. Floor tube in the Prince Albert recovery boiler shows the shield protecting the thermocouple that is in contact with the crown of the tube.

Data are collected from the array of 25 thermocouples about every 10 s, and these data are plotted as a function of time to identify the time periods when significant activity is occurring. Results obtained from the thermocouples indicate that brief, sudden temperature fluctuations occur, and that these fluctuations occur less often along the spout wall and more frequently with increasing distance from the wall. An example of one of these fluctuations is shown in Fig. 4. This event occurred shortly after 1:30 p.m. on September 9, 1998. At the 4914-s mark, floor temperatures ranged from 260 to 330°C. Ten seconds later, the temperature at thermocouple 4 on tube 50 increased over 100°C. Over the next 60 s, the temperatures drop to near their initial level, and, during the subsequent 3 min, they drop another 20°C.

3. Measurement of Residual Stresses

One of the purposes of residual-stress studies has been to provide information to help identify the cracking mechanism operative in composite tubes subjected to kraft recovery boiler service conditions. Both stress-corrosion cracking and thermal fatigue have been

suggested as likely explanations for the observed cracking. In either case, the residual-stress state in the clad layer plays an important role, in that tensile residual stresses at the surface could facilitate crack initiation, and tensile residual stresses below the surface layers assist the propagation of cracks. If, however, the surface is under a compressive residual stress, neither cracking mechanism would be expected to be active. During this period, the residual stresses have been measured in as-fabricated Sanicro 63 (Alloy 625)/ carbon steel tubes, initial measurements were conducted using a furnace that enables measurements under simulated operating conditions, and X-ray measurements were made in support of fatigue studies of floor tube panels and smelt spout openings.

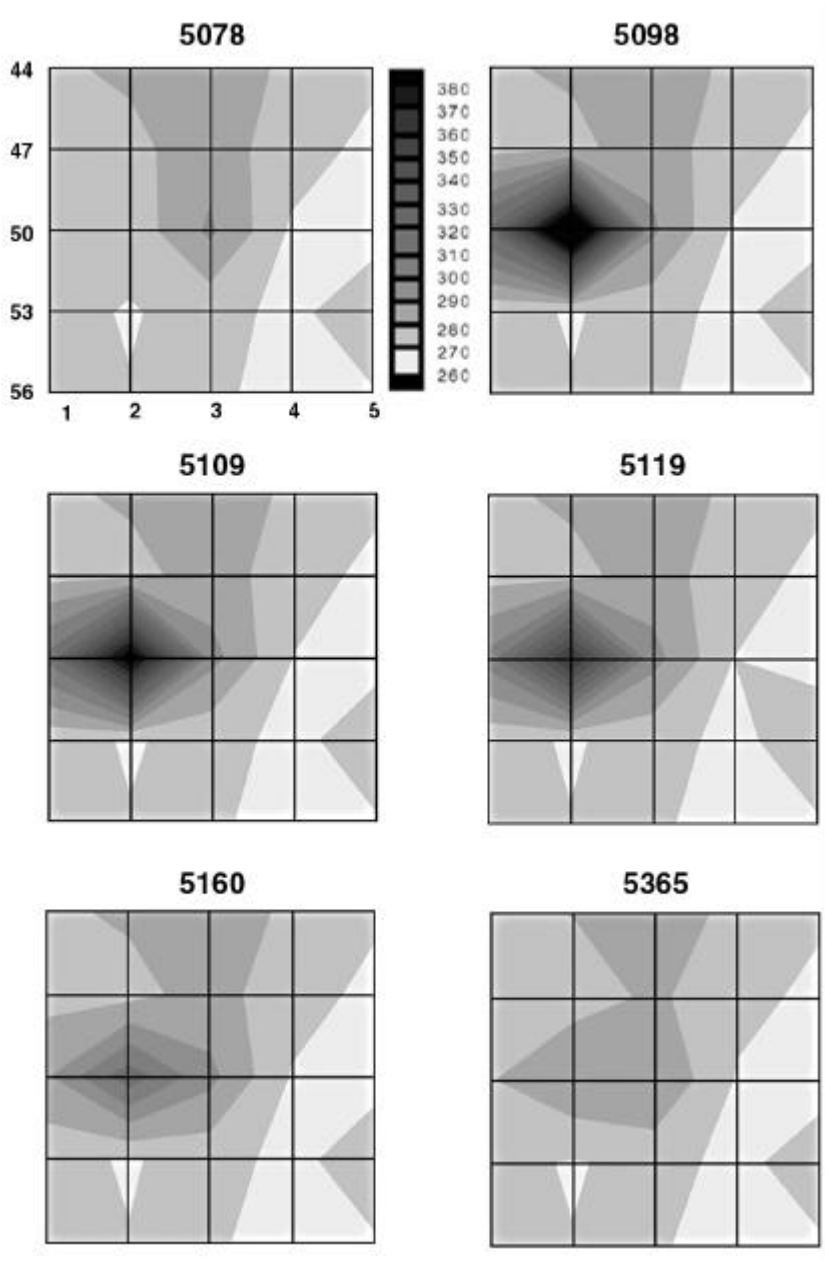

Fig. 4. Temperature profiles of a portion of the Prince Albert recovery boiler floor from early afternoon on September 9, 1998. As indicated in the upper left display, the horizontal lines represent tubes, with the tube number shown on the left axis, while the vertical lines indicate thermocouple numbers corresponding to one less than the distance (in feet) from the spout wall. The elapsed time (in seconds) is given by the number above each profile.

3.1 Residual stresses in Sanicro 63/carbon steel tubes

One of the materials being considered for replacement of the 304L clad on composite tubing is nickel-based alloy 625. Indeed, this is a material whose properties fall into the boundaries defined by a parametric finite-element study. Finite-element modeling has shown that for panels made of 625 composite tubing, the mechanical behavior during a normal boiler's heating and cooling cycle remains elastic. This is because the thermal expansion alloy of 625 almost matches that of the carbon steel, and the alloy has a rather high yield strength. Thus for panels made of 625 composite tubing, knowledge of the initial manufacturing stresses becomes critically important as they dictate the stress state in the panel under operating conditions. Neutron and X-ray diffraction was used to determine residual stresses in an as-manufactured Sandvik 63 composite tube (2.5-in. OD). The experimental data are shown in Fig. 5. As can be seen, the residual stresses are fairly small throughout the Sandvik 63 tube, within ±100 MPa. This result is consistent with the matching thermal expansion between the carbon steel core and the Alloy 625 clad alloy. It also confirms that the large residual stresses previously observed in 304L and Sanicro 38 (Alloy 825) tubes result from a thermal-expansion mismatch. Note that each of the data points in Fig. 5 is actually an average over measurements made at four angular locations, and the estimated standard deviation of the four measurements was assigned as the error bar (for clarity, only error bars for the hoop stress component were plotted). Thus the relatively large error bar observed for most data points is really an indication of the spread of residual stresses around the circumference, rather than the precision of individual measurements. The variation of residual stresses around the circumference has been observed previously in other composite tubing with 304L- and Alloy 825–clad layers and was attributed to the straightening process following the annealing. The X-ray data obtained at the surface of the tube are in agreement with through-thickness neutron diffraction measurements.

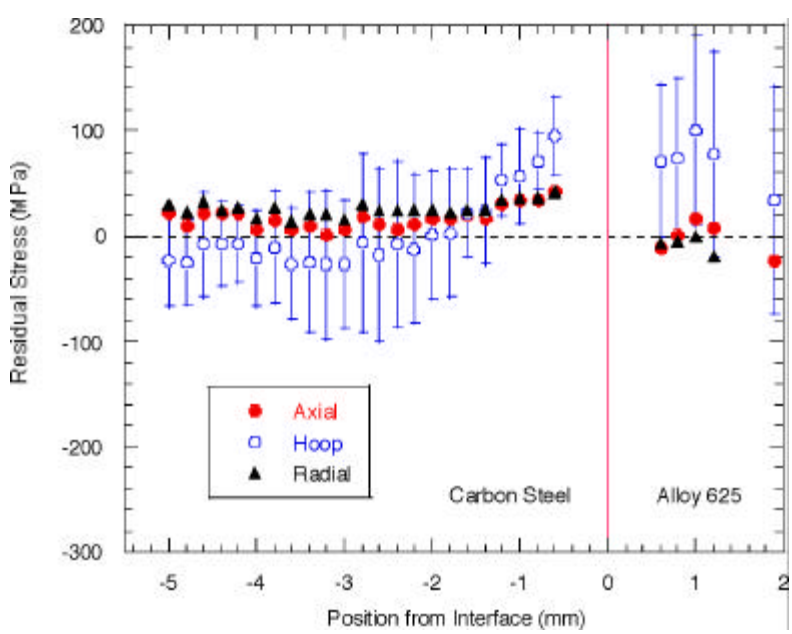

Fig. 5. Residual stresses in 2.5-in. OD Sandvik 63 composite tubing. Data on the surface of the Alloy 625–clad layer was obtained with X-ray diffraction, while the rest of the data were obtained with neutron diffraction.

3.2 Residual stresses measured under simulated operating conditions

To study the effect of thermal cycling, a furnace was designed and tested for in situ heating and cooling experiments on single tubes and tube panels. The heating element is a steel coil that fits within the inner diameter of the Alloy 625/carbon steel composite tube. Two thermocouples were mounted on the inner and the outer surface of the tube to monitor the actual temperatures and assess the temperature gradient through the thickness. The assembly was encapsulated in an alumina tube for insulation. Initial tests were carried out with controlled heating up to 350°C. Figure 6 shows the thermal strain determined at the middle thickness of the carbon steel as a function of temperature readings from the two thermocouples. With the inner surface thermocouple, a linear thermal-expansion coefficient of 12.3×10^{-6} K^{-1} was obtained. With the outer thermocouple, on the other hand, the derived linear thermal-expansion coefficient was 18.9×10^{-6} K^{-1}. A comparison to the published coefficient of thermal expansion for carbon steel and Alloy 625 suggests that either there is a through-thickness temperature gradient or the temperature reading from the outer thermocouple is in error.

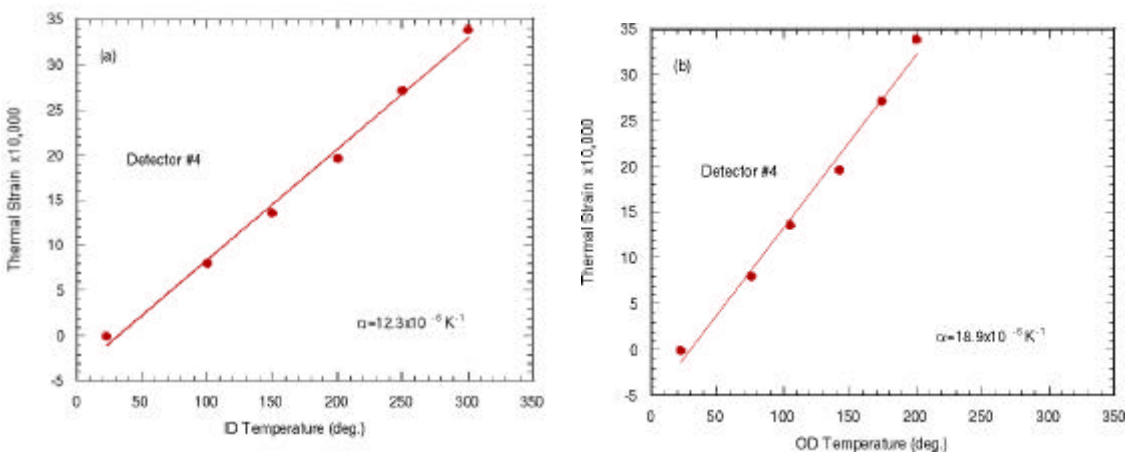

(a) **(b)**

Fig. 6. Thermal strain is plotted against temperature readings from thermocouples mounted at (a) inner and (b) outer surfaces, respectively.

In subsequent experiments, a through-thickness scan over a 4-mm range in the carbon steel revealed a change of no more than 2×10^{-4} in strain. This shows that the temperature gradient in the carbon steel must be less than 15°C, indicating that indeed the outer thermocouple did not give the correct temperature. To further improve the accuracy of measured temperatures, new thermocouples with better insulation have been ordered and will be spot welded to various positions on the inner and outer surfaces to ensure that the measured temperatures are representative of the tube. To ensure uniform heating, the coil heating element will be replaced by a quartz lamp. In addition, heating tapes will be wrapped around the outer surface to minimize any temperature gradient there might be. After successful testing on single tubes, the same idea can be extended to composite tube panels, where each tube comprising the panel is heated to different temperatures using individual heating elements.

3.3 Residual-stress measurements in previously exposed components

In parallel with in situ neutron diffraction measurements, X-ray residual-stress measurements were carried out on a composite tube panel used in thermal-fatigue tests. This panel, which was fabricated from Sumitomo 304L composite tubing by ABB C-E, had the center tube cycled 1000 times between 250 and 540°C. X-ray residual-stress data collected at the crown are shown in Fig. 7. The temperature profile across the panel shows that tubes experiencing a greater temperature difference (hot spot) have smaller compressive stresses. Previous X-ray measurements showed that the surface residual stresses in an as-manufactured ABB composite tube panel are compressive, of the order of –400 MPa. Thus the experimental data in Fig. 7 show that thermal cycling results in a tensile stress in the clad layer. This result, which can be qualitatively understood by considering the initial work hardening in the clad layer and the elastic-plastic behavior during thermal cycling, is in agreement with finite-element calculations.

In support of failure analysis of a spout opening, X-ray experiments were carried out to determine the surface residual stresses in a section of a smelt spout opening removed from a mill in southwestern Alabama. Figure 8 shows the analyzed specimen with markings indicating the locations of sites where X-ray measurements were made and the experimental results. As can be seen, the residual stresses are tensile on the fire side and compressive on the cold side. This result is consistent with TEM observations that showed significant thermal-cycling effects on the fire side of the specimen.

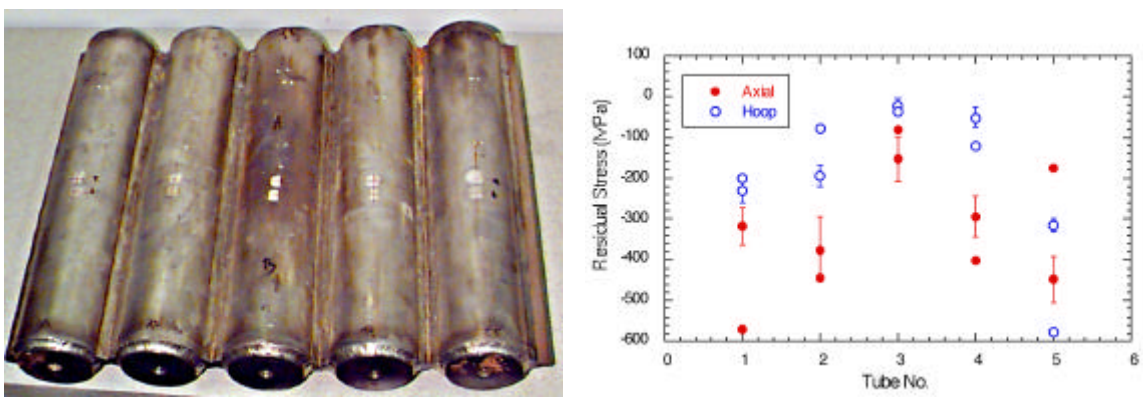

Fig. 7. (l) Tube panel used in thermal-cycling residual-stress studies and (r) results of surface residual-stress measurements in this composite tube panel.

4. Modeling of Residual Stresses

The modeling efforts in support of this project are focused mainly on thermal and mechanical analyses to determine stresses in the tubes under various service conditions. Prior work on 304L stainless steel/SA210 carbon steel composite tubes has shown that due to the large mismatch in the coefficients of thermal expansion of the stainless steel–clad layer and the carbon-steel base, fairly high tensile stresses develop in the clad layer even after a normal operating cycle. The tensile stresses also appear at operating temperature after a brief temperature excursion, thereby providing favorable conditions for development and propagation of cracks.

A more generic response surface study carried out in earlier efforts considered various combinations of thermal-expansion coefficient and yield stress for the clad layer. A normal operating cycle and cycles with small and large temperature excursions from operating temperature were analyzed to seek materials that satisfy the criteria that stresses remain compressive and do not exceed the yield stress. While no material was found to satisfy both criteria for all cycles, Alloy 625 satisfied both conditions for a normal operating cycle, while Alloy 825 satisfied the first condition for a normal cycle.

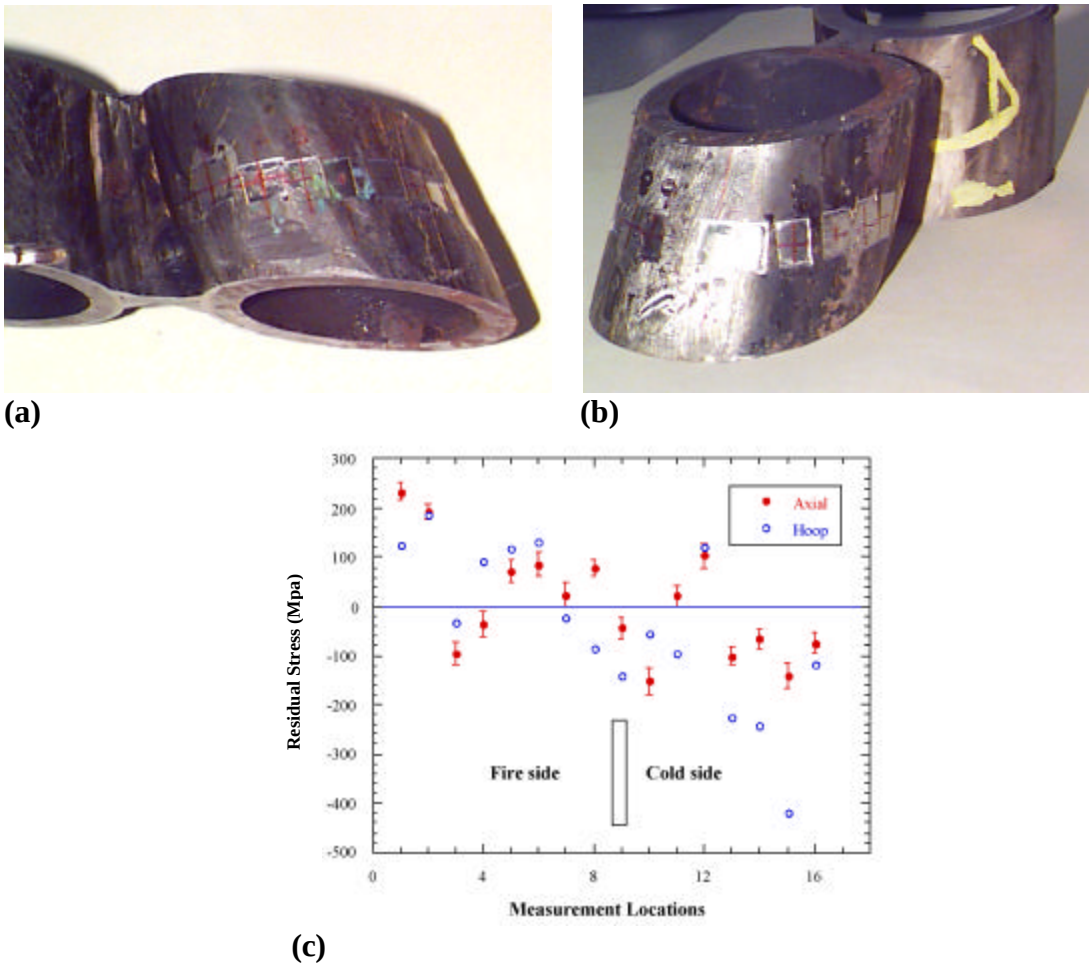

Fig. 8. (a, b) Sections of Alloy 625/carbon steel smelt spout opening showing locations of X-ray measurement points and (c) the results of X-ray residual-stress measurements.

4.1 Modeling of a floor tube panel adjacent to the walls.

Previous modeling work was aimed at examining the tubes in the floor of the boiler in a region away from the walls. Since severe cracking has been found in some tubes close to the walls in some boilers, it was considered important to analyze this case. A new set of

finite-element models was developed for floor tubes adjacent to the wall, because proximity to the furnace walls leads to different service conditions compared to those in the center of the floor. A 2-D finite-element model was developed to compute the manufacturing residual stresses in the floor tube next to the wall. The welding of the membrane that connects the adjacent tube was simulated first, followed by the welding of the seal-plate attachment at the crown of the floor tube that connects it to the wall. Both 304L stainless and Alloy 625 were considered for the clad layer in the analyses. Figure 9 shows the tangential and axial stress distribution for the analyses with Alloy 625/carbon steel composite tubing. The tangential stresses are tensile in the clad layer, with high values close to the welds, and compressive in the carbon steel. Axial stresses are high in tension in the weld regions. Similar overall distributions were obtained for the 304L/CS composite tube.

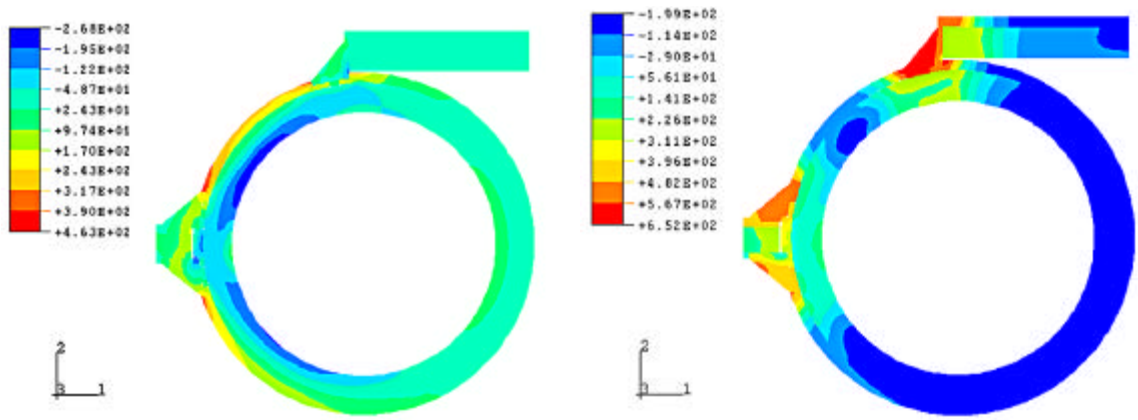

(a) **(b)**

Fig. 9. (a) Tangential and (b) axial stresses (MPa) in the floor tube adjacent to the wall computed using a 2-D model.

The residual stresses obtained from the welding analysis were mapped to a 3-D model for calculating the stresses under service conditions in a tube panel adjacent to the wall. For the tube next to the wall, the initial stress state was assumed based on the residual stresses from the 2-D analyses just described. For the remaining tubes, the residual stresses were obtained from the earlier 2-D analyses of floor tubes away from the walls. The panel was subjected to a normal operating cycle and a temperature excursion over a portion of the seal plate and the associated crown of the tube to simulate conditions when molten smelt running down the wall causes excessive local heating as shown in Fig. 10.

The variation in stresses for the two composite tube panels is shown in Fig. 11 for the tube fire-side surface at a point midway between the membrane and seal-plate welds. For the 304L/CS tube, the large thermal mismatch again plays a dominant role in determining the stress distribution. The tensile residual stresses from assembly welding become compressive at operating temperature. A brief temperature excursion causes another reversal, with stresses remaining tensile through the remainder of operation. The tensile stresses increase in magnitude at boiler shutdown and become compressive when the boiler is brought back to operating temperature. Assumption of 180° steam blanketing instead of full contact with cooling water leads essentially to the same stress distribution.

The results for those adjacent to the wall are not very different from those for a tube far away from the wall, indicating that the thermal-expansion mismatch effect for the 304L/SA210 tubes dominates all other effects, such as initial residual stresses, internal pressurization, and location of tubes.

For the Alloy 625/SA210 tube panel, the axial stresses are slightly compressive at the operating temperature but become tensile after a temperature excursion, as shown in Fig. 11. While the temperature excursion causes significant changes in the axial stresses, it does not have much effect on the tangential stresses, which remain tensile throughout the operating cycle. The axial stresses are not affected significantly by shutdown and subsequent restart of the boiler. These results show that the initial stress levels play a greater role in determining the stresses during service for the Alloy 625–clad material, since the thermal-expansion mismatch with SA210 is quite small and hence not a major factor.

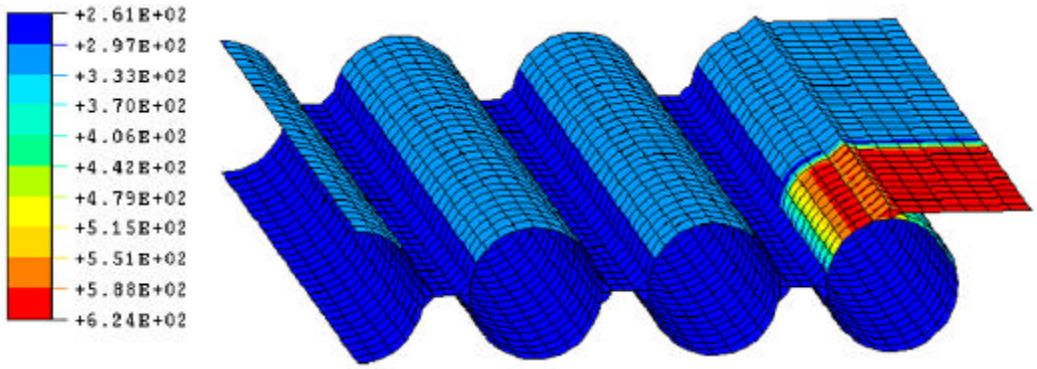

Fig. 10. Three-D model for the floor tube panel adjacent to the wall showing temperature (℃) excursion for a portion of the seal plate and the floor tube.

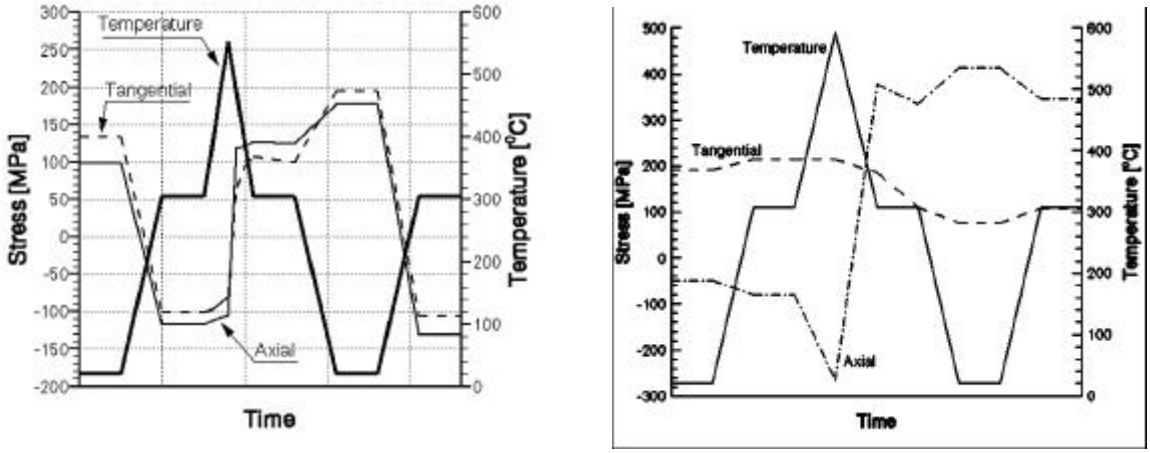

(a) **(b)**

Fig. 11. Temperature cycle and stress variation on the fireside surface of a floor tube adjacent to the wall for (a) 304L/SA210 and (b) Alloy 625/SA210 composite tubes.

4.2 Analyses of windbox attachment

In addition to floor tubes, significant cracking also has been found on the wall tubes near the openings for the smelt spout and the air ports. A preliminary analysis of the wall tubes at the windbox attachment beneath the air ports was carried out using a new finite-element model developed for this purpose. The analysis was restricted to a 304L/SA210 composite tube panel, assuming symmetry boundary conditions in the axial and transverse directions and neglecting the residual stresses due to attaching the windbox.

Figure 12 shows the 3-D model and the temperature distribution used in the analysis, including a temperature excursion to 550°C. The resulting stress distributions at the crown of the tube on the fire side and on the adjacent membrane show that the stress variation is very similar to that obtained in earlier analyses of the floor tubes. There is a possibility that the residual stresses from the wind-box attachment have some effect on the final stresses. However, based on the results in the previous section for the panel adjacent to the wall, a reasonable conclusion is that for the composite tubes with 304L stainless steel as the clad material, the thermal-expansion mismatch dominates all other effects. The mismatch also causes high tensile stresses in the tube whenever there is an increase followed by a decrease in temperature. Other materials such as Alloys 625 and 825, whose thermal-expansion coefficients are closer to that of SA210 carbon steel, may show greater effect of initial stresses, but this remains to be investigated.

4.3 Detailed 2-D analyses with refined mesh

Another focus of recent modeling work has been development of a new 2-D model with greater refinement, especially near the interface between the base material and clad materials on the fire side of the tube. Using the refined model, the stresses in a 304L/SA210 composite tube were computed for operating conditions and after subsequent cooling to room temperature. Figure 13 shows the axial stresses in the tube for the two conditions, with compressive stresses in the clad layer at service conditions becoming tensile after cool down. The base layer shows the opposite trend, with stresses that are predominately tensile at operating temperature becoming mostly compressive at room temperature.

The refined model is able to capture the variations in stresses through the thickness due to the temperature gradients, as well as due to differences in properties across the interface. The detailed simulations using this model can form a valuable tool to better understand the effect of through-thickness variations and interface constraints on the stress fields that develop under various service conditions.

5. Stress Corrosion Testing

The various tasks in this project have produced results that strongly indicate that stress-corrosion cracking plays a very important role in the cracking of the stainless steel layer on composite tubes. The available evidence leads to a hypothesis that the cracking occurs during shutdown of the boiler. One of the issues remaining to be resolved in this project is the identification of the corrodent and the environment under which stress corrosion

occurs. Efforts are under way at both paper institutes, the Pulp and Paper Research Institute of Canada (Paprican) and the Institute of Paper Science and Technology (IPST), to resolve this issue. In the following section, the results of studies at both institutes are described.

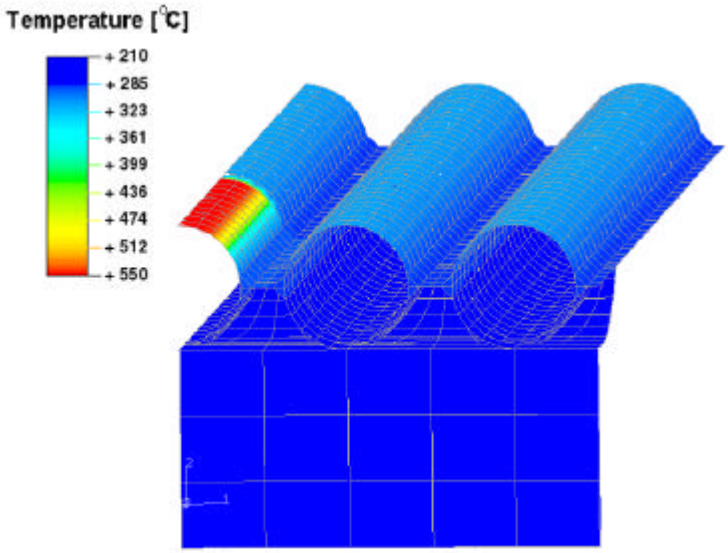

Fig. 12. Three-D model for the wall tube panel at the windbox attachment showing temperature excursion for a portion of the tube.

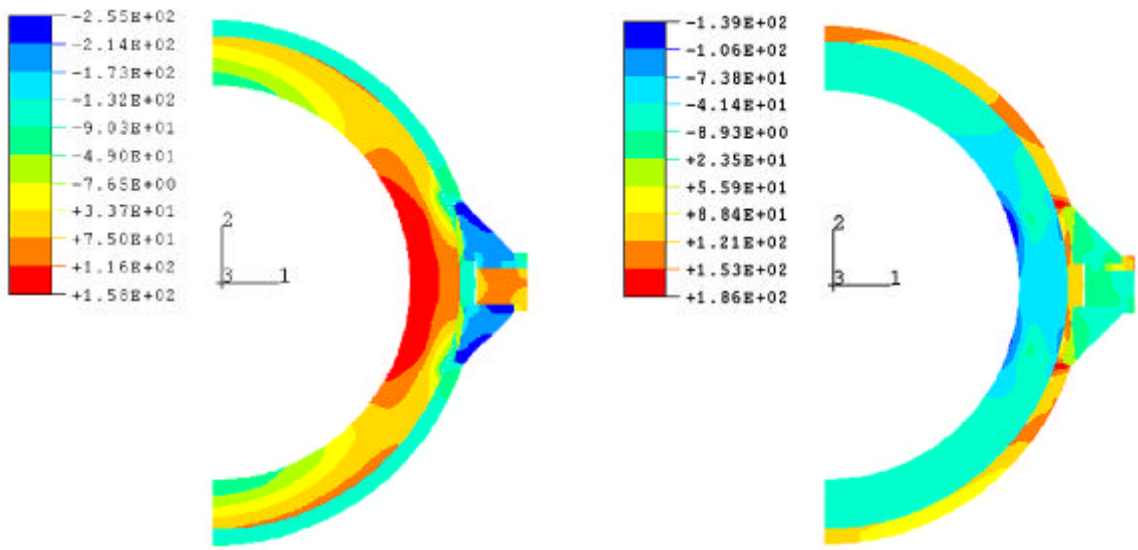

(a) **(b)**

Fig. 13. Axial stresses (MPa) in the tube (a) at operating conditions and (b) after cooling to room temperature.

5.1 Stress-corrosion cracking studies: Paprican

Studies have continued into the stress-corrosion cracking of type 304L stainless steel in salts containing hydrated sodium sulfide. The emphasis has moved from using U-bend and C-ring specimens towards using proof rings that apply a known load and measure time to failure. There also have been two visits to mill sites to observe floor inspections.

5.1.1 U-bend tests

A test has been carried out to show that type 304L stainless steel can undergo stress-corrosion cracking in a solution of smelt collected from a recovery boiler. The smelt was taken from a spout, cooled, crushed, and partially dissolved in distilled water at 60°C under a blanket of nitrogen gas. The solution obtained was dried onto the surface of a polished U-bend specimen. The temperature was maintained at 160°C with a nitrogen purge and water drip at 1 ml/min. After 20 h the U-bend was removed and examined, but cracks could not be seen. The temperature was raised to 170°C, and the experiment was continued. After another 40 h, small cracks were detected.

In the experiment just described, the Na_2S : Na_2CO_3 ratio in the solution was 1 : 2.2. In the following experiment, laboratory chemicals were mixed in the ratio 1 : 19 to find out if 304L stainless steel is susceptible to stress corrosion in mixtures containing lesser concentrations of Na_2S. The experimental procedure was similar; however, the drip volume and interval were changed to 15 ml/min, and the temperature set point was raised to 200°C. Significant cracking was noted after 90 h.

5.1.2 Proof-ring tests

In the proof-ring apparatus, it has been difficult to obtain the same degree of stress-corrosion cracking as has been achieved with the U-bends. Differences are attributed to a number of factors, such as changes in geometry and method of heating. Tests using the $Na_2S \bullet 9H_20$–10% NaOH mixture have been discontinued because the hydroxide content of the salt is considered to be unrealistically high in comparison with that of recovery-boiler smelt.

A number of experimental approaches have been attempted to find a method that consistently produces stress-corrosion cracks in 304L stainless steel. The most successful method to date uses a temperature set point of 190°C. Molten $Na_2S \bullet 9H_20$ (200 ml) is poured into the crucible at the start of the experiment. Nitrogen is flowed continuously, and water additions (10 to 15 ml) are made at 10-min intervals, starting when the temperature set-point is reached. Before commencing the test, the ¼-in.–diam gage length of the specimen is dry-blasted with 100-mesh alumina grit to remove machining marks. A tensile load, equivalent to 2/3 of the 0.2% proof stress at room temperature is applied.

The first test using the above conditions produced a failure in 197 h. A repeat test gave a time to failure of 171 h. The stress-corrosion cracks appear to be transgranular and do not show the pronounced intergranular features that were prominent on fracture faces formed in the $Na_2S \bullet 9H_20$–10% NaOH mixture. It has not yet been decided whether this test

method will be used to measure the time to failure of other boiler tube materials (e.g., 309 and 310 stainless steels and alloys 825 and 625). Additional refinements still are being sought in order to reduce the time to failure.

5.1.3 Characterization of corrosion product associated with stress corrosion

Type 304L stainless steel proof-ring specimens have been examined by SEM/EDX with a view to finding out whether anything of value could be deduced from the morphology or composition of the surface layer of corrosion product. The corrosion product is generally thin, nondescript, and difficult to characterize by such techniques. However, some interesting observations have been made. On specimens where there are stress-corrosion cracks, the layer of corrosion product was generally richer in chromium than the product in uncracked areas. However, the corrosion product that had formed inside the cracks was found to be depleted in chromium and richer in iron. In both cases the corrosion products contained sulfur and oxygen.

On the uncracked specimens, there were areas that appeared very shiny and reflective to the naked eye. On close examination, these had an etched appearance with a network of corrosion product at the grain boundaries. Other areas were marked by the presence of patches of corrosion product with a dried-mud morphology.

An attempt also has been made to characterize the corrosion product on a composite tube removed from a 5-year-old floor. The floor contained shallow cracks (100 to 200 µm) and pitting corrosion in the stainless steel layer. There was a thin layer of corrosion product that appeared to be enriched in both chromium and sulfur. Clearly, the corrosion products are difficult to characterize, but formation of a certain type of chromium-rich, sulfur-containing film seems to be necessary for stress corrosion to take place. Further investigation by a more advanced technique such as XPS or AES may be warranted.

5.1.4 Observations from mill visits

Two floor inspections have been attended recently. At both mills, it was claimed that there were no cracks in the floor. The first was at a 5-year-old mill in western Canada. The boiler operates at 61 atm (900 psi) and has a sloping floor with 13 composite tubes (304L/SA210) on each side. An inspection was done in the spring of 1998, and no cracks were found. The two smelt runs were inspected with water-soluble dye penetrant; again, no cracks were revealed. Specific portions were reinspected after additional grinding with emery paper and rinsing with acetic acid, and still no cracks were detected. The composite tubes near the spout openings were not examined because the residue of the smelt bed and the refractory had not been removed. A small area of the smelt bed (roughly 2½ ft by 1 ft) in one corner of the boiler was cleared by chipping and prizing away the remaining layer. No cracks were found in this area either.

In the past, the boiler was washed several times each year, but washing is necessary now only at 6-month intervals. The policy always has been to burn the bed down thoroughly before a water wash. During this particular shutdown, the bed was burned down for 24 h until very little material remained in contact with the floor. It was then cooled for almost

6 h before the wash was started. Thermocouples installed in the boiler floor indicated that the floor temperature was 60 to 100°C when wash water entered the furnace.

The second mill is in Eastern Canada. It has an older boiler, operating at 60 atm (875 psi). The lower furnace had been replaced completely with 304L/SA210 composite tubes 13 years ago. An inspection was carried out 12 months ago with dye penetrant, and no cracks were found. On this occasion, the entire boiler floor was thoroughly cleaned by hydroblasting, and then it was inspected by the eddy-current method. The inspection was extremely thorough, and not a single crack was found.

At this boiler it always has been common practice to completely burn out the bed before water washing. This takes up to 6 h and is followed by a 6-h cooling period before the wash commences. There are no thermocouples in the floor, but the superheater thermocouples always read below 150°C when washing starts. This boiler has never had problems with fouling and usually is washed at 6-month intervals.

5.1.5 Summary

Laboratory tests show that solutions formed from recovery boiler smelt can cause stress corrosion in type 304L stainless steel. Furthermore, it has been found that sodium sulfide concentrations as low as 5% can cause stress-corrosion cracking in salt mixtures.

Observations from mill visits suggest that 304L/SA 210 composite tubes may not crack by stress corrosion if the char-bed is thoroughly burned down and allowed to cool sufficiently before starting the water wash. The presence of small amounts of smelt after thoroughly burning down the char-bed appears not to give rise to stress corrosion during boiler startup.

There is a shortage of reliable information from boilers about the time taken for cracks to form. If there is any substance to the report that cracking of floor tubes can occur in an interval of 6 months, then it is possible that the time taken to form cracks in laboratory tests may be greater than the time available to form cracks during water washes. This discrepancy needs to be reconciled if the existing theory is to explain the phenomenon of cracking in composite floor tubes.

5.2 Stress-corrosion cracking studies at IPST

5.2.1 Slow strain rate tests

Stress-corrosion cracking susceptibility of 304-L stainless steel in different wash-water compositions and temperatures is being studied. Type 304L tensile specimens are tested using the slow-strain-rate test method. The gage lengths of the tensile specimens are exposed to the test environment, and the specimens are strained at a constant extension rate, giving very slow ($<1 \times 10^{-6} s^{-1}$) initial strain rates. Specimens generally are tested until they fracture. There are a number of different parameters that can be compared to quantify these results (i.e., % reduction in area, % elongation, and crack velocity).

However, the presence of visible stress-corrosion cracks on the specimen surface and/or fracture surfaces are of prime importance in these tests.

Test environments used in this study include the artificial wash-water compositions shown in Table 1. However, individual constituents of wash water or their different combinations also were tested and are listed in Table 5. Tests are carried out at different temperatures. Experiments conducted at temperatures above 100°C were carried out in a special slow-strain rig with an autoclave. The test specimens were electrically isolated from the test rig in all tests.

Figure 14 shows an example of the specimen with stress-corrosion cracks on its surface. After the tests were complete, the specimens were examined for surface cracks, and the crack-depth measurements were made. One-half of the specimen was sectioned, mounted, and polished to measure crack lengths and examine the mode of cracking.

Table 1. Composition of Artificial Wash Waters Used in These Tests

Chemicals	Artificial WW#1	Artificial WW#2	Artificial WW#3
Sodium Carbonate	65%	60.50%	33.333%
Sodium Sulfate	17%	14%	
Sodium Sulfide	15%	15%	33.333%
Sodium Thiosulfate	2%	5%	
Sodium Chloride	0.50%	5.00%	
Sodium Hydroxide	0.50%	0.50%	33.333%

Fig. 14. Micrograph of test specimen #30, showing stress-corrosion cracks on a tensile specimen tested at a slow strain rate.

5.2.2 Constant extension tests

Constant extension or constant strain tests were done in Na_2S + NaOH solution to determine the threshold strain required to initiate a stress-corrosion crack in this system and to establish the effects of applied total strain on the crack-growth rate in this system. In these tests, the specimens were strained to a given initial strain, and the strain was held constant for 24 h. After 24 h of exposure, the specimens were examined for surface cracks, sectioned, mounted, and polished to measure crack depths. The data clearly indicate that the threshold strain for the initiation of SCC in this system is around yield point of the material.

5.2.3 Results summary: wash water #1

A series of tests were conducted in artificial wash water #1. Tests conducted below temperatures of 200°C did not show any signs of SCC, as is shown in Table 2. High-temperature test specimens showed severe SCC in this environment. Cracks were transgranular and branched. Some tight, unbranched transgranular cracks also were found on the specimens in areas away from the final fracture. Tests also were carried out with applied potential, as is shown in Table 2. Type 304-L specimens tested with applied potential in the tested range did not show any SCC in wash water #1. Further tests are planned to cover a broad range of potential values to establish the electrochemical conditions required for SCC in this system.

5.2.5 Results summary: wash water #3

Wash water #3 had higher amounts of sodium hydroxide and sodium sulfide compared with amounts in #1 and #2 wash waters. A series of tests were conducted in artificial wash water #3, and the results are listed in Table 3. In the presence of higher NaOH and higher Na_2S, even the specimen tested at 150°C showed tight branched transgranular SCC under open-circuit conditions. Tests done at 125°C or below showed no signs of SCC in these tests.

5.2.4 Results summary: wash water #2

A series of tests were conducted in artificial wash water #2, which had higher chloride and thiosulfate concentrations than wash water #1. Again, like in wash water #1 tests, tests conducted below temperatures of 200°C showed no signs of SCC, as is shown in Table 4. Specimens tested at 200°C showed severe transgranular SCC in this environment.

Table 2. Slow Strain Rate Test Data for Specimens Tested in Wash Water #1

SP#	Test Solution	Temp. ^{o}C	E, mv (SCE)	Remarks
13	Artificial WW# 1	90	OCP	No Crack
14	Artificial WW # 1	200	OCP	Multiple SCC Cracks
16	Artificial WW # 1	150	OCP	No Crack
20	Artificial WW # 1	200	OCP	Multiple SCC Cracks
22	Artificial WW # 1	200/90	OCP	No Crack
24	Artificial WW # 1	200/150	OCP	Multiple SCC Cracks
		Applied Potential Tests		
25	Artificial WW # 1	100 C	-0.740	No Crack
29	Artificial WW # 1	100 C	-0.650	No Crack
32	Artificial WW # 1	100 C	-0.100	No Crack
35	Artificial WW # 1	90 C	-0.850	No Crack
36	Artificial WW # 1	90 C	-0.950	No Crack
41	Artificial WW # 1	90 C	-0.740	No Crack
44	Artificial WW # 1	90 C	-0.100	No Crack
47	Artificial WW # 1	90 C	-0.650	No Crack
48	Artificial WW # 1 (P.H 13.938)	90 C	-0.900	No Crack
51	Artificial WW # 1	90 C	-0.740	No Crack

5.2.6 Individual constituents of wash water and their combinations

Individual constituents of wash water as well as simple mixtures of different constituents of wash water were tested to study their influence on the SCC of 304L at temperatures of 100°C or below. As shown in Table 5, Na_2S solutions tested at 25°C, 90°C, or 100°C did not show any signs of corrosion or SCC, as expected. However, concentrated (~30%) NaOH solution at 100°C did show tight transgranular SCC. When Na_2S was present with NaOH in the solution, the cracking could be found at temperatures as low as 50°C.

Table 3. Slow Strain Rate Test Data for Specimens Tested in Wash Water #3

SP#	Test Solution	Temp. °C	E, mv (SCE)	Remarks
26	Artificial WW # 3	200C	OCP	Multiple SCC Cracks
30	Artificial WW # 3	200C	OCP	Multiple SCC Cracks
46	Artificial WW # 3	150 C	OCP	Multiple SCC Tight Cracks
49	Artificial WW # 3	125 C	OCP	No Crack
50	Artificial WW # 3	100 C	OCP	No Crack
		Applied Potential Tests		
27	Artificial WW # 3	100 C	-0.740	No Crack
28	Artificial WW # 3	100 C	-0.650	No Crack
37	Artificial WW # 3	90 C	-0.850	No Crack
38	Artificial WW # 3	90 C	-0.950	No Crack
45	Artificial WW # 3	90 C	-0.100	No Crack
53	Artificial WW # 3	90 C	-0.650	No Crack
54	Artificial WW # 3	90 C	-0.740	No Crack

Table 4. Slow Strain Rate Test Data for Specimens Tested in Wash Water #2

SP#	Test Solution	Temp. °C	E, mv (SCE)	Remarks
15	Artificial WW # 2	90	OCP	No Crack
33	Artificial WW # 2	150 C	OCP	No Crack
34	Artificial WW # 2	200 C	OCP	Multiple SCC Cracks
		Applied Potential Tests		
39	Artificial WW # 2	90 C	-0.950	No Crack
40	Artificial WW # 2	90 C	-0.850	No Crack
42	Artificial WW # 2	90 C	-0.650	No Crack
43	Artificial WW # 2	90 C	-0.100	No Crack

Table 5. Slow Strain Rate Test Data for Specimens Tested in Test Solutions Described in Table

SP#	Test Solution	Temp. ^oC	E, mv (SCE)	Remarks
4	(1N)Na_2S $9H_2O$	25	OCP	No Crack
7	(1N)Na_2S $9H_2O$	25	OCP	No Crack
8	(1N)Na_2S $9H_2O$	102	OCP	No Crack
3	(1N)Na_2S $9H_2O$	90	OCP	No Crack
17	Crystals of Na_2S and H_2O (Sat. sol.)	100	OCP	No Crack
58	90 gm Na_2S + 300 ml H_2O	100	OCP	No Crack
6	(1N)Na_2S $9H_2O$ +Na_2CO_3	25	OCP	No Crack
5	(1N)Na_2S $9H_2O$ +Na2CO_3	90	OCP	No Crack
21	300 gms NaOH + 50 ml H_2O	100	OCP	No Crack
57	90gm NaOH + 300 ml H_2O	100	OCP	Multiple SCC Tight Cracks
61	90 gm NaOH + 300 ml H_2O	75	OCP	No Crack
19	150 g Na_2S+150 g NaOH +50 ml H_2O	100	OCP	Multiple SCC Cracks
23	150 g Na_2S+150 g NaOH +50 ml H_2O	100	OCP	No Crack
31	150 g Na_2S+150 g NaOH +50 ml H_2O	75	OCP	No Crack
52	150 g Na_2S+150 g NaOH (No H_2O)	100	OCP	No Crack
55	150 g Na_2S+150 g NaOH +75 ml H_2O	100	OCP	Multiple SCC Cracks
56	150 g Na_2S+150 g NaOH +75 ml H_2O	100	OCP	Multiple SCC Cracks
59	150 g Na_2S+150 g NaOH +75 ml H_2O	75	OCP	Multiple SCC Cracks
60	150 g Na_2S+150 g NaOH +75 ml H_2O	75 C	OCP	Multiple SCC Cracks

Specimens that had stress-corrosion cracks after slow strain rate tests also had a black film on the surface. The film on most of these specimens was shiny and black; however, some specimens had dull black film as well. The film was very similar in appearance to the magnetite film formed on the surface of carbon steels. Tests are being conducted to identify this film in order to understand the environmental and electrochemical conditions that may cause SCC of 304L stainless steels in kraft recovery boilers during shutdown conditions.

5.2.7 Constant extension tests

Constant extension or constant strain tests were carried out in Na_2S + NaOH solution. The main objective of these tests was to determine the threshold strain required to initiate a stress-corrosion crack in this system and to establish the effects of applied total strain on the crack-growth rate in this system. Results from these tests indicate that a large plastic strain is not required to initiate a stress-corrosion crack in this system. The threshold stress or strain for the initiation of SCC is around yield point of the material. Crack-growth rate measurements still are not finished, but the initial data indicated that the crack-growth rate increases with the increase in initial strain.

5.2.8 Conclusions

Results from wash water #1 and #2 show that 304L stainless steel does not undergo stress-corrosion cracking at temperatures up to 150°C. However, at 200°C severe stress-corrosion cracking was noticed under tested open-circuit conditions.

Applied potential tests did not produce conditions required for stress-corrosion cracking. Further tests under controlled potential will be conducted to understand the mechanism of this phenomenon.

Results to date indicate that the presence of higher concentrations of hydroxides can lead to transgranular stress-corrosion cracking. In the presence of sulfides, hydroxides can cause cracking at temperatures lower (~50°C) than those required for pure hydroxide solutions (100°C or higher).

A black surface film is associated with the stress-corrosion cracking of 304L specimens under all of the tested conditions. Work is continuing to characterize this film to understand the mechanism of cracking in the kraft recovery boilers. The threshold stress/strain for the initiation of SCC is around the yield point of the material.

6. Thermal Fatigue Studies of Composite Tubes

The activity on thermal fatigue of composite tubes involves the (1) review of thermal and mechanical fatigue in composite tube materials, (2) compilation and production of the physical and mechanical properties needed for the modeling, (3) isothermal and thermal/mechanical fatigue of tubes, and (4) determination of cracking patterns for various thermal/mechanical loading. Materials of concern include carbon steel (equivalent to SA210, Gr A-1), 304L stainless steel, Fe-Cr-Ni alloy 825, nickel-base alloy 625, 309L stainles steel filler metal, 312 stainless steel filler metal, and chromized carbon steel.

The review completed during 1995 (1) reached nine conclusions that bear on the experimental and analytical work: (1) the physical and mechanical properties of the 309L and 312 stainless steel filler metals are needed; (2) the tensile properties of very fine grained 304L are required; (3) exploratory fatigue data to 600°C are needed for the very fine grained 304L stainless steel, the 309L-deposited filler metal, the 312 stainless steel–deposited filler metal, and Alloy 825; (4) the isothermal fatigue curves are required;

(5) the exploratory thermal-mechanical fatigue data were needed for Alloy 825, Alloy 625, 312 stainless steel, and 309L stainless steel; (6) the procedures for the fatigue damage under multiaxial strains recommended in the ASME Code Section III are applicable; (7) fatigue crack-growth testing is not required; (8) the constitutive equations recommended in DOE RDT F9-5T (2) are suitable for use in elastic-plastic analysis of composite tubes; and (9) transient stress fatigue testing of tubing is needed to confirm the validity of the analysis methods.

All physical properties measurements were obtained for the materials used in the composite tubing, including simulated chromized steel. Here, data for carbon steel at two chromium levels, namely 27% and 40% chromium, were gathered. For 27% chromium, the literature data for 446 stainless steel were used. For the 40% chromium steel, a special material was produced that contained 40% Cr, 0.5% Mn, and 0.25% Si. Physical properties such as thermal expansion, thermal diffusivity, and specific heat were produced. Mechanical properties included tensile and hardness numbers. Samples for fatigue testing were machined.

Thermal fatigue tests were completed on both five-tube and three-tube panels (Fig. 15) (3). For the five-tube panel, 7.5-kW bank furnace was used to heat the crown of the center tube in the panel. The hot spot in the panel cycled 1000 times between 540 and 250°C and experienced a maximum through-thickness gradient of 30°C. No cracks were produced in the hot section. Very little change in hardness was observed. Residual-stress measurements described in a previous section indicated a change in the surface stress of the hot section of the tube panel. This change was away from a high residual stress toward zero stress. The dislocation substructure observed by TEM of the hot section revealed characteristics very similar to tubes exposed in service. However, the micro-structure was not characteristic of the microstructure observed in uniaxial test samples subjected to thermal/mechanical fatigue. It was concluded that the relatively severe thermal cycling of the hot spot in the panel did not produce significant fatigue damage. A three-tube panel was prepared for further testing. In this case, cycling to above 600°C was undertaken to better represent possible fatigue conditions in spout-opening tubes.

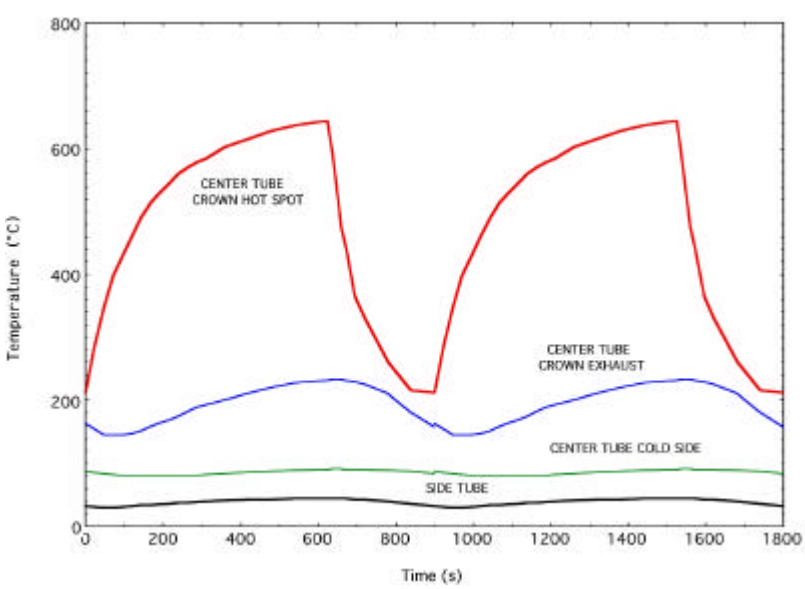

Fig. 15. Temperatures at several locations during the thermal cycling of a three-tube panel to simulate thermal fatigue of a composite smelt spout opening.

7. Transmission Electron Microscopy Characterization of Composite Tubes

Previous work on unexposed and various exposed 304L/SA210 composite floor tubes showed highly strained dislocation substructures in the 304L cladding, just below the tube surface. By contrast, the mid-thickness of the cladding had low dislocation contents typical of annealed material. In-service exposure produced plastic strain and dislocation structures, including cellular and kinked dislocation network substructures within the grains, which were similar to those found in 304L thermal-fatigue control specimens (cycled at 300 to 600°C to total plastic strains of 0.45%). Additional careful work to examine various tubes from service in different recovery boilers (built by different manufacturers) all showed the similar and important result of no difference in the characteristic service-induced dislocation substructure between cracked and uncracked portions of the tubes.

This year, specimens were examined from composite tubes taken from different parts of the lower boiler including wall tubes and spout-opening tubes. Typical near-surface dislocation substructures are shown from nearby cracked and uncracked portions of 304L cladding, taken from wall tubes that were in service in a mill in western Canada (Fig. 16). The dislocation substructures in these wall tubes looked quite similar to those observed previously in floor tubes. Furthermore, the strain-induced dislocation structures are generally similar between cracked and uncracked regions. However, subtle, fine differences in details of the dislocation network structure (the degree of kinking and loops) are consistent with the uncracked tube being at a somewhat higher temperature.

Near-surface dislocation substructures also were analyzed in specimens taken from a spot opening that was in service in a mill in the south central United States. These tubes are bent compared to the straight wall and floor tubes that have been examined. Specimens from cracked and uncracked regions had identical, heavy cellular dislocation substructures beneath the exposed surface that indicate significantly more plastic strain (Fig. 17). Comparison of this in-service dislocation structure with that of the thermal fatigue–test control specimen (0.45% plastic strain) clearly indicates that there was more plastic strain in the spout opening due to thermal cycling (Fig. 18). However, despite much more thermal fatigue–induced plastic strain, such mechanical strains and stresses are the same in cracked and uncracked regions, indicating that corrosion must play some role in causing the cracking, at least in the crack-initiation stage.

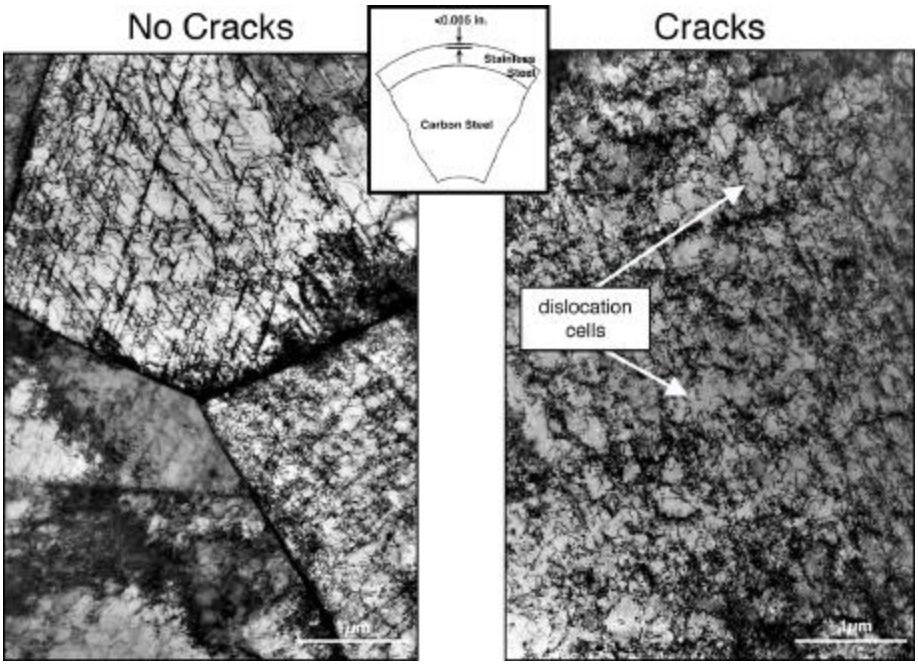

Fig. 16. Comparison of TEM analysis of dislocation substructures from uncracked and cracked portions of 304L clad from composite wall tubes from a western Canada mill. Although there are subtle differences, both samples have similar cellular dislocation structures induced by plastic strain during thermal cycling.

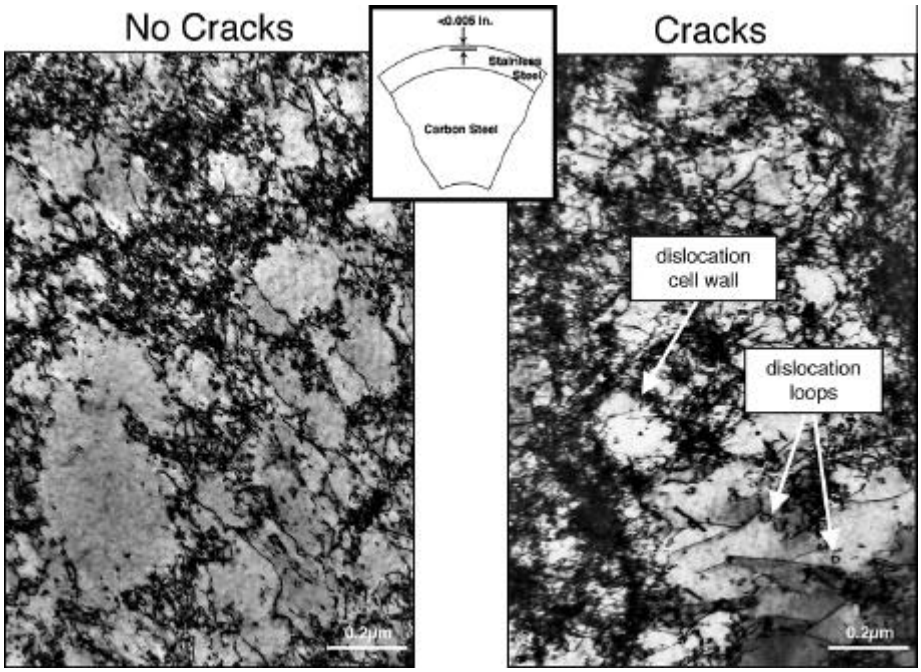

Fig. 17. Comparison of TEM analysis of dislocation substructures from uncracked and cracked portions of 304L clad from composite smelt spout-opening tube. There is no detectable difference in the cellular dislocation substructures induced by plastic strain due to thermal cycling between cracked and uncracked tubes.

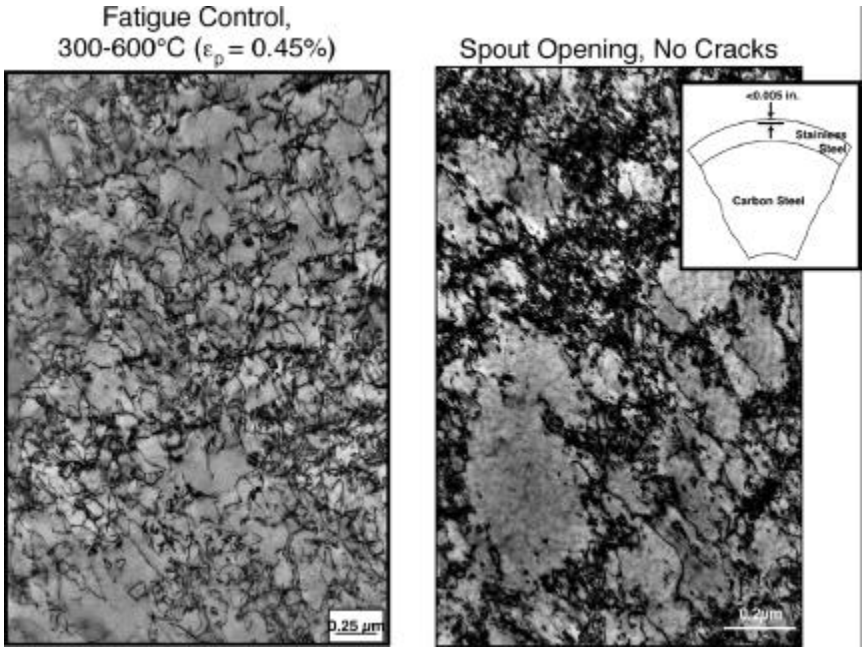

Fig. 18. Comparison of TEM analysis of dislocation substructures in 304L specimens, one from a thermal-fatigue control test and the other from near the surface of the 304L cladding from an uncracked composite spout-opening tube. Clearly, the spout-opening tube has seen considerably more plastic strain than the thermal-fatigue control specimen.

A test section of floor tubing was fatigue tested at ORNL in a hot-spot and constraint configuration to try to simulate the kind of thermal-fatigue strain such tubes see in service. The hot spot contained a near-surface, strain-induced dislocation substructure that is very similar to the typical structure found in various floor tubes removed from service (Fig. 19). This hot-spot thermal-fatigue dislocation substructure has considerably less plastic strain than the 0.45% strain produced in a thermal fatigue–test control specimen. This indicates that the hot-spot test does simulate the small thermal cycling–induced strains developed during service in floor tubes.

Finally, efforts began this year to examine other advanced composite tube materials such as Alloy 625. A straight as-fabricated tube (Sandvik 63/carbon steel) showed a low level of near-surface strain-induced dislocation substructure, consistent with a well-annealed and straightened tube as shown in Fig. 20(a). Examination of a cracked spout-opening tube (Sumitomo 625/carbon steel) taken from a mill in southwestern Alabama showed a highly strained dislocation structure, as shown in Fig. 20(b), indicative either of bending to make the spout opening or thermal fatigue during service, or both. This structure in Alloy 625 does not have the cellular structure characteristic of the softer 304L cladding. More work on Alloy 625 or other advanced cladding materials is planned next year.

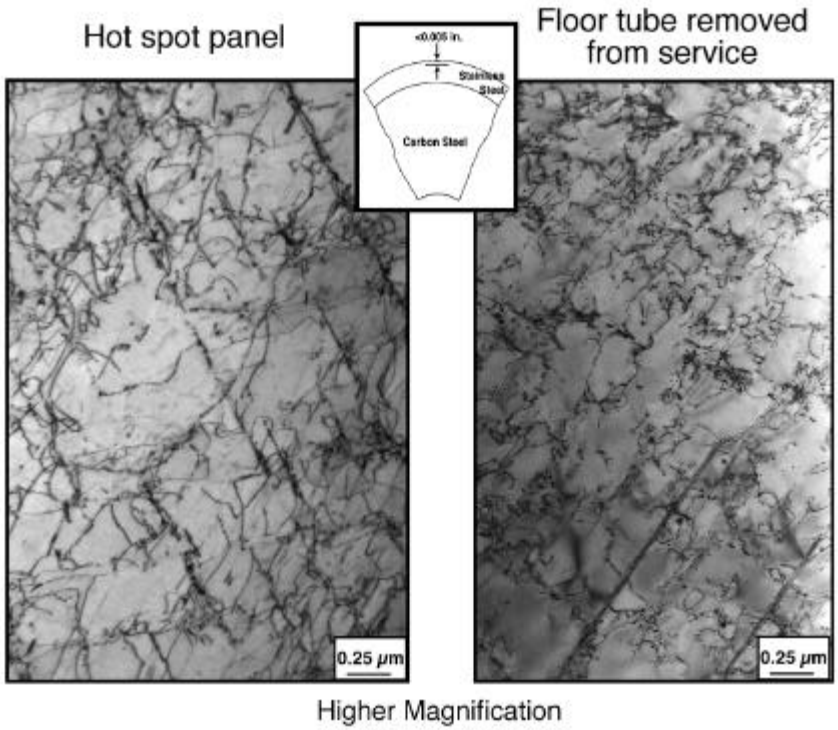

Fig. 19. Comparison of near-surface TEM analysis of strain-induced dislocation substructures in 304L cladding from the hot-spot thermal-fatigue simulation and from a floor tube removed from service.

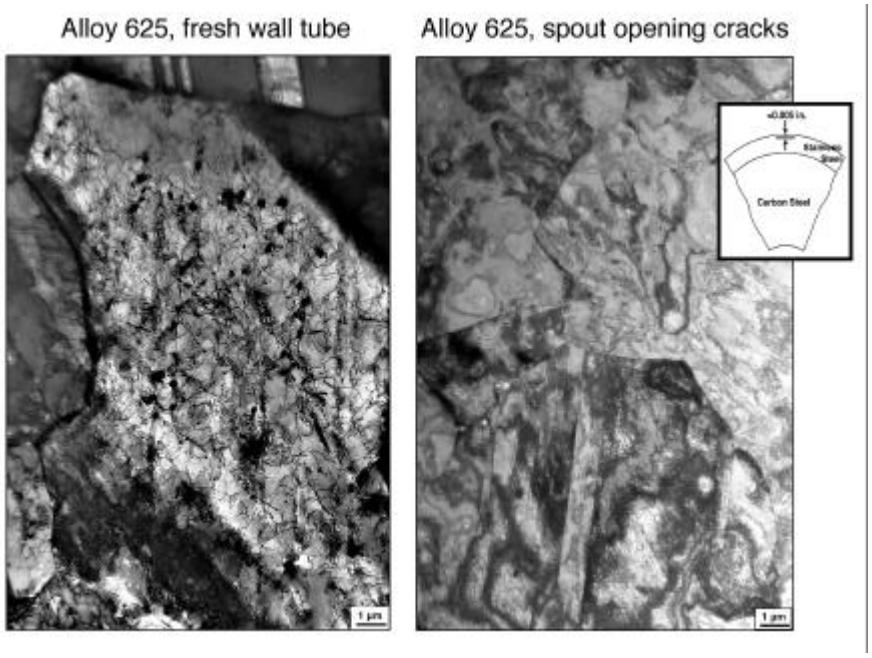

(a) **(b)**

Fig. 20. Comparison of near-surface TEM analyses of Alloy 625 (a) from cladding of a straight Sandvik tube and (b) from a cracked Sumitomo spout-opening tube.

REFERENCES

1. R. W. Swindeman, *A Review of Thermal/Mechanical Fatigue in Composite Tube Materials*, Oak Ridge National Laboratory Draft TM-13474 (to be published).

2. RDT Standard F9-5T, *Guidelines and Procedures for Design of Nuclear System Components at Elevated Temperatur*e (September 1974).

3. R. W. Swindeman, J. R. Keiser, P. J. Maziasz, and D. L. Singbeil, "Fatigue Cracking of Coextruded 304L/CS Tubes," pp. 209–12 in *9th International Symposium on Corrosion in the Pulp and Paper Industry, Preprints of Publication*, Canadian Pulp and Paper Association, Montreal, Canada, May 1998.

Materials for the Pulp and Paper Industry

Section 2. Corrosion and Failure Analysis Studies in Support of the Pulp and Paper Industry

J. R. Keiser, S. J. Pawel, R. W. Swindeman, and H. F. Longmire
Metals and Ceramics Division
Oak Ridge National Laboratory
P.O. Box 2008, Oak Ridge, Tennessee 37831

INTRODUCTION

Technical support is being provided to various pulp and paper companies and related industries to help determine the cause of material-degradation problems and to identify alternate materials to prevent such degradation. During the past year, activities have included examinations of superheater tubes, economizer tubes, soot-blower components, tubes from the lower section of recovery boilers, and inspection of continuous digesters. The results of the analyses and inspections were communicated to the plant operators, and, in some cases, recommendations were made.

TECHNICAL PROGRESS: FY 1998

Examination of Failed Coextruded Wall Tube

An examination was conducted on a composite wall tube removed from the spout wall of a North American boiler after some damage was observed during an inspection. The damage was thought to have occurred during a prior ESP when the char-bed reportedly slumped against the spout wall. Inspectors reported that the stainless steel cladding was severely thinned below and in the vicinity of the primary air ports. The tube was cut into 19 samples. Some of these were given to an independent testing company, some were retained by the mill operator, but the majority of the samples were sent to ORNL for examination.

The samples sent to ORNL were cut, mounted, and polished for metallographic examination. The examination showed that the stainless steel layer was totally gone in some areas and the carbon steel in those areas showed evidence of severe overheating. At higher and lower positions on the tube, some cladding remained on the tube, and the evidence of overheating was less. Even farther from these severely degraded areas, the amount of degradation was less, as indicated by the thicker stainless layer and fewer changes in the carbon steel microstructure. The thinning of the stainless layer as a function of position on the tube is shown in Fig. 1.

It was concluded that local overheating of the tube very likely had occurred during the ESP when the majority of the water had been drained from the tubes. The wall tubes probably experienced this unusually large amount of heating because the char-bed slumped against the wall. As a result of this damage, the wall required repairs in order to resume operation.

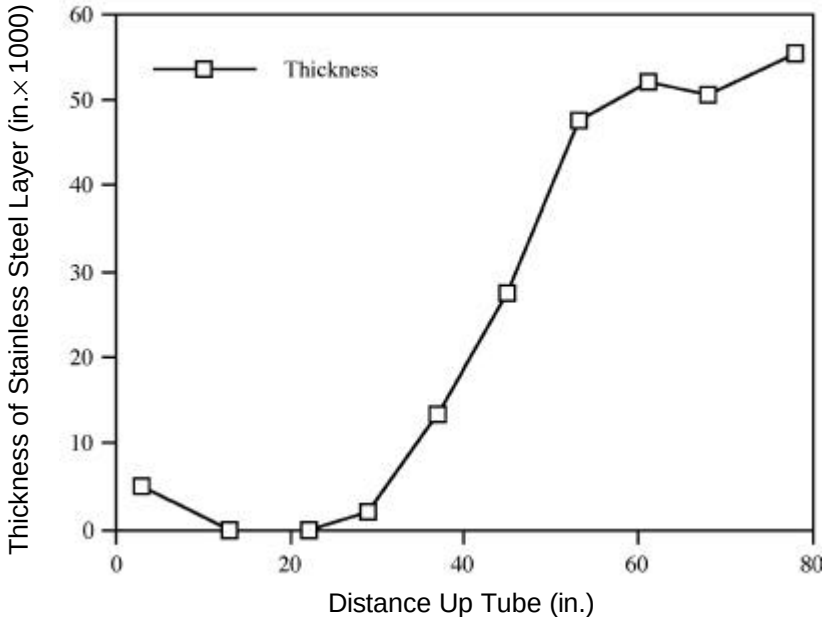

Fig. 1. Thickness of the stainless steel layer on 304L/CS composite tubing vs position on a tube that had experienced degradation because of overheating during an ESP.

PUBLICATIONS

J. R. Keiser, B. Taljat, X.-L. Wang, R. W. Swindeman, L. E. Meyers, P. J. Maziasz, R. L. Thomas, D. L. Singbeil, R. Prescott, J. P. Gorog, and P. M. Singh, "Overview of the DOE Studies of Recovery Boiler Floor Tube Cracking," in *Proceedings of the TAPPI 1998 International Chemical Recovery Conference*, Tampa, Florida, pp. 71–86, June 1–4, 1998.

B. Taljat, T. Zacharia, X.-L. Wang, J. R. Keiser, R. W. Swindeman, and C. R. Hubbard, "Mechanical Design of Steel Tubing for Use in Black Liquor Recovery Boilers," in *Proceedings of the 9th International Symposium on Corrosion in the Pulp and Paper Industry*, Ottawa, Ontario, pp. 193–217, May 26–29, 1998.

R. Prescott, P. Eng and D. L. Singbeil, "Stress Corrosion Cracking of Type 304L Stainless Steel in Kraft Recovery Boiler Environments," in *Proceedings of the 9th International Symposium on Corrosion in the Pulp and Paper Industry*, Ottawa, Ontario, pp. 185–188, May 26–29, 1998.

R. W. Swindeman, J. R. Keiser, and P. J. Maziasz, "Fatigue Cracking of Coextruded 304L/CS Tubes," in *Proceedings of the 9th International Symposium on Corrosion in the Pulp and Paper Industry*, Ottawa, Ontario, pp. 209–12, May 26–29, 1998.

J. R. Keiser, B. Taljat, X.-L. Wang, R. W. Swindeman, P. J. Maziasz, L. E. Meyers, R. L. Thomas, S. T. Elliott, D. L. Singbeil, R. Prescott, and J. P. Gorog, "Causes and Solutions for Cracking of Coextruded and Weld Overlay Floor Tubes in Black Liquor

Recovery Boilers," in *Proceedings of the 9th International Symposium on Corrosion in the Pulp and Paper Industry*, Ottawa, Ontario, pp. 213–20, May 26–29, 1998. **Winner of Conference Best Paper Award**

PRESENTATIONS

All researchers make oral presentations on their work at the triannual program reviews. Invited presentations reviewing the program's progress have been made annually at AF&PA Recovery Boiler Committee and BLRBAC meetings, at NACE International's T-5H-1 committee meeting, at TAPPI's Steam and Power Committee meeting, and, when invited, at meetings organized by various paper companies. Four papers were presented at the 9th International Symposium on Corrosion in the Pulp and Paper Industry, held in Ottawa in May 1998, and one paper was presented at the International Chemical Recovery Conference held in Tampa in June 1998. Additional papers were presented at other society meetings.

INDUSTRIAL INPUT AND TECHNOLOGY TRANSFER

An advisory committee composed of representatives of paper companies, boiler manufacturers, tube fabricators, and consulting companies meet three times a year to review the progress on the program. In addition, frequent contacts are made with representatives of several paper companies to discuss program activities.

ESTIMATED ENERGY SAVINGS

Recovery boilers typically provide about 60% of the power for kraft mills, so continued operation is critical. Reductions in the downtime will provide an energy savings that is proportional to the number of operating days gained.

Synthesis and Design of Silicide Intermetallic Materials

J. J. Petrovic, R. G. Castro, D. P. Butt, Y. Park,
R. U. Vaidya, K. J. Hollis, and H. H. Kung
Los Alamos National Laboratory
Los Alamos, New Mexico 87545

INTRODUCTION

The overall objective of this program is to develop structural silicide-based materials with optimum combinations of elevated-temperature strength/creep resistance, low-temperature fracture toughness, and high-temperature oxidation and corrosion resistance for applications of importance to the U.S. processing industry. A further objective is to develop silicide-based prototype industrial components. The ultimate aim of the program is to work with industry to transfer the structural silicide materials technology to the private sector in order to promote international competitiveness in the area of advanced high-temperature materials and important applications in major energy-intensive U.S. processing industries.

The program currently has a number of developing industrial connections, including a CRADA with Johns Manville Corporation targeted at the area of $MoSi_2$-based high-temperature materials and components for applications in fiberglass melting and processing. We also are developing an interaction with the Institute of Gas Technology (IGT) to develop silicides for high-temperature radiant gas–burner applications, for the glass and other industries. With Combustion Technology Inc., we are developing silicide-based periscope sight tubes for the direct observation of glass melts. With Accutru International Corporation, we are developing silicide-based protective sheaths for self-verifying temperature sensors that may be used in glass furnaces and other industrial applications.

SUMMARY OF TECHNICAL PROGRESS: OCTOBER 1997–JUNE 1998

CRADA with Johns Manville Corporation

The kinetics of corrosion of plasma-sprayed and extruded $MoSi_2$ materials were investigated in molten alkali borosilicate glass under static and dynamic conditions at 1000 to 1550ºC for 0.5 to 1510 h. The corrosion behavior was compared with that of zirconia, alumina, yttria, mullite, yttria-alumina garnet (YAG), alumina-zirconia-chrome-silica refractory (AZCS), YAG-molybdenum disilicide composites, zirconia-molybdenum disilicide composites, molybdenum, niobium, and a molybdenum–5 wt % titanium alloy. The corrosion rates were evaluated by measuring dimensional changes above, at, and below the molten glass line. It was shown that the $MoSi_2$ materials were generally superior in performance to the other refractory materials with the exception of MgO-stabilized zirconia and AZCS, which were superior to $MoSi_2$ at the glass line but exhibited relatively similar corrosion rates above and below the glass line.

The mechanisms of corrosion were investigated. The corrosion behavior was evaluated by measuring dimensional changes above, at, and below the molten-glass line and through microstructural studies using transmission and scanning electron microscopy and X-ray diffraction. The mechanisms of corrosion vary with location in or above the glass melt due to changes in the activity of oxygen and the propensity for dissolution of Si. It was demonstrated that above the glass line, $MoSi_2$ forms a relatively good protective layer of silica. Below the glass line, Si depletion through dissolution leads to the development of a protective Mo-rich layer composed of Mo_5Si_3 and discontinuous Mo oxides, Mo particles, and crystalline SiO_2. At the glass line, neither a protective silica layer nor an Mo-rich layer forms due to the combined effect of rapid dissolution of SiO_2 and simultaneous vaporization of Mo products caused by the locally high oxygen activity. Thus, the rate of corrosion of pure $MoSi_2$ at the glass line is comparatively rapid. Although the mechanisms are different, the corrosion rates above and below the glass line were relatively similar. Dynamic glass-corrosion tests demonstrated that the corrosion rates were independent of glass-flow rate, suggesting that the processes are not rate limited by cation or anion transport through the melt. A phenomenological model was developed to describe the overall processes of corrosion at each of the three locations.

Interaction with Institute of Gas Technology

The testing of a suite of materials in a gas radiant tube furnace facility was performed at IGT during March 10–27, 1998. The materials, in the form of rectangular bend bar–type specimens, were placed at three locations inside and outside of the IGT radiant burner U-tube. The specimens inside the U-tube were exposed to the combustion gas environment. The specimens outside the U-tube were exposed to an endothermic environment. The test ran for 339 h.

The materials tested by IGT were the following:

- Plasma-sprayed $MoSi_2$ (73 samples)
- Plasma-sprayed Mo_5Si_3 (61 samples)
- SCRB210 SiC (101 samples)
- $MoSi_2$ "C" hot-pressed discs (32 samples)
- $MoSi_2$-A10/SiC hot-pressed composites (32 samples)
- $MoSi_2$-E10/Si_3N_4 hot-pressed composites (32 samples)
- IC221M – A1–24 (24 samples provided by ORNL)
- FA386M2 – B1–24 (24 samples provided by ORNL)
- IC438 – C1–13 (13 samples provided by ORNL)

The test conditions were the following. The nominal air flow and natural gas flow to the radiant-burner U-tube at high-fire conditions was 3030 SCFH and 300 SCFH, respectively. The low-fire rates were 780 SCFH of air and 75 SCFH of natural gas. The average temperatures of the specimens inside the U-tube were approximately 15 to 30ºF

hotter than that of the furnace temperature once the furnace was equilibrated. There were peak temperatures as high as 1925ºF during startup. At high-fire conditions, the average temperature of the samples on the outside of the burner (carburizing side) was approximately 1830ºF when the furnace was pressurized with nitrogen, and approximately 1815ºF in the endothermic atmosphere. At low-fire conditions, the temperature varied between 1845 and 1815ºF in the nitrogen atmosphere and 1835 to 1805ºF in the endothermic atmosphere.

The samples inside the U-tube were exposed to higher combustion temperatures. The highest temperature observed was 2000ºF in the early stages of the test, and it decreased to 1950ºF once the system equilibrated. The average temperature at all three internal sample holders was 1875ºF during the endothermic atmosphere and approximately 1890ºF when the furnace was pressurized with a nitrogen atmosphere. The temperature of the internal specimens was approximately 1872ºF with respect to an average furnace temperature of 1810ºF. Temperature swings of approximately 75ºF were observed during both high- and low-firing conditions.

The total operating time of the furnace was 339 h, which included 210 h in a nitrogen atmosphere and 129 h in an endothermic atmosphere. The test was terminated at 339 h due to the detachment of some of the specimen holders on the inside and outside of the radiant U-tube.

Initial visual test results showed significant degradation of plasma-sprayed Mo_5Si_3 when exposed to both the combustion and the endothermic environments. Plasma-sprayed $MoSi_2$ also showed significant degradation when exposed to the combustion environment, with an improved performance when exposed to the endothermic heat-treating environment. Minimal damage was observed for the rest of the samples tested.

Interaction with Combustion Tec Inc.

We have been interacting with Combustion Tec Inc. to explore the development of a $MoSi_2$-based periscope sight tube, for use with its video monitoring system for viewing molten-glass surfaces on the inside of glass furnaces. Techniques were developed to plasma spray from a $MoSi_2$ tube approximately 6 in. in length and 1.5 in. in diameter. A fabricated $MoSi_2$ periscope sight tube was sent to Combustion Tec for performance testing. The performance test, which will require the insertion of the $MoSi_2$ tube into the glass melter, will cause a thermal-shock condition of the tube from room-temperature to approximately 1500ºC in a 30-s time period. Removal of the sight tube, which occurs over a 5-s time period, also provides a thermal-shock condition.

Interaction with Accutru International Corporation

We have been interacting with the Accutru International Corporation to explore the development of $MoSi_2$-based protection sheaths for their self-verifying temperature-measurement system. The Accutru self-verifying temperature-measurement system allows for the in situ calibration of a thermocouple while it is still in place in the high-temperature environment. The use of the Accutru system to measure the temperature of

molten-glass baths and/or the temperatures inside of glass furnaces requires that the temperature sensor elements be protected by a sheath material that is resistant to these highly corrosive high-temperature conditions. Our objective is to develop $MoSi_2$-based closed-end tubular protective sheaths by plasma spray–forming techniques that will be compatible with Accutru sensor systems and that can be tested in glass-melting furnaces.

Interaction with Oxford University

We have been interacting with Oxford University in the United Kingdom to explore the production of continuously reinforced SiC fiber–$MoSi_2$ matrix composites using a plasma-spray monotape technology. Such SiC fiber–$MoSi_2$ matrix composites would possess high fracture toughness and thermal-shock resistance.

$MoSi_2$ was successfully plasma sprayed onto the SiC fiber monotape, with good penetration of the $MoSi_2$ around the SiC fibers. Damage to the SiC fibers as a result of the $MoSi_2$ plasma-spraying process was observed to be minimal.

High Temperature Structural Silicides Conference

An Engineering Foundation High Temperature Structural Silicides Conference was held May 25–29, 1998, in Hyannis, Massachusetts. The conference had 50 attendees that were from the United States, Japan, China, United Kingdom, Germany, and Sweden. The conference chairs were A. K. Vasudevan, Office of Naval Research; J. J. Petrovic, Los Alamos National Laboratory; S. G. Fishman, Office of Naval Research; C. A. Sorrell, U.S. Department of Energy; and M. V. Nathal, NASA-Lewis Research Center.

The objective of the conference was to assess the state of the art of international materials research on high-temperature structural silicides. Forty-two technical presentations were given in the areas of Materials, Mechanical Behavior, Atomic Mechanisms, Fabrication, Properties, and Applications. The refereed proceedings of the conference are to be published in the *Journal of Materials Science and Engineering A* in 1999.

TECHNICAL PROGRESS: JULY–SEPTEMBER 1998

CRADA with Johns Manville Corporation

Glass-corrosion studies this quarter focused primarily on Mo_5Si_3 plasma-sprayed coatings. A static corrosion study was done at 1300°C for 1 h. Dimensional analysis of the corrosion coupons is in progress. Due to the thin thickness of the coating and catastrophic oxidation of materials at and above the glass line as shown in Fig. 1, a comparison of material loss could not be obtained. Next quarter, we are planning to compare material loss only below the glass line.

Figure 1 shows SEM morphologies of the plasma-sprayed Mo_5Si_3 exposed at 1300°C for 1 h. As shown in Fig. 1, the glass-line region split due to severe corrosion/oxidation at and above the glass line. The SEM microstructures and EDS analysis showed that Mo_5Si_3 oxidizes in the oxygen environment, forming mostly SiO_2 and Mo oxides (EDS showed

mostly MoO_3). The approximate ratio of SiO_2 and Mo oxides under SEM was 50 : 50. As we reported previously, a protective, continuous SiO_2 oxide layer could not form on the surface of Mo_5Si_3 due to pesting of nonprotective Mo oxide formation as products.

The severe corrosion at and above the glass line shown in Fig. 1 also prevented the observation of microstructural changes below the glass line after the corrosion test. Thus, the study of microstructural changes occurring during the corrosion of Mo_5Si_3 will be focused only on corrosion taking place below the glass line.

Next quarter, we also will initiate corrosion studies of single-crystal $MoSi_2$ and Mo_5Si_3 in molten-glass environments.

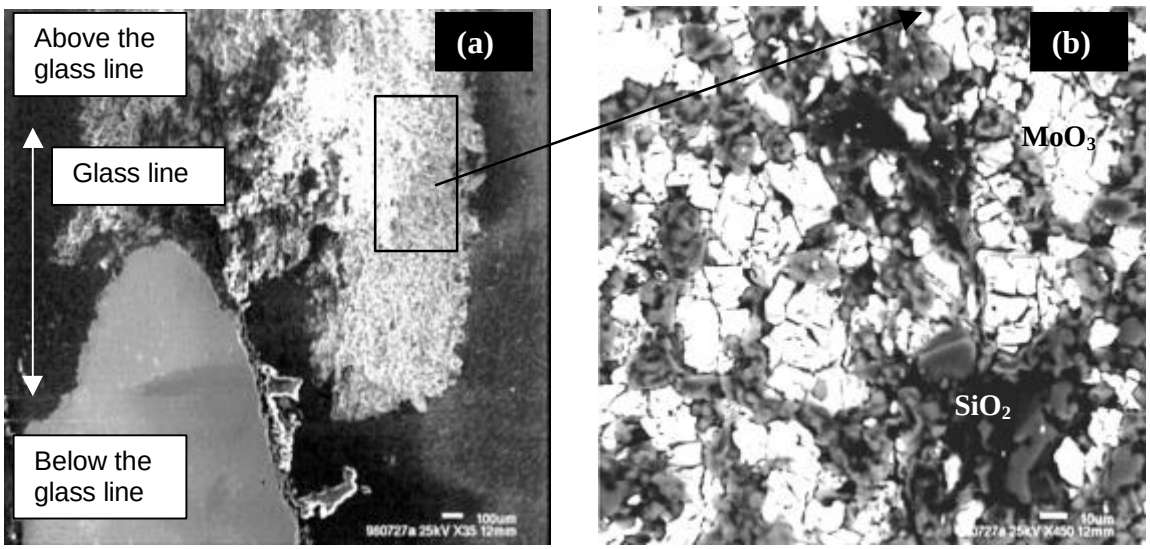

Fig. 1. SEM observation of plasma-sprayed Mo_5Si_3 near the glass line exposed at 1300°C for 1 h. View (a) shows near-glass-line morphology exhibiting severe corrosion/oxidation at the glass line, and view (b) shows above-the-glass-line morphology observed from the square regions exhibiting SiO_2 and MoO_3 formation as products.

Institute of Gas Technologies Interaction

We have continued investigations on the stability of molybdenum-based silicides in combustion and endothermic heat-treating environments. The temperature history of the four-point bend samples varied depending on the location of the sample holders on the radiant U-tube. In general, the test samples on the interior of the U-tube (combustion environment) experienced a higher temperature than the samples on the exterior of the tube (endothermic environment). A summary of the temperature history observed during the furnace operation is given in Table 1.

Table 1: Summary of the Temperature History During Furnace Operations

Four-point bend samples exposed to the endothermic environment: Ao, Bo, and Co • Average temperature of the four-point bend samples on the outside of the U-tube (endothermic environment) was approximately 15 to 30ºC hotter than the furnace temperature. • Temperatures of the samples were approximately 1000ºC when the atmosphere in the furnace was nitrogen and approximately 990ºC in the endothermic atmosphere. • The temperature varied from one location to another by approximately 25ºC depending on high- or low-fire conditions. • Samples located in the A position had the highest temperature during the high-fire operation and the lowest temperature during low-fire conditions.
Four-point bend samples exposed to the combustion environment: Ai, Bi, and Ci • Samples located inside the U-tube were exposed to the higher temperatures of the combustion flame. The highest peak temperature recorded was approximately 1095ºC. • The average temperature at all three holders was approximately 1025ºC during the endothermic atmosphere and approximately 1030ºC when the furnace was under a nitrogen atmosphere. • The average temperature of the internal coupons was 1020ºC with respect to the average furnace temperature of 985ºC. • The temperature varied from one location to another by approximately 25ºC, depending on the high- or low-firing operation conditions. • The samples located in the A position had the highest temperature during high fire and the lowest temperature during low fire.

Visual inspection of the four-point bend samples showed significant oxidation of the plasma-sprayed Mo_5Si_3 when exposed to the combustion and endothermic environments. Plasma-sprayed $MoSi_2$ also showed significant oxidation when exposed to the combustion environment, with an improved performance when exposed to the endothermic heat-treating environment. The accelerated oxidation that was observed in the plasma-sprayed materials was not present in the hot-pressed $MoSi_2$ and the $MoSi_2$ composites. Analysis of these samples revealed the presence of both SiO_2 and Mo oxides on the surface of the four-point bend samples. Differences in the oxidation behavior can be attributed to the loss of silicon during the plasma-spray process, which results in a molybdenum-rich, silicon-depleted material. As a result of this silicon loss, a large volume fraction of Mo_5Si_3 can be present throughout the $MoSi_2$ matrix, Fig. 2. Mo_5Si_3 has been shown to have poor oxidation resistance at elevated temperatures**.** The observed catastrophic failure of the plasma-sprayed Mo_5Si_3 in the combustion and endothermic environments also demonstrates the poor oxidation resistance of this material.

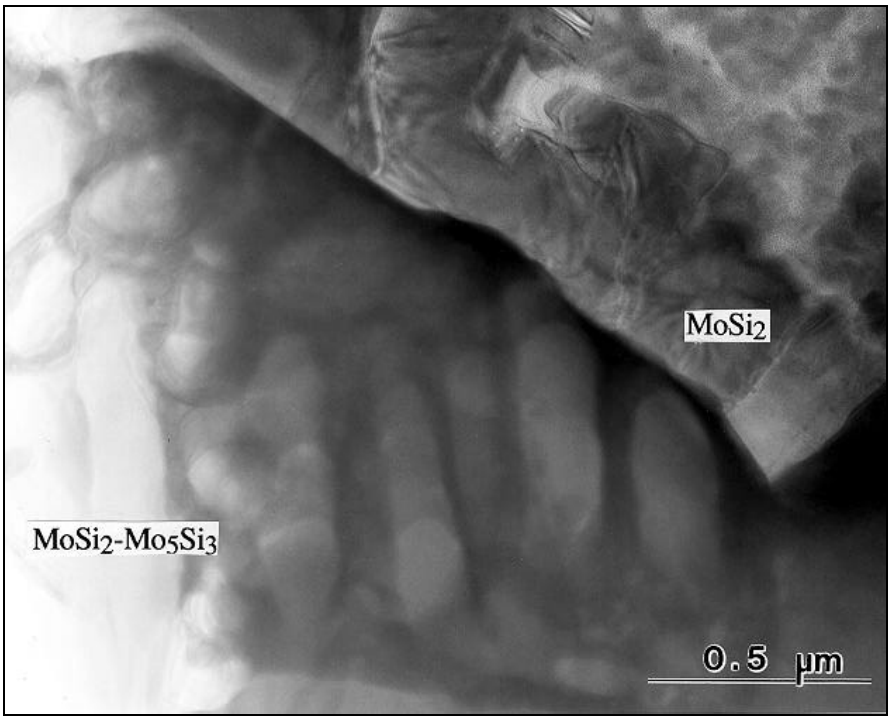

Fig. 2: TEM micrograph of as-sprayed $MoSi_2$ showing the presence of a $MoSi_2$-Mo_5Si_3 eutectic.

The surface morphologies of the materials were characterized by SEM and EDS. The morphologies are shown in Fig. 3 for hot-pressed $MoSi_2$, plasma-sprayed $MoSi_2$, and $MoSi_2$-Si_3N_4 composites. The EDS results in Table 2 show that all of the $MoSi_2$, Mo_5Si_3, and $MoSi_2$-SiC, $MoSi_2$-Si_3N_4 materials exhibit SiO_2 and Mo oxide formation from the molybdenum silicide and SiO_2 from the SiC and Si_3N_4 materials. The formation of products in the endothermic environment for each material will be characterized. To date, more Mo oxide formation in the combustion environment has been observed, a result of the accelerated formation of Mo oxides/less formation of SiO_2 caused by the lower oxygen activities in the combustion environments as compared with those in pure air.

Due to severe oxidation of the plasma-sprayed samples, four-point bend testing after exposure to the endothermic and combustion environments was not possible. In addition, bend test samples that were adjacent to the plasma-sprayed samples in the holders were also damaged/cracked as a result of the expansion that occurred during oxidation of the plasma-sprayed samples. Four-point bend strength results of the silicide-based materials in the as-machined condition and after exposure to the endothermic and combustion environments are summarized in Table 3.

Test results indicated a 28% increase in strength of the $MoSi_2$/30SiC samples, from 341.5 MPa to approximately 438 MPa after exposure to both the combustion and endothermic environments. Investigations currently are being performed to determine the cause of the observed strength increase. Changes in the strength of $MoSi_2$/30Si_3N_4 samples were relatively small and not statistically significant. The strength of the plasma-

sprayed (157.9 MPa) and hot-pressed (153.8 MPa) $MoSi_2$ in the as-machined condition were similar but below the strength levels of plasma-sprayed Mo_5Si_3 (251.8 MPa).

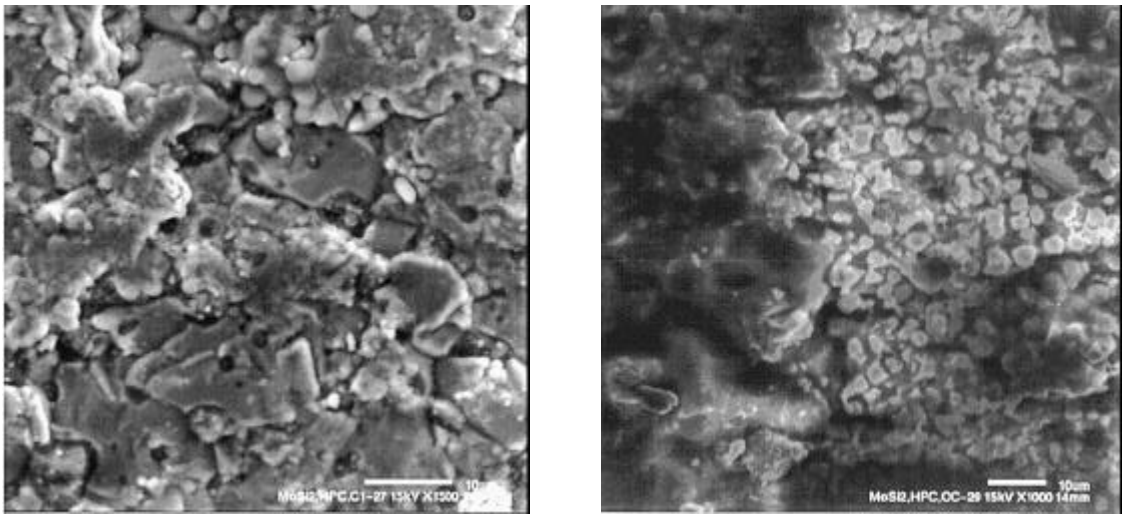

Outer surface morphology of hot-pressed $MoSi_2$ exposed (l) inside of radiant U-tube (CI-27) and (r) outside of radiant U-tube (OC-29).

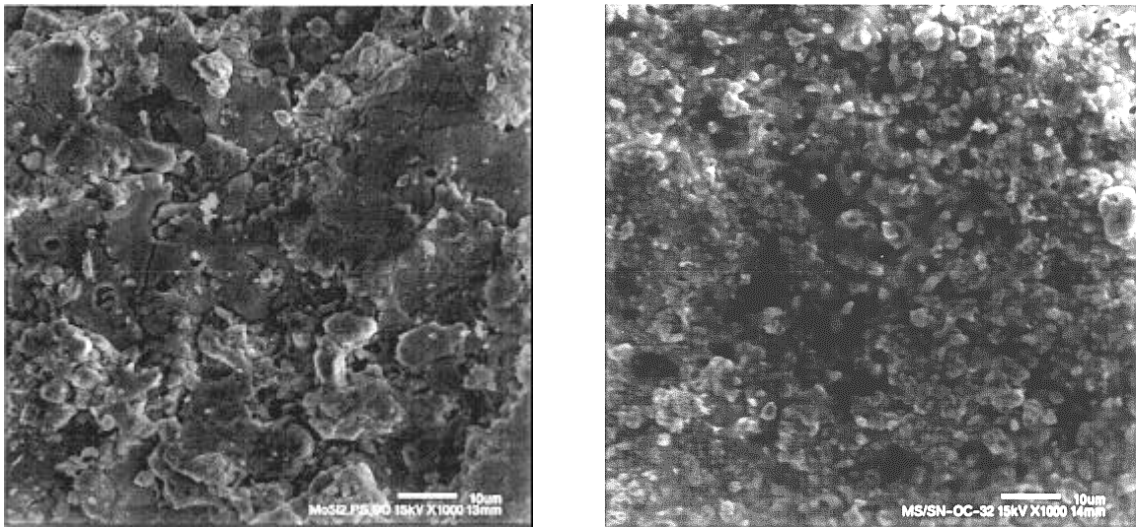

Outer surface morphology of plasma-sprayed (l) $MoSi_2$ and (r) $MoSi_2$–30% Si_3N_4 composite exposed outside of radiant U-tube.

Fig. 3. SEM observation of hot-pressed $MoSi_2$, plasma-sprayed $MoSi_2$, and $MoSi_2$–30% Si_3N_4 composites exposed at 1000 to 1020°C.

Table 2: EDS Results from the Outer Surface of the Specimens Exposed in Combustion Environments

(S: small intensity peak)

Sample	Mo	Si	O	Fe	Ca	Al	S	Remarks
$MoSi_2$								
HPC C1-27	0	0	0					SiO_2/Mo oxides
HPC OC-29	S	0	0	0				Mostly SiO_2 (little Mo oxides)
PS C1-11	S	0	0	0				Mostly SiO_2 (little Mo oxides)
PS CO	0	0	0					SiO_2/Mo oxides
$MoSi_2$-Si_2								
OC-37		0	0				0	SiO_2 with S impurity
$MoSi_2$-SiC								
C1-37		0	0	S				SiO_2
$MoSi_2$-Si_3N_4								
C1-32	0	0	0	0	0			SiO_2/Mo oxides
OC-32	0	0	0		0			SiO_2/Mo oxides
SCRB-210								
C1-8		0		0	0		0	SiO_2 with impurities
OC-8		0	0		0		0	SiO_2 with Sulfur
Mo_5Si_3								
C1-PS	0	0	0					Mostly SiO_2 (little Mo oxides)
CO-19PS		0	0	0				SiO_2 with Fe (less Mo oxides)

Table 3: Four-Point Bend Strength (MPa) of Plasma-Sprayed (PS) $MoSi_2$ and Mo_5Si_3 and Hot-Pressed (HP) $MoSi_2$, $MoSi_2$/30SiC, and $MoSi_2$/30 Si_3N_4

Condition	PS $MoSi_2$	PS Mo_5Si_3	HP $MoSi_2$	HP $MoSi_2$/30SiC	HP $MoSi_2$/30Si_3N_4
as-machined	157.29	251.86	153.8	341.5	462.3
Combustion	oxidized	oxidized	broke	438.7	464.3
Endothermic	oxidized	oxidized	broke	438.0	484.8

Oxford University Collaboration

Oxford University has successfully completed a 4-layer Sigma 1140+ fiber-reinforced $MoSi_2$ and $MoSi_2$+SiAlON composite with excellent fiber spacing and minimal fiber damage. After heat-treating at 1500ºC followed by furnace cooling, no matrix cracking was observed in the composites. Future investigations will focus on the use of an SCS-9 SiC fiber that has a carbon core. The Sigma 1140+ fiber has a tungsten core and is not suitable for high-temperature applications above 1000ºC. An SiC-coated SCS-9 fiber also will be evaluated to minimize interfacial reaction between the fiber and the $MoSi_2$ matrix. Consolidation of the continuously reinforced layered composite will be evaluated using hot isostatic pressing (HIP) and hot pressing. The physical and mechanical properties of the composite will be evaluated, including the CTE of matrix, electrical conductivity, pesting and oxidation properties, interfacial strength, fiber tensile properties, bend strength, fracture toughness, and creep properties. Consolidation of the composite material will be investigated at LANL.

DOE/OIT Glass Call ’99 Proposal

A proposal titled “Molybdenum Disilicide Composites for Glass Processing Sensors” was submitted to the DOE/OIT Glass Lab Call ’99 in June 1998. We proposed a program to develop strong, tough, and thermal shock–resistant molybdenum disilicide hybrid composite tubes by plasm spray–forming techniques that can be employed for a variety of advanced sensors and controls for the glass industry. LANL will test these tubes as protective sheaths for the advanced temperature sensors being developed for the glass industry by the Accutru International Corporation and as periscope sight tubes for closed-circuit video glass-furnace sensors marketed by Combustion Tec. Inc. The research performed at LANL has shown that $MoSi_2$ materials are highly resistant to corrosion in molten glasses and their performance in molten glass is similar to the refractory ceramic AZS, which is used widely in the glass industry. $MoSi_2/Si_3N4$-SiC fiber composites possess the mechanical characteristics necessary for applications inside glass furnaces where thermal stresses and thermal-shock conditions require materials that can stand up to these severe mechanical requirements. Preliminary studies have established the feasibility of plasma spray forming both $MoSi_2/Si_3N_4$ particulate–reinforced composites and $MoSi_2$/SiC fiber composites. $MoSi_2$-oxide laminate tube geometries also have been produced by plasma-spray forming and are under consideration for glass industry sensor applications.

Our Proposal was selected for funding by DOE/OIT. These activities have commenced in October 1998. There will be a 50% cost sharing each year from our industrial partners Accutru International Corporation, Combustion Tec Inc., Plasma Process Inc., and Exotherm Inc. In FY 1999, we will establish and optimize plasma spray–forming techniques for $MoSi_2$-oxide laminate composite and $MoSi_2/Si_3N_4$-SiC fiber hybrid composite tube geometries and evaluate the composite mechanical properties and corrosion resistance in molten glasses. In FY 2000, we will fabricate prototype composite temperature-sensor sheath and periscope sight tubes and perform preliminary tests in glass-melting furnaces in association with Accutru and Combustion Tec. In FY 2001, we will demonstrate an Accutru glass furnace temperature-measurement sensor system and a

Combustion Tec closed-circuit glass furnace video-monitoring system that will use composite tubes as critical components for dramatically improved glass sensor performance.

Facility Upgrades

A Fanuc S-10 industrial robot was purchased and installed in the thermal-spray booth at LANL. The robot has six axes of motion and will be capable of spraying long (~ 36-in.) sheathing tubes for glass-processing sensors. An acceptance test and training course on the operation of the robot was conducted September 28–29, 1998, at LANL. An SG-100 plasma-spray torch has been mounted on the robot arm, and a demonstration has been performed on coating Al_2O_3 thermocouple tubes with $MoSi_2$. The robot will be used to support the development of $MoSi_2$-based glass-processing sensors.

PUBLICATIONS

Journals

J. J. Petrovic, M. I. Pena, I. E. Reimanis, M. S. Sandlin, S. D. Conzone, H. H. Kung, and D. P. Butt, "Mechanical Behavior of $MoSi_2$-Reinforced Si_3N_4 Matrix Composites," *J. Am. Ceram. Soc.* **80**, 3070–76 (1997).

H. Kung, Y. C. Lu, A. H. Bartlett, R. G. Castro, and J. J. Petrovic, "Structural Characterization of Combustion Synthesized $MoSi_2$-Si_3N_4 Composite Powders and Plasma Sprayed $MoSi_2$-Si_3N_4 Composites," *J. Mater. Res.* **13**, 1522–29 (1998).

J. J. Petrovic and A. K. Vasudevan, "Key Developments in High Temperature Structural Silicides," accepted for publication in *Materials Science and Engineering A*, 1999.

K. K. Chawla, J. J. Petrovic, J. Alba, and R. Hexemer, "Phase Identification in Reactively Sintered Molybdenum Disilicide Composites," accepted for publication in *Materials Science and Engineering A*, 1999.

A. M. Baker, P. S. Grant, R. G. Castro, and H. Kung, "Preliminary Characterization of a Plasma Sprayed $MoSi_2$/Sigma SiC Fibre Monotape," accepted for publication in *Materials Science and Engineering A*, 1999.

Y. Park, D. P. Butt, R. Castro, J. Petrovic, and W. Johnson, "Durability of Molybdenum Disilicide in Molten Alkali Borosilicate Glass," accepted for publication in *Materials Science and Engineering A*, 1999.

Y. S. Park, R. G. Castro, K. J. Hollis, J. J. Petrovic, and D. P. Butt, "Corrosion of Molybdenum Disilicide Materials in Molten Alkali Borosilicate: I Kinetics and Comparison to Other Refractories," submitted to *J. Am. Ceram. Soc.*, 1998.

Y. S. Park, R. D. Field, J. J. Petrovic, and D. P. Butt, "Corrosion of Molybdenum Disilicide Materials in Molten Alkali Borosilicate Glass: II: Microscopy and Mechanisms," submitted to *J. Am. Ceram. Soc.*, 1998.

S. D. Conzone, D. P. Butt, and A. H. Bartlett, "Joining $MoSi_2$ to 316L Stainless Steel," *J. Mater. Sci.* **32**, 3369–74 (1997).

R. U. Vaidya, P. Rangaswamy, M. A. M. Bourke, and D. P. Butt, "Measurement of Bulk Residual Stresses in Molybdenum Disilicide/Stainless Steel Joints Using Neutron Scattering," accepted for publication in *Acta Materialia*, 1997.

R. U. Vaidya, A. H. Bartlett, H. H. Kung, and D. P. Butt, "Joining of $MoSi_2$ to Itself and Reactions with Aluminum Interlayers," accepted for publication in *J. Mater. Sci. Letters*, 1997.

Other Publications

J. J. Petrovic, "High Temperature Structural Silicides," *Ceram. Eng. Sci. Proc.* **18**, 3–17 (1997).

D. E. Alman, J. A. Hawk, J. J. Petrovic, C. H. Henager, and M. Singh, "Abrasive Wear Behavior of $MoSi_2$-SiC Composites," pp. 51–61 in *Wear of Engineering Materials*, ed. J. A. Hawk, ASM International, c. 1998.

R. G. Castro, R. U. Vaidya, A. Ayala, B. D. Bartram, D. E. Gallegoes, and H. S. Kurek, "Evaluation of Molybdenum-Based Silicides in a Combustion and Endothermic Environment," to be published in *Proceedings of the United Thermal Spray Conference*, Dusseldorf, Germany, March 17–19, 1999.

R. U. Vaidya, A. H. Bartlett, S. D. Conzone, and D. P. Butt, "Investigations into the Joining of $MoSi_2$ to 316L Stainless Steel," in *Ceramic Joining*, eds. I. Reimanis, C. Henager Jr., and A. Tomsia, pp. 63–74, American Ceramic Society, Westerville, Ohio, c. 1997.

Y. S. Park, D. P. Butt, K. J. Hollis, R. G. Castro, and J. J. Petrovic, "Viability and Degradation of Molybdenum Disilicide Materials in Molten Glass Environments," *Proceedings, 22nd Cocoa Beach Conference on Composites, Advanced Ceramics, Materials and Structures*, American Ceramic Society Engineering Ceramics Division, January 1998, Cocoa Beach, Florida.

R. G. Castro, K. J. Hollis, H. H. Kung, and A. H. Bartlett, "Molybdenum Disilicide Composites Produced by Plasma Spraying," *Proceedings, 15th International Thermal Spray Conference*, May 25–29, 1998, Nice, France, Vol. II, pp. 1199–1204.

J. J. Petrovic, "Ceramic-Silicide Composites," to be published in *Proceedings of the World Ceramics Congress*, June 14–19, 1998, Florence, Italy.

PRESENTATIONS

Invited Presentations

J. J. Petrovic, "Key Developments in High Temperature Structural Silicides," Keynote Presentation, Engineering Foundation High Temperature Structural Silicides Conference, May 25–29, 1998, Hyannis, Massachusetts.

K. K. Chawla, J. Alba, J. J. Petrovic, and R. L. Hexemer, "Phase Identification in Reactively Sintered Molybdenum Disilicide Composites," Engineering Foundation High Temperature Structural Silicides Conference, May 25–29, 1998, Hyannis, Massachusetts.

J. J. Petrovic, "Ceramic-Silicide Composites," World Ceramics Congress, June 14–19, 1998, Florence, Italy.

Other Presentations

Y. S. Park, D. P. Butt, K. J. Hollis, R. G. Castro, and J. J. Petrovic, "Viability and Degradation of Molybdenum Disilicide Materials in Molten Glass Environments," 22nd Cocoa Beach Conference on Composites, Advanced Ceramics, Materials, and Structures, American Ceramic Society Engineering Ceramics Division, January 1998, Cocoa Beach, Florida.

A. M. Baker, P. S. Grant, R. Castro, and H. Kung, "Preliminary Characterization of Plasma Sprayed $MoSi_2$/Sigma SiC Fibre Monotapes," Engineering Foundation High Temperature Structural Silicides Conference, May 25–29, 1998, Hyannis, Massachusetts.

Y. S. Park, R. G. Castro, K. Hollis, J. J. Petrovic, and D. P. Butt, "Durability of Molybdenum Silicide Materials in Molten Alkali Borosilicate Glass," Engineering Foundation High Temperature Structural Silicides Conference, May 25–29, 1998, Hyannis, Massachusetts.

R. G. Castro, H. Kung, K. J. Hollis, and J. J. Petrovic, "Applications of Molybdenum Disilicide Composites Produced by Plasma Spraying," Engineering Foundation High Temperature Structural Silicides Conference, May 25–29, 1998, Hyannis, Massachusetts.

R. G. Castro, K. J. Hollis, H. H. Kung, and A. H. Bartlett, "Molybdenum Disilicide Composites Produced by Plasma Spraying," 15th International Thermal Spray Conference, May 25–29, 1998, Nice, France.

R. G. Castro, J. J. Petrovic, D. P. Butt, K. J. Hollis, H. H. Kung, and Y. Park, "Durability of $MoSi_2$ in High Temperature Industrial Applications," DOE/OIT Advanced Industrial Materials Annual Meeting, June 23–25, 1998, Jackson Hole, Wyoming.

J. J. Petrovic, R. G. Castro, D. P. Butt, K. J. Hollis, and Y. Park, "Advanced High Temperature Materials for Glass Applications," DOE/OIT Glass Industry Project Review, August 12–13, 1998, Argonne, Illinois.

HONORS AND AWARDS

J. J. Petrovic was a Co-Organizer of the Engineering Foundation High Temperature Structural Silicides Conference, May 25–29, 1998, Hyannis, Massachusetts.

PATENTS/DISCLOSURES

None.

Licenses

None.

INDUSTRIAL INPUT AND TECHNOLOGY TRANSFER

Johns Manville Corporation

We have a CRADA with Johns Manville Corporation to develop $MoSi_2$-based materials for fiberglass processing.

Institute of Gas Technology (IGT)

We are interacting with IGT to perform tests on $MoSi_2$-based materials in radiant gas combustion tube environments.

Exotherm Corporation

We have been investigating the plasma spraying of advanced $MoSi_2$, Mo_5Si_3, and composite powders from the Exotherm Corporation.

Combustion Tec, Inc.

We are interacting with Combustion Tec to develop a $MoSi_2$ sight tube for a glass-furnace monitoring system that can withstand 3000ºF at the glass-furnace wall.

Accutru International Corporation

We are interacting with Accutru International to develop $MoSi_2$-based composite protection sheaths for their self-verifying temperature-measurement system for glass furnaces.

Plasma Process Inc.

We are interacting with Plasma Process Inc. to transfer the plasma spray–forming technology that we have developed for $MoSi_2$-based materials and composites.

Oxford University

We are interacting with Oxford University to examine the plasma-spray fabrication of continuous SiC fiber–$MoSi_2$ matrix composites.

Uniform-Droplet Spray Forming

C. A. Blue and V. K. Sikka
Metals and Ceramics Division
Oak Ridge National Laboratory
P.O. Box 2008, Oak Ridge, Tennessee 37831

J.-H. Chun
Massachusetts Institute of Technology
Laboratory of Manufacturing and Productivity
77 Massachusetts Avenue, Cambridge, Massachusetts 02139

T. Ando
Department of Mechanical Engineering
Northeastern University, 334SN
Boston, Massachusetts 02115

INTRODUCTION

This report summarizes the joint study, "Uniform-Droplet Spray Process," sponsored by the U.S. Department of Energy, Assistant Secretary for Energy Efficiency and Renewable Energy, Office of Industrial Technologies, Advanced Industrial Materials (AIM) Program, under contract DE-AC05-96OR22464 with Lockheed Martin Energy Research Corp. It was conducted at Oak Ridge National Laboratory (ORNL), Massachusetts Institute of Technology (MIT), and Northeastern University with the objective of studying the uniform-droplet spray (UDS) process (1–5) for advanced industrial materials processing.

Two important areas of advanced materials processing are addressed: advanced particulate production and controlled spray deposition. While the former area deals with the production and controlled solidification of UDSs, the latter area deals with controlled deposition of UDSs.

Products in the particulate area are spherical balls and flakes of metals and alloys produced by the solidification of a UDS. Strong interest already has been identified in electronics packaging in which UDS-processed ball grid array (BGA) solder balls are expected to replace those produced by conventional, cut-wire spheroidization. The advantage of the UDS process is expected to drive the technology toward higher-melting–temperature BGA balls with smaller diameters required in higher-density packaging. Other applications of UDS-processed particulate materials are expected to follow with the development of methods for multiple-orifice spraying, controlled secondary quenching, melt cleaning/filtration, high-temperature melt delivery, and stable jet breakup in finer droplet-size ranges, all of which are important aims in the joint study.

Products in the spray-deposition area vary from coatings to near-net-shape or net-shape spray deposits and are characterized by ultimate levels of microstructural control permitted by the decoupled spray parameters. Among the new opportunities envisioned

are porosity-free deposition, precise microstructural control, production of novel microstructures and materials, and the potential for net-shape and near-net-shape processing. The joint study has generated significant fundamental knowledge on the droplet generation, droplet manipulation, in-flight solidification, and droplet deposition, with the particular objective of applying the UDS process to the continuous production of flat products (e.g., sheet, strip, and coatings). Current efforts are focused on aluminum sheet production.

OAK RIDGE NATIONAL LABORATORY TECHNICAL PROGRESS: FY 1998

Summary

The main focus of the work at ORNL has been in the area of extending the UDS process to high-temperature engineering alloys. This development started with the construction of a low-temperature (300°C) apparatus, which was utilized to gain the appropriate base technology and verify results previously produced by MIT. Upon completion of this phase, a medium-temperature apparatus was developed and constructed that is capable of spraying at temperatures up to approximately 1200°C. This work continued in the 1998 calendar year. With this system, aluminum- and copper-based alloys have been successfully sprayed: 6061 Al, Cu–8% P, Cu–10% Sn, and Cu (all in the 150- to 300-μm powder-size range).

This year consisted of finishing the work with the medium-temperature system while developing the high-temperature system. Challenges with the high-temperature system include materials compatibility, temperature gradients through high-temperature crucibles, orifice clogging, and orifice placement. When spraying higher-melting alloys, reaction kinetics have been looked into extensively for each material to be sprayed. In an effort to try to spray as many materials as possible with the same crucible, alumina was chosen for preliminary high-temperature spraying. This is the same material used for the nozzle. Calculations and experimental data have revealed temperature gradients as large as 300°C from the inside to the outside of the crucible. This has caused freezing in the nozzle. External insulation on the bottom of the ceramic crucible has been incorporated to minimize these temperature gradients. The other area of critical importance is orifice placement in the bottom of the crucible. A series of high-temperature adhesives and an orifice housing design have been implemented to eliminate orifice blowout. Work with Hoeganaes (Riverton, New Jersey) and Jim Ingram (Hoeganaes Pilot Plant Manager) was accomplished in order to extract industrial spraying experience. Currently, ORNL has UDS capabilities up to 1500°C. Because ORNL has the highest temperature spray capabilities, three separate companies [Uniform Metals Technologies, Inc. (Watertown, Massachusetts), Micro Engineering (Cinnaminson, New Jersey), and ACuPowder International (Union, New Jersey)] spent time and worked with ORNL to better understand the UDS process and systems.

This year, the primary focus has been in the area of multinozzle spraying and high-temperature spraying. The multinozzle work has been accomplished in conjunction with the splat and spreading work accomplished at MIT and Northeastern University in order

to develop the necessary parameters for spraying aluminum sheet. The basic work here will be translatable to other materials.

The initial high-temperature spraying has commenced in the area of low-temperature intermetallics. This area has experienced temperature problems. Due to the large temperature gradient at the bottom of the crucible, much higher temperatures have to be obtained in the melt to prevent the jet from freezing in the nozzle. Three heating assemblies have been burned out. Currently, induction is being routed to the high-temperature UDS apparatus to eliminate this problem. This also is being looked at because if commercial implementation of the technology is to occur, induction melting is a common tool utilized in industry. Upon successful completion of this work and gaining further high-temperature knowledge, work with high-temperature intermetallics and stainless steels will continue.

Multiple-Orifice Spraying

Due to interest shown by Alcoa Aluminum in aluminum sheet forming and a task outlined for this year's work of multiple-orifice spraying on aluminum sheet, a spray plate containing two orifices was fabricated. Two orifices were mounted, and a parallel plate system was fabricated to charge the molten droplets as they are systematically broken at the jet tip. Initially, the system was tested with the low-temperature system to minimize variables. The material used was tin, with an orifice diameter of 100 μm. Initial testing was very encouraging. Simultaneous breakup of both jets using one piezoelectric jet destabilization system was accomplished. Sufficient spacing between the two orifices was used to ensure that field overlap between the droplets was not a issue. This will be discussed further in the work by Northeastern University.

NORTHEASTERN UNIVERSITY TECHNICAL PROGRESS: FY 1998

The accomplishments at Northeastern University are identified in several areas as summarized below.

Processing of Engineering Alloys

Our most important goal is to develop applications of the UDS process to engineering alloys in the areas of both particulate production and controlled spray deposition.

The UDS process can produce particulate in either spherical ball or flake form. In-flight solidification and fluid quenching produce spherical balls, while substrate quenching produces flakes. In the UDS process, secondary quenching of droplets can be done in any designated thermal state. The first commercial application of UDS-processed particulate has been the solder balls used in BGA electronics packaging (6). Potential areas of other particulate applications include fine, uniform spherical powders for injection molding and hot isostatic pressing, development of powders of difficult-to-process alloys (e.g., immiscible alloys), and advanced alloy powders with ultimate structural uniformity and metastability.

In the area of controlled spray deposition, our efforts have two foci. One of them concerns the application of UDS to the production of flat products of aluminum. The specific goals in this area of our work are to (1) develop a lab-scale, multiple-orifice linear UDS nozzle, (2) study the conditions for the production of porosity-free aluminum strip with the linear nozzle, and (3) characterize and evaluate the resultant strip. The other important area in our study of controlled spray deposition is the production of novel microstructures by such new approaches as epitaxial growth of rapidly solidified single-crystal alloys, reactive spray deposition to produce intermetallic coatings, and spray deposition of functionally graded coatings.

The following describes our current activity during FY 1998 in some of the above major areas.

1. Processing of aluminum and copper alloys

During the past 12 months, one of our major efforts has been to develop a UDS apparatus suitable for lab-scale experiments with aluminum and copper alloys and to study the processing conditions required for these materials. Figure 1 shows the UDS system developed at Northeastern University.

In our aluminum and copper projects, major challenges have been the high melt temperatures and aluminum's affinity with oxygen. To overcome these hurdles, we designed and built a new furnace system and an atmosphere-control system. The new furnace system consists of higher-temperature clamshell heaters and a boron nitride–coated graphite-melting crucible, both of which are contained in a new stainless steel furnace section. The furnace section has side view ports for monitoring and a top plate that permits power and gas supplies, as well as connection to the vibration system. The graphite crucible adopts a design that permits the use of an orifice-holder insert. The insert can contain one or more orifices depending on the type of experiments. The chamber atmosphere must be controlled to be inert to ensure stable uniform breakup of the molten jet ejected from the orifice(s). It also affects the solidification of the droplets as will be discussed in a later section. The atmosphere-control system consists of a rotary vacuum pump, an oxygen-gettering furnace, an in-line desiccator, a circulation pump, a chamber pressure controller, and an oxygen monitor.

Aluminum experiments typically require that the oxygen content be kept below 1 ppm, especially in the region near the orifice. To maintain such a low oxygen content, the chamber atmosphere must be maintained at a slightly positive pressure at all times during an experiment in order to prevent any migration of air into the system through tubing connections and other fittings used in the system. Experiments with copper alloys do not require oxygen removal by ion-getting and can be performed under regular nitrogen gas atmosphere while venting the excess chamber gas to the atmosphere.

A typical view of uniform breakup of an aluminum jet is shown in Fig. 2. The alloy processed was Al-6 Cu-0.4 Zr (in weight percent). A 152-μm–diam sapphire orifice was used to eject the melt at a crucible pressure of 74 kPa. The experiment was performed at a melt temperature of 1023 K, which corresponded to a melt superheat of 100 K for the alloy. The chamber atmosphere was ultrahigh-purity argon in which the oxygen content

was controlled at 0.4 ppm using the atmosphere-control system. At a vibration frequency of 7.33 kHz, the 152-μm jet broke into uniform droplets whose solid mean diameter was determined to be 282 μm. Due to a chamber height limitation, the uniform droplets were quenched into silicone oil at a flight distance of 0.25 m to allow for full solidification into spherical particles. Use of a taller chamber and finer orifice diameter permits full in-flight solidification of the droplets.

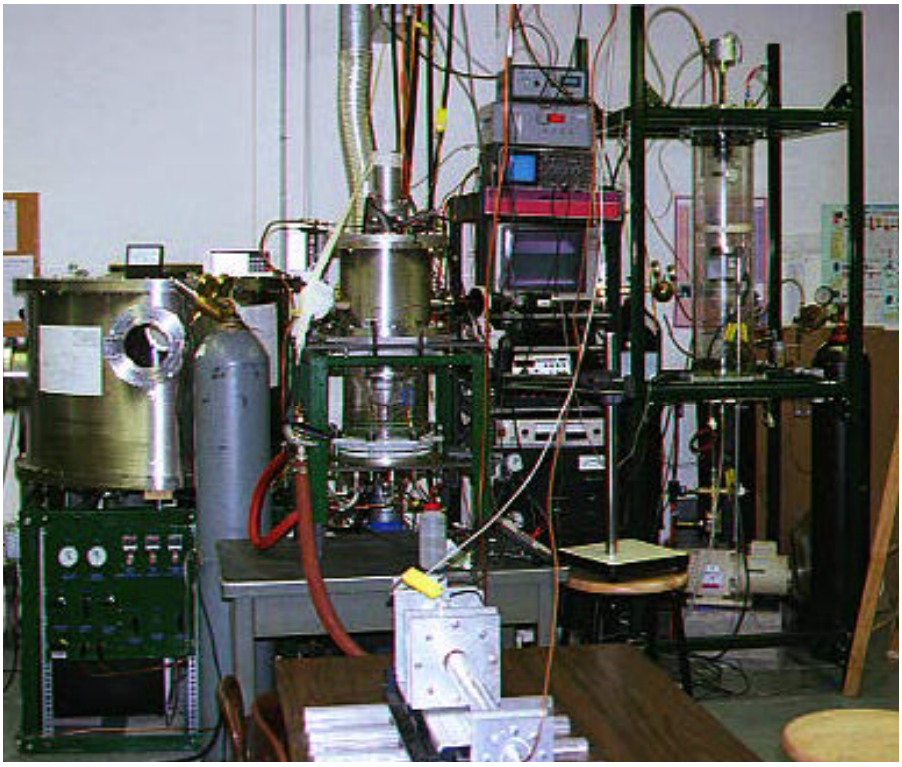

Fig. 1. The uniform-droplet spray apparatus at Northeastern University.

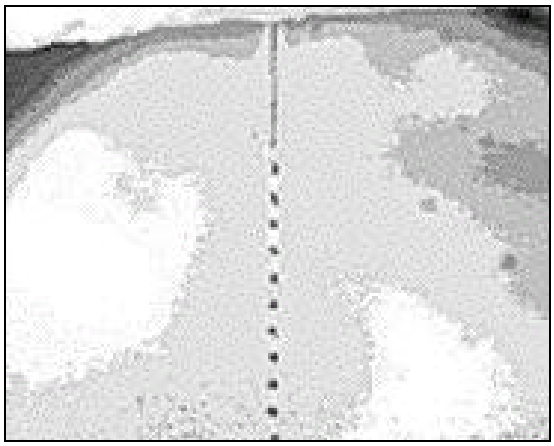

Fig. 2. Uniform breakup of aluminum jet.

Although the two particles have the same diameter and belong to the same powder, the particle in Fig. 3(a) presents a much finer microcellular microstructure than the particle in Fig. 3(b). The majority of the particles from this powder presented a fine microcellular structure similar to the one in Fig. 3(a). The different cell sizes come from different prior undercoolings experienced by the two particles. Notice that the particle in Fig. 3(a) maintains a truly spherical shape while the particle in Fig. 3(b) presents a somewhat irregular shape. This indicates that the latter particle already had started solidifying when quenched in the silicone oil, while the other particle was fully molten and undercooled at the flight distance 0.25 m at which it was quenched.

The runs with Cu–30 wt % Zn brass also used the same chamber and a 152-μm sapphire orifice. The melt temperature was set at 1267 K, corresponding to a 40-K initial superheat for the brass, which had a liquidus temperature of 1227 K. A regular nitrogen gas atmosphere, whose residual oxygen content was controlled at < 200 ppm, permitted stable uniform breakup of the brass jet. Due to chamber height limitation, the droplets were quenched into silicone oil at a flight distance of 0.25 m.

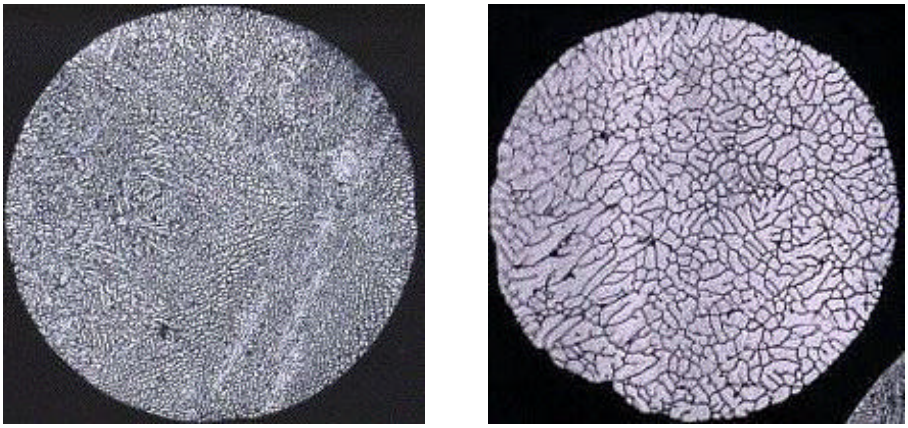

(a) **(b)**

Fig. 3. Microstructures of 282-mm uniform-droplet-sprayed Al-6Cu-0.4Zr balls: (a) large prior undercooling and (b) small prior undercooling.

Figures 4 and 5, respectively, show typical microstructures and the appearance of a 250-μm uniform brass powder produced in this way. Again, microstructures representing high and low degrees of prior undercoolings and solidification rates as seen in Fig. 4 are noted. However, as opposed to the aluminum powders discussed earlier, most particles of the brass powder presented a cellular microstructure similar to Fig. 4(b). Although not shown in Fig. 4, many particles also presented a shrinkage cavity in their interior.

Therefore, the flight distance of 0.25 m was sufficient to cause in-flight nucleation in the majority of the brass droplets, whose initial superheat was only 40 K as opposed to 100 K used in aluminum runs. The latter was confirmed using the simulation model (7, 8) we developed during this project.

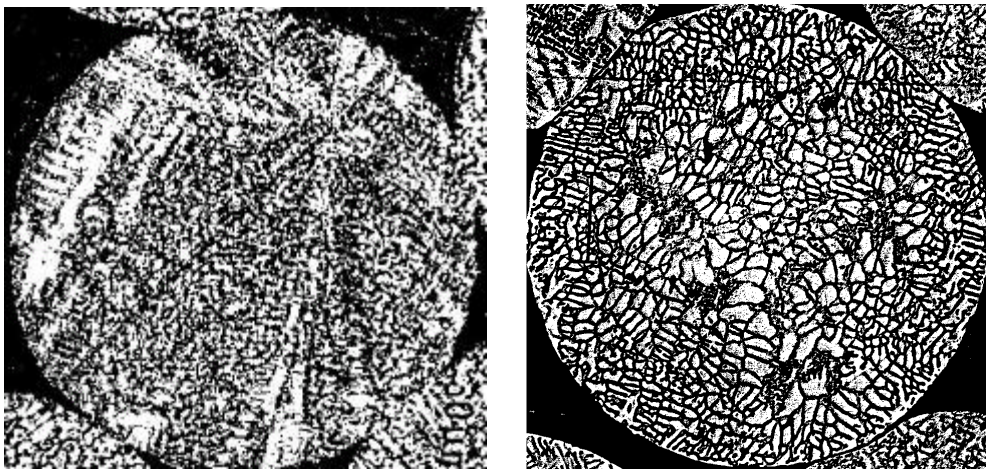

(a) **(b)**

Fig. 4. Microstructures of 250-mm uniform-droplet-sprayed Cu–30 wt % Zn balls: (a) large prior undercooling and (b) small prior undercooling.

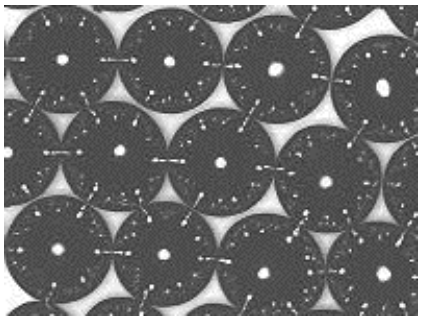

Fig. 5. Uniform-droplet-sprayed, 252-mm Cu–30 wt % Zn balls.

2. Multiple-orifice nozzle

As we develop basic methodologies for aluminum and copper processing using a single-orifice apparatus, a multiple-orifice linear UDS nozzle is being developed that can produce a linear UDS of aluminum. The linear UDS nozzle will be used to produce a 1-in.–wide aluminum strip as stated in our FY 1998 proposal. We have designed and fabricated a three-orifice UDS nozzle and tested it with tin-lead alloys to obtain data for optimum designs of the multiple-orifice UDS nozzle for aluminum. Figure 6 shows a video clip from a test run with a Sn–5 wt % Pb alloy. The nozzle uses three 152-µm sapphire orifices placed linearly with a spacing of about 8 mm. Stable uniform breakup, as shown in Fig. 6, continued for 15 min until the crucible was completely emptied. Adding more orifices does not add any fundamental technical difficulty. Multiple-orifice

nozzles with nonlinear configurations are easy modifications and will be developed for increased productivity, which is desired especially in particulate-production applications. The linear UDS nozzles will be used in conjunction with a computer-controlled movable substrate to produce a 1-in.–wide aluminum strip.

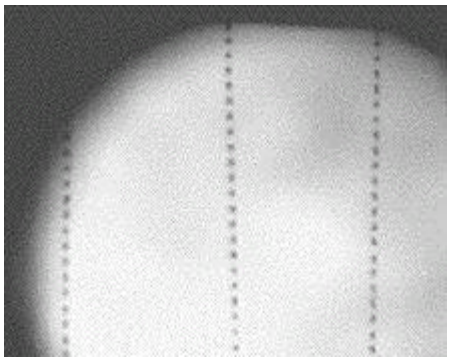

Fig. 6. Multiple-orifice uniform breakup of Sn–5 wt % Pb.

Single-Crystal Spray Deposition

One of the most attractive applications of UDS is the controlled-droplet deposition (or spray forming) of materials with novel microstructures. Our prior work with MIT reported on the production of uniform equiaxed microstructures and the rapid solidification, columnar structures by incremental epitaxial growth (9–11). A recent work at Northeastern University has further advanced this capability and produced single crystals by the incremental epitaxial solidification of uniform droplets. Figure 7 shows cross sections of single-crystalline spray deposits of pure tin and a Sn–5 wt % Pb alloy produced in our recent experiments. The results, obtained with tin-lead alloys, will be extended to higher-melting-point engineering alloys as we complete necessary modifications for higher-temperature processing.

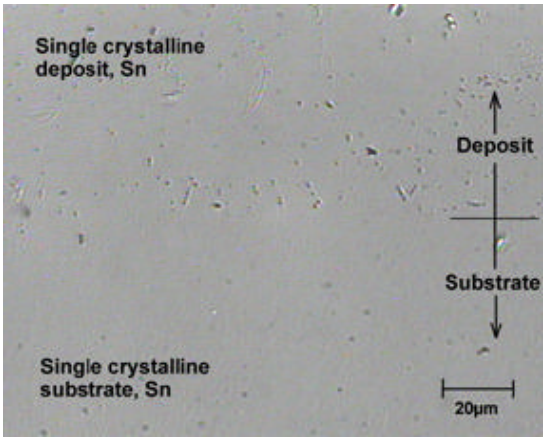

(a)

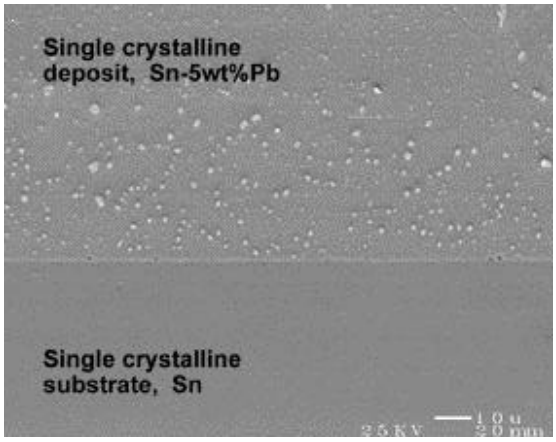

(b)

Fig. 7. Incremental epitaxial growth of rapidly solidified single-crystalline deposits: (a) Pure tin single-crystal deposit on a single-crystal tin substrate and (b) Sn–5 wt % Pb single-crystal deposit on a single-crystal tin substrate.

Thermal State and Solidification of Uniform Droplets

Successful applications of the UDS process to advanced materials processing hinges on the ability to control the in-flight solidification of the droplets at ultimate levels. To achieve this goal, an entirely new approach that permits active control of the kinetics of the heterogeneous nucleation in the droplets is being taken using the nonadiabatic calorimetric method we developed during the project (12–14). The results in Fig. 8, obtained with a Sn–5 wt % Pb alloy, indicate that the prior undercooling depends on the droplet diameter and the chamber atmosphere, parameters that can be adjusted in the UDS process to actively control the undercooling. Our study will generate data in the form of CCT diagrams that are critical to the industrial application of the UDS process. The method will be applied to engineering alloys.

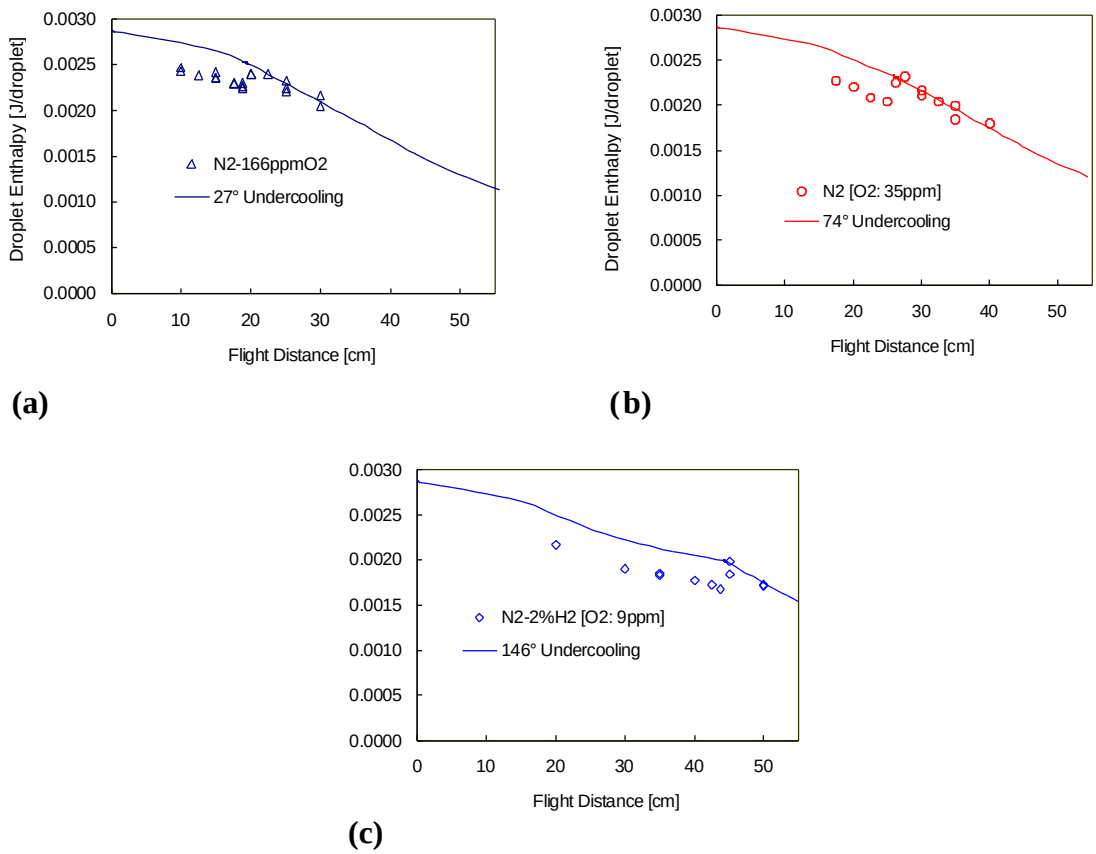

Fig. 8. Measured and simulated droplet enthalpy values. Sn–5 wt % Pb alloy: (a) 185 mm, N_2 (166 ppm O_2); (b) 185 mm, N_2 (35 ppm O_2); and (c) 185 mm, N_2–2% H_2.

Significant Accomplishments

- An analytical model has been developed to explain the fundamental mechanism of droplet splashing.
- Multiple splat interactions were studied to show that surface porosity can be reduced by increasing the ratio of the splat solidification time to the time between merged splats.
- A droplet trajectory-control system that precisely delivers droplets to a target at a desired deposition rate was built.
- The production of uniformly sized powders was advanced by implementing an integral controller to the on-line vision-control system.
- A new deposition chamber was constructed to study the evolution of microstructure in spray-formed sheet products.

Task 1. Study of the Impact Behavior of Uniform Droplets

A. Fundamental study of droplet spreading

Experimental and theoretical studies are being performed to better understand the dynamic and thermal behavior of rapidly spreading, molten microdroplets. The goal of the experimental study is to evaluate the effects of factors, such as the thermal state of impacting droplets and the target condition, on the spreading and solidification behavior of droplets. Although the bulk solidification time scale is much longer than the spreading time scale in most rapidly spreading droplets, the local solidification at the contact area between the droplet and the substrate has a significant effect on final splat shapes. Observations of splats that were produced by the UDS process and deposited on various substrate conditions have led to the construction of spreading-regime maps. These maps are based on the ratio of local solidification time to dynamic spreading time.

It is desirable to avoid droplet splashing upon impact in spray-forming applications to minimize the formation of porosity. An analytical model has been built to explain the fundamental mechanism of splashing (15). Based on the linear perturbation method applied to a radially expanding liquid sheet, the model can predict the rate of the unstable amplitude growth. The model predicts that a small Weber number, a smooth target surface, and the suppression of the initial expansion of liquid sheet (e.g., by way of enhanced solidification rate) are necessary to minimize splashing.

B. Surface porosity of sprayed deposits

A physical model describing the formation of surface porosity of deposits that were sprayed onto flat substrates has been developed (16). Using one-dimensional heat conduction and scaling analysis, it was predicted that surface porosity is reduced by increasing the ratio of the solidification time of an individual splat to the average time for

a splat to merge with a previous splat. This ratio was shown to control surface porosity by performing a series of systematic experiments that varied droplet flux, droplet size, and substrate material and temperature. As the ratio increased from 0.007 to 14.85, surface porosity decreased from 10.3 to 2.2%.

C. Controlled deflection of charged droplets

A droplet trajectory controller was developed to precisely deliver droplets to desired locations (17). This is important for high-speed imaging of droplet spreading as well as for applications of the UDS process to rapid prototyping. The trajectory-control system uses deflection plates and a pulsed-signal provider to the charging plate. The system was shown to be capable of depositing droplets to the same target at different deposition rates. Low-frequency deposition produced a vertical pillar, while high-frequency deposition produced a solidified ball. An optical imaging system will be developed to capture the spreading behavior of individual droplets delivered by this trajectory system.

Task 2. Applications to Engineering Alloys and Processes

A. Closed-loop control of the UDS apparatus for the production of uniform powders

After the SPC control algorithm was shown to produce a high variation in ball size distribution, a new control approach was considered. This new control algorithm is based on the dynamics of the UDS process, such as the change in hydrostatic pressure in the melt crucible. Using a numerical simulation of the UDS process, an integral controller was implemented and tested to obtain the gain values that provide the best steady-state and transient responses. The gain value that produced no overshoot and the fastest settling time was chosen as the optimal integral gain. From this value, fine-tuning of the controller was done by conducting experiments with the UDS system.

It is important to note that the optimal gain value corresponds to a specific target diameter. However, the gain values for other target diameters can be obtained using the numerical simulation alone. Fine-tuning is not required, since we now know the optimal response characteristics. Experiments proved that the optimal gain of the integral controller produces no steady-state error, a settling time of less than 5 s, and a very stable response.

B. Spray forming of aluminum alloy sheet material

The goal of this research is to investigate microstructural evolution in spray-formed products. Aluminum alloy sheet material will be fabricated through layerwise deposition using a multiple-orifice UDS generator. Maintaining a constant ratio of the local solidification time to the deposition cycle time of each layer seems to be the key to producing uniform microstructure through the thickness of the deposit. To do so, active control over the substrate height and temperature during spray forming are being implemented.

As shown in Fig. 9, a new spray-deposition chamber that allows for translation of the substrate in the x, y, and z directions has been built. By varying the height of the substrate during deposition, the enthalpy flux into the deposit can be controlled. The temperature of the substrate also will be controlled with cartridge heaters and/or cooling channels to maintain the deposit cooling rate.

Fig. 9. New spray deposition chamber at Massachusetts Institute of Technology.

An improved high-temperature droplet generator was built to increase melt capacity and heater power. It has been successful in producing uniform droplets of 6111 aluminum alloy and pure copper. A high-speed, data-acquisition system currently is being developed to measure droplet temperature with microelectronic sensors. This information is necessary to control microstructural evolution in the spray-formed sheet material.

REFERENCES

1. C. H. Passow, M.S. Thesis, Dept. of Mechanical Engineering, Massachusetts Institute of Technology, 1990.
2. C. H. Passow, J.-H. Chun, and T. Ando, *Metall. Trans. A* **24A**, 1187 (1993).
3. T. Ando, J.-H. Chun, and S. Sahu, *Proc. '93 PM World Congress, Part II.*, (Kyoto, Japan: Jap. Soc. of Powder and Powder Metall., 1993, p. 971.
4. C.-A. Chen, S. Sahu, J.-H. Chun, and T. Ando, *Science and Technology of Rapid Solidification and Processing*, NATO ASI Series, Series E-Vol. 278, (Dordrecht: Kluwer Academic Publishers, 1994, p. 123.
5. C.-A. Chen, J.-H. Chun, and T. Ando, in *Proc. 1994 Powder Metall*. (Toronto, 1994).

6. P. W. Yim, J.-H. Chun, T. Ando, and V. K. Sikka, *Int. J. Powder Metall*. **32**(2), 155–64 (1996).

7. A. G. DiVenuti, M.S. Thesis, Tufts University, 1996.

8. A. G. DiVenuti and T. Ando, "A Dendrite Growth Model Accommodating Curved Phase Boundaries and High Peclet Number Conditions," *Metall. Trans. A*. **29A**(12) (in press).

9. C. A. Chen, P. Acquaviva, J.-H. Chun, and T. Ando, "Spray Forming of an Sn–5 wt % Pb Alloy with a Uniform-Droplet Spray at a Low Deposition Rate," *Scripta Met. Mater*. **34**(5), 689–96 (1996).

10. C.-A. Chen, S. Sahu, J.-H. Chun, and T. Ando, "Spray Forming with Uniform Droplets," in *Proc. Science and Technology of Rapid Solidification and Processing*, NATO Workshop, June 21–24, 1994, Westpoint, New York, pp. 123–34.

11. C.-A. Chen, P. W. Yim, J.-H. Chun, and T. Ando, "Production of Novel Microstructures in Tin-Lead Alloys by Uniform-Droplet Spray Forming," in *Proc. PRICM-2*, Kyongju, Korea: Korean Inst. Metals and Materials, 1995, pp. 189–97.

12. C. D. Tuffile, M.S. Thesis, Tufts University, 1996.

13. C. D. Tuffile, A. G. DiVenuti, T. Ando, and J.-H. Chun, *J. Materials Synthesis and Processing* **5**(1), 31–37 (1997).

14. T. Tuffile, T. Ando, and J.-H. Chun, "Characterization of the In-Flight Solidification of Sn-Pb Uniform Droplets," *Solidification 1998*, eds., S. P. Marsh, J. A. Dantzig, R. Trivedi, W. Hofmeister, M. G. Chu, E. J. Lavernia, and J.-H. Chun (Warrendale, Pennsylvania: TMS, 1998), pp. 359–71.

15. H.-Y Kim, Z. C. Feng, and J.-H. Chun, "Instability of a Liquid Sheet Emerging from a Droplet upon Colliding with a Solid Surface," submitted to *Physics of Fluids*.

16. S. Chey, "A Study of Surface Porosity Formation in Deposits Sprayed onto Flat Substrates by the Uniform Droplet Spray Process," Ph.D. Thesis, Massachusetts Institute of Technology, 1998.

17. J. Shin, "Feasibility Study of Rapid Prototyping Using the Uniform Droplet Spray Process," B.S. Thesis, Massachusetts Institute of Technology, 1998.

Publications

P. W. Yim, J.-H. Chun, T. Ando, and V. K. Sikka, "Production and Characterization of Mono-Sized Sn–38 wt % Pb Alloy Balls," *Int. J. Powder Metall*. **32**(2), 115–64, (1996).

C. D. Tuffile, A. G. DiVenuti, T. Ando, and J.-H. Chun, "Calorimetric Enthalpy Measurement of Traveling Uniform Droplets," *J. Mater. Synthesis and Processing* **5**(1), 31–37 (1997).

C. D. Tuffile, T. Ando, and J.-H. Chun, "Characterization of the In-Flight Solidification of Sn-Pb Uniform Droplets," submitted to the *Proceedings 1998 TMS Annual Meeting*.

A. G. DiVenuti and T. Ando, "A Dendrite Growth Model Accommodating Curved Phase Boundaries and High Peclet Number Conditions," *Metall. Trans. A.* **29A**(12) (in press).

C. Tuffile, T. Ando, and J.-H. Chun, "Characterization of the In-Flight Solidification of Sn-Pb Uniform Droplets," *Solidification 1998*, eds., S. P. Marsh, J. A. Dantzig, R. Trivedi, W. Hofmeister, M. G. Chu, E. J. Lavernia, and J.-H. Chun, (Warrendale, Pennsylvania: TMS, 1998), 359–71.

J.-P. Cherng, J.-H. Chun, and T. Ando, "In-Flight Solidification Behavior of Aluminum Alloy Droplets Produced by the Uniform Droplet Spray Process," *Solidification 1998*, eds., S. P. Marsh, J. A. Dantzig, R. Trivedi, W. Hofmeister, M. G. Chu, E. J. Lavernia, and J.-H. Chun, (Warrendale, Pennsylvania: TMS, 1998), 317–25.

PRESENTATIONS/THESES

C. A. Blue, V. K. Sikka, J.-H. Chun, and T. Ando, "Uniform-Droplet Process," poster, ASM Educational Symposium, Oak Ridge, Tennessee, April 7, 1995.

P. W. Yim, J.-H. Chun, T. Ando, and V. K. Sikka, "Production and Characterization of Mono-Sized Sn–38 wt % Pb Alloy Balls," Int. Conf. on Powder Metallurgy and Particulate Materials, Seattle, Washington, May 14–17, 1995.

J.-H. Chun, C. A. Blue, V. K. Sikka, and T. Ando, "The Uniform-Droplet Spray Process," poster, Advanced Industrial Materials Program Annual Meeting, Washington, DC, June 14–16, 1995.

C. A. Blue, V. K. Sikka, J.-H. Chun, and T. Ando, "Uniform-Droplet Spray Forming," poster, Advanced Industrial Materials Program Annual Meeting, Oak Ridge, Tennessee, June 24–26, 1996.

C. A. Blue, V. K. Sikka, J.-H. Chun, and T. Ando, "Uniform-Droplet Spray Process," poster, Advanced Industrial Materials Program Annual Meeting, Albuquerque, New Mexico, June 16–18, 1997.

Rajesh Shingavi, "Processing and Characterization of Uniform-Droplet Sprayed Sn and Sn-Pb Alloys," M.S. Thesis, Tufts University, 1995.

Charles D. Tuffile, "Characterization of the Thermal State and Solidification in the Uniform-Droplet Process," M.S. Thesis, Tufts University, 1996.

Alfred G. DiVenuti, "Modeling of the Solidification of the Solidification in the Uniform-Droplet Process," M.S. Thesis, Tufts University, 1996.

T. Ando, C. Tuffile, X. Dong, W. Fortner, Y. Abesi, "Materials Processing with Uniform-Droplet Sprays," poster, Centennial Poster Session, Northeastern University, May 4, 1998.

T. Ando, C. Tuffile, X. Dong, W. Fortner, Y. Abesi, and Michael Beauregard, "Materials Processing with Uniform-Droplet Sprays," poster, Materials Showcase, Northeastern University, September 24, 1998.

C. A. Blue, V. K. Sikka, J.-H. Chun, and T. Ando, "Uniform-Droplet Spray Process," poster, Advanced Industrial Materials Program Annual Meeting, Jackson Hole, Wyoming, June 23–25, 1998, invited special technical presentation.

HONORS AND AWARDS

None.

PATENTS/DISCLOSURES

Disclosure: ERID No. 0263, S-87,628, "Materials Forming Using Directed Droplet Stream"

LICENSES

Uniform Metals Technologies, Inc. (Watertown, Massachusetts)

Aeroquip Corporation (Ann Arbor, Michigan)

INDUSTRIAL INPUT AND TECHNOLOGY TRANSFER

Aeroquip Corporation (Ann Arbor, Michigan).

Alcoa Aluminum (Alcoa Center, Pennsylvania)

Hoeganaes (Riverton, New Jersey)

Micro Engineering (Cinnaminson, New Jersey)

Uniform Metals Technologies, Inc. (Watertown, Massachusetts)

Contacts who have an interest in the UDS process:

ACuPowder International, LLC (Union, New Jersey)
Allvac (Monroe, North Carolina)
Ametek Specialty Metal Products Division (Wallingford, Connecticut)
Eckart America L.P. (Louisville, Kentucky)
Ervin Industries, Inc. (Ann Arbor, Michigan)
Homogeneous Metals (Clayville, New York)
Los Alamos National Laboratory (Los Alamos, New Mexico)
Postle Industries Inc. (Cleveland, Ohio)
SCM Metal Products, Inc. (Research Triangle Park, North Carolina)
Wright-Patterson Air Force Base (Kettering, Ohio)